Isolation and characterization of circulating small extracellular vesicles: A step towards method validation and clinical biomarker application.

Dissertation

zur Erlangung des Grades
Doktor der Naturwissenschaften

am Fachbereich Biologie
der Johannes Gutenberg-Universität Mainz

Christoph Kleinert

geboren am 16.06.1991 in Heidelberg

Mainz, 2023

1. Betreuer: [redacted]

2. Betreuer: [redacted]

Tag der Verteidigung: 03.05.2023

Table of Content

Zusammenfassung

Diese Studie zielt darauf ab, die Diagnose oder Überwachung von Krankheiten zu vereinfachen, indem kleine extrazelluläre Vesikel (sEVs) im Blut analysiert werden, anstatt auf Biopsien oder Liquorentnahmen angewiesen zu sein. Von Zellen sezerniert, spiegeln sEVs zu einem gewissen Grad die molekulare Zusammensetzung der Ursprungszelle wider. Es werden verschiedene Methoden zur Isolierung von sEVs aus Plasma verglichen und bewertet (1), darunter Größenausschlusschromatographie, Differentialzentrifugation, Immunisolation, Fällung auf Polymerbasis und Membranaffinitätsisolierung. Die Ausbeute und Reinheit jeder Isolierungsmethode wird durch die Untersuchung typischer EV-Marker, der Abreicherung von Plasmakontaminanten sowie der Partikelmenge und -größenverteilung beurteilt. Darüber hinaus wurden ausgewählte Isolierungsmethoden in einer validierungsähnlichen Umgebung getestet, um ihre Reproduzierbarkeit zu zeigen (2). Im Folgenden wurde die interindividuelle Variation (3) für eine ausgewählte Isolierungsmethode bewertet.

1) Alle verwendeten sEV-Isolierungsmethoden sind für die Aufreinigung aus Plasma geeignet, die Isolate unterscheiden sich jedoch deutlich in Bezug auf Ausbeute und Reinheit. Es wurden besonders sEV-reiche Aufreinigungen ausgewählt, um die Eignung für die weitere Analyse klinischer Proben zu bewerten.

2) Die ausgewählten Methoden, die auf Ultrazentrifugation und Größenausschlusschromatographie basieren, erwiesen sich als reproduzierbar, mit weniger als 30 % Abweichung vom Mittelwert für 2/3 der analysierten Proben. Das Größenausschlusschromatographie-Verfahren qEVsingle 35 Tween hat die größten Abweichungen, aber eine geringe Kontamination mit Gesamtprotein und HDL.

3) Der Test auf interindividuelle Variabilität durch Aufreinigung und Charakterisierung von 10 individuellen menschlichen Plasmaproben ergab eine große Variabilität der Ergebnisse, die mit verschiedenen Charakterisierungsmethoden verifiziert wurden. Außerdem wurden die technischen Anforderungen und der Durchsatz der verschiedenen Isolierungs- und Charakterisierungsmethoden bewertet.

Insgesamt kommt die Studie zu dem Schluss, dass die Isolierung von sEV die Erforschung von Biomarkern unterstützen kann. Obwohl alle in der Studie verwendeten Methoden für die

Aufreinigung von sEVs aus Plasma geeignet sind, unterscheiden sich die Isolate erheblich in Bezug auf Ausbeute und Reinheit. Einige Isolierungsmethoden sind reproduzierbarer als andere, was insbesondere bei frühen Biomarker-Projekten berücksichtigt werden sollte. Die bevorzugte Methode qEVsingle 35 Tween ist in der Lage interindividuelle Unterschiede der EV-Menge und des Phenotyps aufzuzeigen. Dies wurde durch einen sEV-Charakterisierungs-Workflow bewiesen, der implementiert wurde, um eine umfassende sEV-Analyse von sEVs aus lediglich 150 µL Plasma zu erhalten. Die Charakterisierungsmethoden wurden verglichen und ihre Stärken und Schwächen gegeneinander aufgeführt. Es wird aufgezeigt welche Methoden dazu geeignet sind die Biomarkerforschung und klinischen Anwendung zu unterstützen.

Summary

This study aims to simplify the diagnosis or monitoring of diseases by analyzing small extracellular vesicles (sEVs) in the blood rather than relying on biopsy or cerebrospinal fluid sampling. Secreted by cells, sEVs reflect to some extent the molecular composition of the originating cell. Different methods for isolating sEVs from plasma are compared and evaluated (1), including size exclusion chromatography, differential centrifugation, bead-based immunoprecipitation, polymer-based precipitation, and membrane affinity isolation. The yield and purity of each isolation method are assessed by investigating the presence of typical EV markers, depletion of plasma contaminants, and particle quantity and size distribution. Further, selected isolation methods were assessed in a validation-like setting to show their reproducibility (2). In the following, the interindividual variation (3) has been evaluated for one chosen isolation method.

1) All sEV isolation methods used are suitable for purification from plasma, but the isolates differ significantly in terms of yield and purity. Particularly sEV-rich purifications were chosen to further evaluate the feasibility of clinical sample analysis.

2) The selected methods, based on ultracentrifugation and size-exclusion chromatography, were shown to be reproducible, with less than 30% deviation from the mean for 2/3 of the analyzed samples. Even though the size exclusion chromatography method qEVsingle 35 Tween shows the highest deviations, low levels of total protein and HDL contaminations were shown.

3) The test for inter-individual variability by purifying and characterizing 10 individual human plasma samples found significant variation in the results obtained, verified with different characterization methods. Further, the technical requirements and throughput of the different isolation and characterization methods were assessed.

Overall, the study concludes that sEV isolation can support biomarker discovery. Even though all methods used in the study are suitable for purifying sEVs from plasma, the isolates differ significantly in terms of yield and purity. Some isolation methods are more reproducible than others which should be considered in early biomarker projects. The preferred method, qEVsingle 35 Tween, can reveal interindividual differences in sEV amount and phenotype. That has been proven by an sEV characterization workflow that was implemented to get a comprehensive sEV description from 150 µl of plasma. The characterization methods were

compared, and their strengths and weaknesses were listed against each other. It is shown which methods are suitable to support biomarker research and clinical applications.

List of Figures

List of Tables

Abbreviations

(K3)EDTA	Ethylenediaminetetraacetic acid (tri potassium)
AD	Alzheimer's disease
APC	Allophycocyanin
ApoA1	Apolipoprotein A1
ApoB100	Apolipoprotein B100
ATP	adenosine triphosphate
Aβ	B-amyloid
BBB	blood-brain barrier
BEST	Biomarkers, endpoints, and other tools
BiP	binding immunoglobulin protein
BSA	Bovine serum albumin
BSA	Bovine serum albumin
CD	Cluster of Differentiation
cfDNA	Cell-free DNA
COPII	Coat Protein Complex II
CSF	cerebrospinal fluid
CTC	Circulating tumor cells
CTLA-4	cytotoxic T-lymphocyte-associated Protein 4
CV%	Relative standard deviation
DPBS	Dulbecco's Balanced Salt Solution
ECL	Electrochemiluminescence
EGFR	endothelial growth factor receptor
EpCAM	Epithelial cellular adhesion molecule
EPI	ExoDx Prostate IntelliScore
ESCRT	endosomal sorting complex required for sorting
EV	Extracellular vesicle
FBS	Fetal Bovine Serum
FDA	Food and Drug Administration
HDL	High density lipoprotein
HEK-293	Human embryonic kidney 293 cells
HeLa	Cervical cancer cells from Henrietta Lacks
HER2	Receptor tyrosine-protein kinase erbB-2
HLA-ABC	Human leucocyte antigen class I molecules, Major Histocompatibility complex class I
HLA-DRDPDQ	Human leucocyte antigen class II molecules, Major Histocompatibility complex class II
HRP	Horseradish peroxidase
HRP	Horse radish peroxidase
HSP	Heat shock protein
IgG	Immunoglobulin G
ILV	intraluminal vesicles
IND	Individual
LDL	Low density lipoprotein

MCSP	melanoma-associated chondroitin sulfate proteoglycan
MHCII	Major histocompatibility complex class 2
MIgG	Mouse Immunoglobulin G
miRNA	micro ribonucleic acids
mRNA	Messenger RNA
MSD	Meso scale discovery
MVB	multivesicular bodies
N/A	Not available
NaCl	Sodium chloride
NSCLC	Non-small cell lung cancer
NTA	Nanoparticle tracking analysis
PANX1	Pannexin 1
PD	Parkinson's disease
PD-1	programmed death receptor
PD-L1	Programmed Cell Death 1 Ligand 1
PET	positron emission tomography
PLS3	Phospholipid Scramblase 3
PS	Phosphatidylserine
PTK7	Protein tyrosine kinase 7
PVDF	Polyvinylidene fluoride
R	Spearman correlation coefficient
REA	Recombinant antibody isotype Control
RNA	Ribonucleic acid
ROCK1	Rho-kinase 1
R-squared	Coefficient of determination
RT	Room temperature
SEC	Size exclusion chromatography
sEV	Small extracellular vesicle
SSEA-4	Stage Specific Embryo Antigen 4
TAPA1	Anti-Proliferative Antibody
TBS	Tris-buffered saline
TIM-4	T-cell membrane protein 4
TMB	3,3',5,5'-Tetramethylbenzidine
Tsg101	Tumor susceptibility gene 101
TSPN	Tetraspanin
WB	Western blot
z-score	Standard score

1. Introduction

1.1. Biomarkers

1.1.1. Definition

The word biomarker, also referred to as surrogate markers or endpoints, can be dated back to the early 1970s. Following the Food and Drug Administration (FDA) definition, a biomarker is specified as a "defined characteristic that is measured as an indicator of normal biological processes, pathogenic processes, or biological responses to an exposure or intervention, including therapeutic interventions" [1]. The underlying principle is to substitute a complex condition (e.g., disease) with a measurable size – the biomarkers – that represents the condition itself. The need for biomarkers is based on two significant advantages. First, the biomarker measurement or analysis is more significant, objective, specific, or accurate in comparison to the analysis of the condition itself. That might be important when the condition is very diverse or mild in its manifestation and evaluating the biomarker status enables clinical decision-making. Simultaneously, the costs, robustness, or turn-around time might also be reduced. Second, the study of biomarkers may allow for a reduction in the time needed to observe alterations. In some cases, the diagnosis of a disease might be possible years or decades before the onset of symptoms. Ideally, the marker is also non- or minimally invasive. [2–4]

On the one hand, a biomarker can be either a concentration of biofluid-content substances, aggregates, cells, or nanoparticles. These can be determined in biofluids like blood, urine, cerebrospinal fluid, saliva, or tissues. On the other hand, a biomarker can be histological, physiological, and radiological characteristics, including sampling-free readings, e.g., imaging methods or blood pressure measurement.[5, 6]

Besides a single measurement of individual data points, a biomarker can also consist of the relative quantity of two markers or a complex pattern of genes or proteins. [4, 7]

1.1.1.1. Extracellular vesicles

A potential source of biomarkers that has been getting increased attention for years is circulating extracellular vesicles (EVs). These vesicular structures are shed by cells throughout the human body and enable to determine their tissue origin and further analyze the cargo. As such, they are heavily studied in different biomarkers research

areas, including cancer, autoimmune diseases, and neurodegeneration. However, the application is still challenging, and there is not yet an FDA-approved biomarker assay on the market. [8, 9]

1.1.2. Application

W. A. Colburn (2003) classifies the biomarkers and the associated needs based on the stages of drug discovery. The requirements will change as drug discovery progresses from early to later phases. In the early stage, the biomarker should reflect the alterations in the hypothesized pathological mechanism. These biomarkers can be valuable for early drug discovery, even though their informative value is limited. In later stages, the biomarker should reflect the progression of the disease and be influenced by the therapeutical interventions. Ultimately, the biomarker predicts specific observed outcomes making it a surrogate marker or showing a good relationship to the best currently used predictor. [10, 11]

A pathology progresses from molecular changes over cellular and tissue alterations until whole organs and their functions are negatively affected. The observable clinical effect is the resulting manifestation. Mechanistic proximity of the biomarker to the pathological outcome gives more significant feedback about the disease state. More distal biomarker changes earlier than the clinical outcome but might lack specificity. [2, 10]

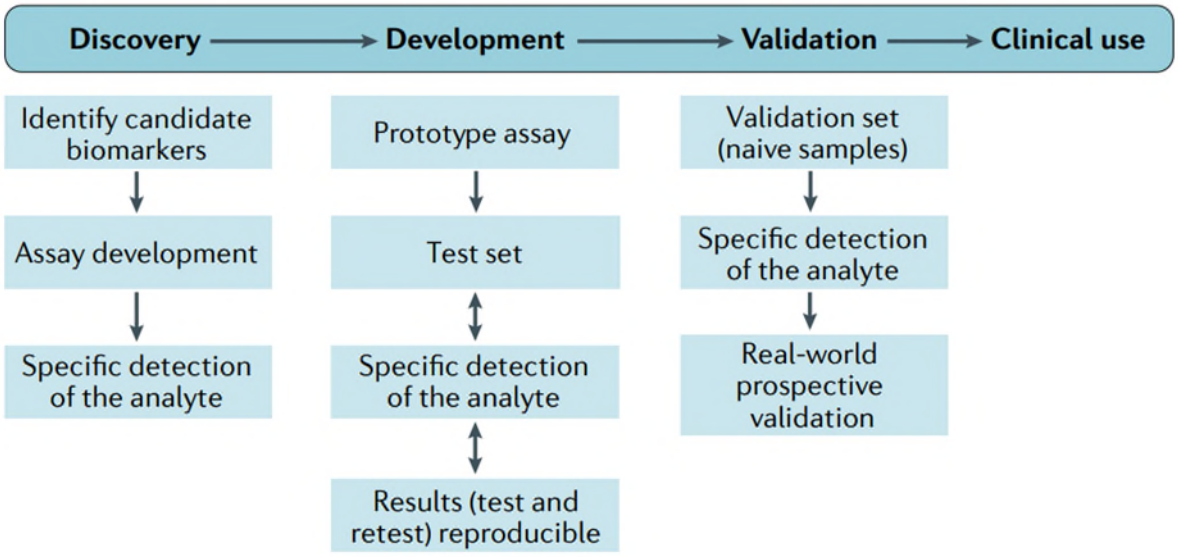

Figure 1 – Steps and challenges of biomarker assays from discovery to clinical use. [12]

The underlying pathological mechanism is critical in the early drug development phase for a biomarker strategy. The comprehensible link to the drug's effect should be hypothesized

during the target selection phase. During the preclinical phase, an assay for testing the biomarker should be designed and validated regarding pre-defined criteria. Further, the feasibility of the assay in the clinical setting needs to be evaluated based on, e.g., the costs, potential risk for the patients during sampling, and the required sample volume. [13]

In theory, the biomarker should have proven to provide relevant information, the feasibility of the measurement for clinical study analysis, and the reliability of the results before the transition to the clinical phase. This includes testing solutions from different manufacturers to avoid software or hardware-specific differences in the outcome as well as cross-user and -site variation in data acquisition and analysis. [11, 14]

In phase I studies, changes in pharmacodynamic biomarkers provide evidence for drug-target interaction with hypothesized modulation and help in drug selection and dosing for upcoming trials. The association between a biomarker and the predicted clinical outcome can be evaluated during phase II trials, where diseased individuals undergo the treatment. Pharmacodynamic biomarkers will help to evaluate the dose-response relationship when comparing the different dosing cohorts. A positive control treatment – mostly the current standard therapy – is indispensable for biomarker validation of a therapeutic with a new mechanism of action. Because, for innovative treatment options there is, by definition, no fully validated biomarker available. Hence, the validation of the biomarker and the therapeutic will be driven simultaneously, reducing the biomarker's initial significance and complicating early decision-making. [11]

In phases II and III, pre-defined biomarkers statuses can serve as exclusion criteria – called enrichment study design. For this, the enrichment strategy is based on characteristics related to the investigated therapeutic's mechanism of action. As an example, a mechanistically involved protein or genetic marker can identify responders from non-responders. The exclusion of the non-responding population would increase the observed therapy effect. Even though it is unlikely that a phase II study definitively determines whether a marker can predict the clinical benefit, investigators may identify an association that can be further investigated in phase III. [14–16]

An overview of the distinct phases from biomarker discovery over development and validation to the clinical application is shown in Figure 1 – Steps and challenges of biomarker assays from discovery to clinical use. [12].

1.1.3. Types of Biomarkers

Over the years, different subtypes of biomarkers have been classified. **Diagnostic markers** confirm the presence of a disease. Besides the status, whether an individual is diseased or not, the biomarkers often allow a more defined classification of the disease. Diagnostic biomarkers often share predictive or prognostic markers characteristics (will be described in the following) as the definitions have a smooth transition. One specific example of a potential diagnostic biomarker is the cargo of circulating extracellular vesicles (EVs). These reveal a great potential in cancer diagnosis by carrying tumor-specific micro ribonucleic acids (miRNAs), e.g., miR-181b-5p and miR-320b (NSCLC), or membrane proteins like EpCAM, HER2, PTK7, and Survivin (Prostate cancer). [1, 17, 18]

If a marker allows evaluation of the likelihood of an effect caused by an intervention or exposure, they are called **predictive biomarkers**. The marker indicates the probability that the treatment is beneficial for the individual. By pre-defining the study participants' selection criteria, the number of individuals needed to demonstrate efficacy can be reduced. One example of a potentially predictive biomarker is programmed death receptor ligand 1 (PD-L1) for treatment with immune checkpoint inhibitors. Immune checkpoint inhibitors are a treatment option for certain cancers, including gastric and NSCLC. In 2011 the FDA approved the first antibody of this class targeting cytotoxic T-lymphocyte-associated Protein 4 (CTLA-4). From 2014 to 2020, the FDA approved another six antibodies targeting the programmed death receptor (PD-1)/PD-L1 axis. The enhanced activation of the PD-1/PD-L1 axis leads to increased tumor growth due to immune escape and is associated with a poor prognosis. [19] Since only a small subpopulation of cancer patients benefit from this new therapy option, the need to have predictive biomarkers was identified soon. This need led to the idea of measuring PD-L1 on the surface of cancer and immune cells. Current FDA-approved predictive biomarker assays require the extraction of cancer tissue and identify the ratio of PD-L1 positive cancer and immune cells. However, the PD-L1 expression as a predictive biomarker is not universal for all cancer types and

varies for the different antibodies within the class of immune checkpoint inhibitors. [19–22]

Tumor-derived EVs have been shown to have similar immunomodulating effects and carry PD-L1. Since these tumor-derived EVs can be found in patient plasma samples, they are an intensively studied potential predictive biomarker. In metastatic melanoma patients, EV-bound PD-L1 levels have been elevated in non-responders prior to immunotherapy. [23, 24]

Prognostic biomarkers reflect the likelihood of changes in the progression of a disease. It should allow for early identification of individuals at risk of a specific outcome like a clinical event or disease recurrence. Prognostic biomarkers can also serve to exclude individuals or groups with higher risks for poor outcomes from clinical studies. In the case of a pure prognostic marker, this would not affect the measured treatment effect but would affect the different outcomes. If, for example, a biomarker indicates a disease's rapid progression, both patient groups (biomarker positive and negative) would have the same potentially beneficial effect from treatment. Nevertheless, the biomarker-positive group would still have a worse clinical outcome (Figure 2 – Theoretic treatment effects on biomarker positive and biomarker negative groups for a purely prognostic and a purely predictive biomarker [28]). For example, it has been shown that the proteins syntenin and binding immunoglobulin protein (BiP) can be detected in EVs isolated from human serum samples. Higher levels of these vesicle-associated proteins indicate an early phase of metastasis development in melanoma patients and thus are associated with a poor outcome. Through knockdown experiments, it has been shown that both proteins are involved in cell motility and invasion. [25–27]

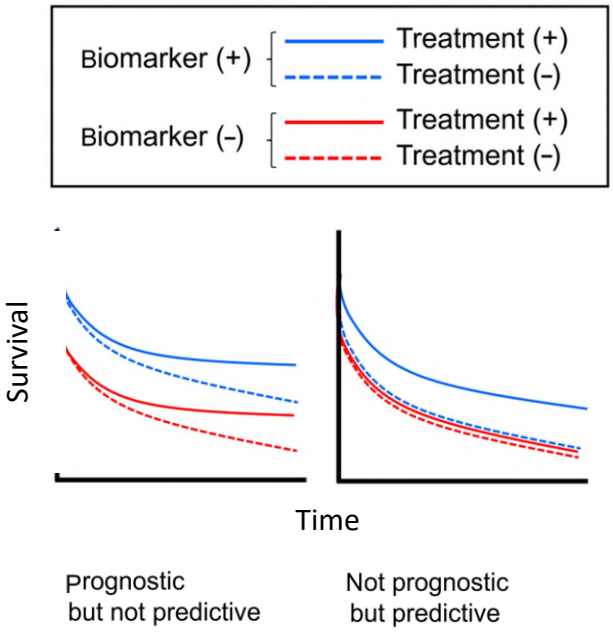

Figure 2 – Theoretic treatment effects on biomarker positive and biomarker negative groups for a purely prognostic and a purely predictive biomarker [28]

If the measurement of a biomarker can be performed serially or even constantly, they are called **monitoring biomarkers**. The aim is here to evaluate the disease status of the effects of therapy, exposure, and environmental influences. If a threshold of the marker is reached, that indicates a pre-defined modification in treatment. That can also take place during, e.g., a clinical trial with a potentially liver-toxic drug. Markers that constantly assess the liver function would indicate early harmful effects and can lead to the exclusion of the concerned individuals from the study. [29]

Pharmacodynamic biomarkers are a helpful tool to evaluate the effects of medical intervention by demonstrating that the drug reaches the drug-target and measuring the resulting effect (target-engagement) [12]. Especially in the early development of an active compound, the biomarker strategy should rely on one or more valid pharmacodynamic biomarkers to evaluate the efficacy. Thereby, the cost of drug development can be reduced by tightening the early phase pipeline. Nevertheless, pharmacodynamic biomarkers also play an essential role in clinical practice. Often the given dosage depends on the change of these markers and the anticipated therapeutic effect. [29, 30]

Markers that characterize the patient's response to the active compound, including absorption, distribution, metabolism, and excretion, are called **pharmacokinetic markers**.

The knowledge about the individual classification leads to a deeper understanding of patient-dependent treatment options, often referred to as precision medicine. [31, 32]

In contrast to a prognostic biomarker, a **risk biomarker** indicates the likelihood of developing a disease or medical condition that did not yet occur. **Safety biomarkers** can be quantified before and after drug exposure to evaluate the presence of adverse events. The measurement demonstrates or refutes toxic effects on specific organs or tissues. Despite the positive impact on the study participant's health, a risk assessment must be conducted to trade the safety consideration against the benefit of the intervention. [29, 33]

1.1.4. Validation

In principle, the validation of biomarkers needs to comprise two levels: I) Biological validation: a hypothesis validation needs to be performed to verify that the changes in the biomarker go along with the changes in the expected clinical outcome. II) Method validation: focuses on the devices and protocols used to analyze the alterations. [34]

Validation of analytical methods for a biomarker should guarantee its sensitivity, specificity, precision, and reproducibility and reveal the intra- and interpatient variability. The specific requirements can vary a lot due to the context of use. The context of use describes the type of biomarker according to the “Biomarkers, endpoints, and other tools” (BEST) criteria and the application during drug development. [35] Another effector of the requirements is the risk assessment. If, for example, a biomarker predicts a disease based on a complex and potentially harmful sampling like a biopsy, the likelihood of a false positive result should be lower compared to a measurement that can easily be performed several times a day, like nasal sampling. According to the validation status, the biomarker has to pass three stages of evidence: 1) exploratory, 2)probable valid, and 3) fit-for-purpose. [36] The term “fit-for-purpose” has replaced the old term “known valid” due to the growing understanding that the validation criteria need to be defined based on the degree of certainty required to answer the specific question. [14, 29]

1.1.5. Liquid Biopsy

Liquid biopsy describes the transition from analyzing tissues obtained by a conventional biopsy to assay biofluids gathered by non-invasive sampling. The concept was established around ten years ago, and since its first usage described the detection of circulating tumor cells, it is closely linked to cancer research. Nevertheless, the basic principle has been introduced into various diagnostic areas. [37, 38]

The biofluids used are primarily blood and urine, but other matrices like saliva and tears have also been described. Besides the decreased risk for patients, liquid biopsy exceeds in cost and time efficiency, fast turn-around time, and consequently allows real-time monitoring of the current health state. In some cases, the tissue is inaccessible due to its anatomical location or unremovable, hindering conventional biopsy. Often the tissue section is not representative of the heterogeneous pathological tissue alterations. Hence, a liquid biopsy would still allow the patients' diagnosis or disease classification.

Even though the advantages of liquid biopsy seem outstanding, it has not yet reached a broad clinical application. [40, 41]

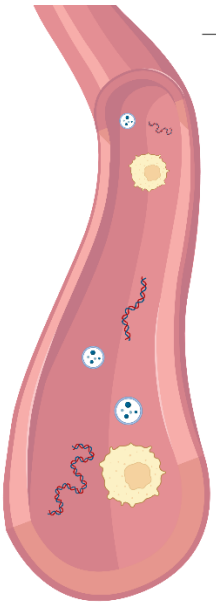

Biomarker types	Biomarker	Strengths	Limitations
Circulating tumor cells	cancer cells with particular surface markers	direct derivation from tumor tissues	low counts and technical challenges
Circulating DNA	mutant ctDNA, e.g., EGFR mutation	easy examination	not suitable for distinct cancer types
Circulating EVs	EV populations and their cargo	protected by lipid-bilayed, crosses biological barriers	technical challenges for isolation, purification

Figure 3 – Schematic overview of liquid biopsy strategies, including circulating tumor cells, DNA, and EVs. [39]

However, three categorical strategies are known: I) circulating tumor cells (CTC), II) cell-free DNA (cfDNA), and III) EVs (see Figure 3 – Schematic overview of liquid biopsy strategies, including circulating tumor cells, DNA, and EVs. [39]).

I) The first CTC biomarker that the FDA has approved is CellSearch®. It is used for the analysis of blood samples from metastatic breast-, colorectal-, and prostate cancer

patients. The method is based on the assumption that peripheral blood should be free from epithelial cells. After capturing predominantly EpCAM-positive cells from the patient's blood, the cells get immunofluorescent labeled, and the CTCs can be detected based on their membrane marker composition. [42]

II) In 2016, the FDA approved the real-time polymerase chain reaction (PCR) based cobas® EGFR Mutation Test v2 as a companion diagnostic test for endothelial growth factor receptor (EGFR) gene mutations in plasma. Due to the moderate sensitivity in detecting mutations in lung cancer patients, the conventional biopsy is still the gold standard and needs to confirm negative results. [38]

With Guardant360 CDx, another cfDNA-based test was approved by the FDA in 2020. This Next Generation Sequencing test analyses a panel of cancer-related gene alterations, including 73 point-mutations, 23 indels, 18 gene amplifications, and six gene fusions. Based on the results, the physicians can identify those NSCLC patients who benefit from an osimertinib (TAGRISSO™) treatment. [43, 44]

III) There is no FDA-approved EV products on the market, including biomarker panels. Nevertheless, tests like the ExoDx Prostate IntelliScore (EPI) are commercially available and show promising results for prostate cancer patients. Together with other clinical variables like prostate cancer antigen levels, family history of prostate cancer, and age, the test can reduce the performed biopsies by ~30 %. The reverse transcriptase polymerase chain reaction test gives a risk score ranging from 0 to 100 based on exosomal RNA patterns (ERG, PCA3, and SPDEF). [9, 45, 46]

1.1.6. The strong demand for more specific biomarkers in neurodegeneration and cancer

1.1.6.1.Neurodegeneration

Neurodegenerative disorders, most prominently Alzheimer's and Parkinson's disease (AD & PD), share different commonalities. In both cases, progressive degradation of brain cells leads to loss of function and subsequent mental deterioration. The tissue breakdown remains unnoticed until the brain can no longer compensate for the deficiency. The onset of the symptoms occurs years or even decades after the beginning of the pathological processes. The pathologies are accompanied by misfolded protein aggregations like tau, β-amyloid, or α-synuclein in the central nervous system (CNS). In many cases, these

misfolded proteins are sources of inflammatory processes in the CNS which was demonstrated in post-mortem brain tissue. [47] The current standard treatment focuses on maintaining the levels of neurotransmitters. Consequently, the underlying progressive degeneration is not slowed or inhibited. [48, 49]

There is a need for reliable biomarkers due to the lack of robust biomarkers for early diagnosis and classification of diseases. Many AD patients get misdiagnosed even in special dementia clinics (25-30%), and there is evidence to assume that the rate is even higher in primary care. For PD, the accuracy is better (20% of misdiagnosis), but for the occurring clinical trials with disease-modifying therapeutics, the risk of including falsely diagnosed patients is high. [48] Inclusion criteria need to be defined based on biomarkers for enrichment studies. Due to the overlap in pathological processes, the heterogeneity of neurodegenerative diseases is high. The alteration might only occur in specific brain regions leading to other phenotypes and, consequently, different classifications.

Further differences relate to the type and level of inflammation. Especially in elderly patients, there is a higher chance for the co-occurrence of different neurodegenerative processes or other impairments. In interventional trials, it might be necessary to start the treatment in the pre-symptomatic or prodromal stage of the disease. Hence, surrogate markers need to indicate treatment effects maybe decades before the onset of the symptoms. Therefore, suitable pharmacodynamic biomarkers are crucial. [48, 50]

For AD, the primary biomarkers are the peptide β-amyloid (Aβ), especially Aβ42, and tau, which can also be measured in different phosphorylated forms (e.g., p-tau$_{181}$). In Lewy body diseases like PD, α-synuclein is measured as well as their phosphorylated or oligomeric forms. These biomarkers can be detected by positron emission tomography (PET) imaging or quantification in biofluids like cerebrospinal fluid (CSF) and blood. Besides PET imaging, CSF best reflects the biochemical state of the brain tissue. Nevertheless, easily accessible alternatives like blood are needed for monitoring to develop new pathogenesis-based treatment options. [49, 51]

1.1.6.2.Oncology

Cancer, in general, is an abnormal, uncontrolled proliferation of cells within an organism. Stepwise pathological changes in the genome of the affected cell line led to an increased

risk for neoplasia. The accumulation of dominant gain of functions (oncogenes) and loss of function (tumor suppressor genes) leads to the key features called hallmarks of cancer, including self-sufficient in growth signals, insensitivity to anti-growth signals, tissue invasion & metastasis, evading apoptosis, and genome instability and mutation [52, 53]

The resistance to anti-growth signals and pathological changes in the DNA replication and repair mechanisms lead to genomic instability. Thus, there is an intra- and intertumoral heterogeneity that is accompanied by different clinical outcomes. This, in combination with the histological types of cancer with their individual underlying properties, gives an idea about the variety of tumor classification and genomic subcategorization. [54–57]
As with neurodegeneration, there is a need for easily accessible detection of biomarkers that enable the earliest possible intervention. Also, the biomarker-driven patient selection improves in both cases the detectable efficacy. [58, 59] There is a demand for non- or minimal-invasive biomarkers throughout treatment to monitor the disease progression at several time intervals. Other than in neurodegeneration, there are several biomarkers available to contribute to the decision-making in drug development and clinical practice. Nevertheless, exploring genetic and phenotypic variability and their consequences on clinical outcomes with and without treatment gives a deeper insight into the pathogenesis and individual treatment options towards precision medicine. [11]

1.1.6.3. Motivation for using EVs in the field of biomarkers

Since the profile of an exosome mirrors the cellular origin and the physiological or pathological state, the conclusion to use the exosomes for diagnosis or disease classification is consequent. Their presence in easily accessible biofluids and the variation in the heterogenic composition appear appealing. EVs carry lipids, metabolites, proteins, and nucleic acids from every cell type to far distant places within the body and cross biological barriers like the blood-brain barrier (BBB). [60–65] The cargo is clustered into analyzable entities and protected from degradation by a lipid bilayer. It has been demonstrated that EVs from diseased tissues can be proven in different biofluids but might also be involved in various pathological processes. Novel detection and

quantification methods constantly improve sensitivity which suggests the significance of EVs will increase. [61, 66, 67]

Therefore, EVs seem to be a promising source of biomarkers, especially in neurodegeneration and cancer research. Even though the aims and conditions are very different is both areas, EV biomarkers might be feasible to meet the diverse requirements.

1.2. Extracellular vesicles

1.2.1. Description

EVs are multicomponent structures that unite cell-membrane lipids with incorporated and enclosed proteins and nucleic acids from the cell of origin in entities. These vesicles are released into the extracellular space and can be found in various biofluids. Due to their entity, they contain important information about the cell and tissue of origin. [68, 68, 69]

1.2.2. Structure

EVs are heterogeneous particles that are released from cells. Like cells, they are bound by a well-defined lipid bilayer encompassing an aqueous core. [70] The thickness of the phospholipid bilayer is typically ~5 nm and allows a theoretically spontaneous self-assembled vesicle of ~15.5 nm or bigger. The composition of the membrane and content is dependent on the cell of origin that release the vesicles into the extracellular space. [71, 72]

1.2.3. Classification

EVs can be classified into three major subtypes: (i) apoptotic bodies, (ii) microvesicles, and (iii) exosomes. [65][73] While this classification is based exclusively on biogenesis, subdivisions refer to the vesicles' size. [74]

(i) Apoptotic bodies are the biggest subtype. Unlike other vesicle types, they have been shown to include cell organelles ranging from 1-4 µm in diameter. Phagocytes rapidly remove apoptotic bodies, so their occurrence is limited. [70, 75, 76]

(ii) Microvesicles or ectosomes shed directly from the outer cell membrane, and the size has been described to be within 100-1000 nm in diameter. The amount of microvesicles varies a lot dependent on the cell type of the cell of origin, its state in the cell cycle, and its microenvironment. [70, 77]

(iii) The smallest types of vesicles are called exosomes ranging between 30 and 150 nm. [74]

If the classification by biogenesis is reasonable is controversial. For instance, it has been reported that the formation of T-cell EVs frequently occurs at the outer cell membrane. The definition based on the biogenesis classifies those as microvesicles, but they share

many of the characteristics of exosomes. There is a lack of specific markers and enrichment or isolation strategies. Depending on the research question, a classification based on the physiochemical properties (by size or surface marker appearance) might be more meaningful for a uniform nomenclature and reporting of the data. [60] The technical separation of different-sized vesicles led to a nomenclature that allows a more accurate report of the EV properties. The vesicles are exclusively defined by their size and, thus, consist of a mixture of apoptotic bodies, microvesicles, and exosomes. Here, the small EVs (sEVs) reflect the size range of the exosomes and are often referred to as < 150 nm. [74, 78]

1.2.3.1. Apoptotic bodies

Description

Apoptosis is a mechanism well-described in multicellular organisms and can be referred to as an active deletion of specific cells. One of the characteristics of a cell undergoing the sequential steps of apoptosis is morphological conversion. Caspase-mediated reorganization of the cytoskeleton leads to a shrinkage of the apoptotic cell. It loses the cellular connections to the surrounding tissue while the outer membrane forms protrusions and blebs. Interestingly, not all cells undergo the disassembly into apoptotic bodies, and it has been shown that it is not required for phagocytic clearance. During apoptosis, the cells do not lose the membrane integrity and thus prevent the release of intercellular constituents into the surrounding interstitial tissue [75] [79]

Cargo

Apoptotic bodies as fragments of a decomposing cell include cytosol and fragmented or even intact organelles. Consequently, a wide variety of biomolecules, for instance, proteins, lipids, metabolites, and nucleic acids, can be found. Due to the systematic fragmentation of the DNA, the chromatin condensation, the deconstruction of the nucleosome, and the breakdown of the cell nucleus, apoptotic bodies contain micronuclei, DNA fragments, and chromatin. Even if the presence of components from the nucleus or endoplasmic reticulum are indicators of apoptotic bodies, these markers lack specificity and have been shown to be found in other vesicles. It is hypothesized that caspase-cleaved proteins like Rho-kinase 1 (ROCK1) and Pannexin 1 (PANX1) are

exclusively found in apoptotic cells and bodies. [80] Phosphatidylserine (PS) is a commonly used marker for apoptotic cells and vesicles. The phospholipids are expressed on the outer leaflet of the apoptotic cell membrane. As a signal for phagocytosis, it triggers the uptake of apoptotic bodies. In macrophages, the surface receptor T-cell membrane protein 4 (TIM-4) and the PS-binding protein annexin-V were identified to initiate this PS-dependent phagocytosis. [75, 81–83]

Biogenesis

The mechanisms and pathways during apoptosis are well described and a continuous focus of research. However, the underlying changes of apoptotic body biogenesis are poorly understood. The proteolytic cleavage of cytoskeletal proteins that accompany the early stages of apoptosis is followed by further well-regulated modifications that lead to the division of the cell and the formation of apoptotic vesicles. [79] How these individual steps are orchestrated is still unclear. Confocal microscopy revealed that dying epithelial stem cells produce 12.9 ±3.2 apoptotic bodies per hour with an average size of 2.3 µm. [84]

Function

Apoptotic bodies play a significant role in immune regulation, cell-to-cell communication, and organ repair, as phagocytosis can stimulate cell proliferation. The fact that distinct cell types deconstruct into different quantities of apoptotic bodies with different compositions is a hint for the regulatory value of apoptotic bodies. [75, 76, 84]

1.2.3.2. Microvesicles

Description

Microvesicles were first described in blood plasma or serum originating from platelets. They have been shown to have pro-coagulant effects, but in recent years they were also discussed to be involved in cell-to-cell communication. In contrast to apoptotic bodies, microvesicles are also released from healthy cells and can be found in all biofluids. Under pathological conditions, the number increases, and their composition differs. [77, 85]

Cargo

Due to the biogenesis of microvesicles, their content is mainly composed of cytosolic proteins, like heat-shock-proteins (HSP). Also, cell membrane-associated proteins and proteins that tend to cluster at the cell membrane can be detected. This includes cytoskeletal proteins and glycosylated and phosphorylated proteins. In contrast to exosomes, the microvesicles can incorporate even smaller organelles like mitochondria. Besides proteins, mRNA, miRNA, bioactive lipids, and metabolites incorporate in microvesicles. [70, 76]

Biogenesis

Microvesicles are formed via the budding of the plasma membrane and occur in every human tissue. The release requires adenosine triphosphate (ATP)-dependent contraction of actin and myosin, promoting a protrusion of the membrane. Hence, the shedding of microvesicles is reduced in cold temperatures and dependent on kinesin and myosin. The vesicle is then released from the membrane by fission of the bud stalk. It has been shown that the formation of microvesicles can be fostered by increasing the calcium ion concentration or inducing cell stress. The initiation of the microvesicle formation can be linked to three observed mechanisms. First, the relocation of the late endosomal protein Tumor susceptibility gene 101 (Tsg101) to the plasma membrane leads to a local change in membrane curvature resulting in budding. Second, protein-protein interactions in the cell periphery may lead to membrane shape changes and de novo vesicle formation. Third, the membrane lipid composition or their leaflet translocation can also contribute to the curvature of the membrane and hence contribute the vesicle creation. [70, 85–88]

Function

Early experiments revealed that platelets shed tissue factor-coated vesicles in response to collagen exposure participating in blood coagulation. Later an immunostimulatory effect was observed. Vesicles shed by neutrophile granulocytes seams to stimulate macrophages to release anti-inflammatory signals. On the other hand, pro-inflammatory effects of microvesicles have been observed by transferring chemokine receptors or stimulating corresponding mediator release. Like other vesicles, microvesicles are highly

heterogeneous in composition and function. Their interaction with targeted cells can be due to receptor interaction of the membrane-bound proteins or the internalization of the cargo by fusion or endocytosis. Here, not only an interaction based on protein can be imagined. Also, mRNA and miRNA transmission would be conceivable. Since these molecules are highly conserved compared to their non-vesicular counterparts, they can reach far-distant recipient cells. [87, 88]

1.2.3.3. Exosomes

Description

The word "exosome" is formed from the Greek words "exo" ("outside") and "soma" ("body"). In 1987 the term was first used to describe vesicles that are formed within the endosomal compartment and can be released to the extracellular space. As apoptotic bodies and microvesicles, exosomes are phospholipid-bilayer-bound entities. Due to the biogenesis, the size has been reported to be anything from the theoretical minimum to up to 200 nm in diameter. In transmission electron microscopy, the morphology of the exosomes is often referred to as cup-shaped, but cryo-electron microscopy, as the more structure-preservative method, does not confirm the results. As they carry cargo from the cell of origin toward close and far distant tissues, their function and utility have been investigated a lot within the last decades. Because their size and density overlap with microvesicles, identifying exosomes is challenging and requires marker analysis. [65, 78, 89]

Cargo

Other than the tetraspanins, exosomes carry proteins connected to the endosomal sorting complex required for sorting (ESCRT) like Alix and Tsg101, heat shock proteins (HSP70 and HSP90), and membrane transport and fusion proteins (Flotillin, Annexins, and GTPases). In theory, the estimated cargo is below 100 proteins per vesicle. Besides proteins, exosomes carry large and small molecules, including nucleic acids (mitochondrial and nuclear DNA and various types of RNA), lipids, and metabolites. Since the RNA content has been reported to be significantly different from the cell of origin, they are highly investigated. miRNA, other non-coding RNA, and mRNA have been

identified as exosome cargos, both full-length and fragmented. Exosomal membranes were shown to incorporate high cholesterol levels, phosphatidylinositol, phosphatidylethanolamine, sphingomyelin, ceramide, and phosphatidylserine. They contain lipid rafts-associated proteins, e.g., cytosolic tyrosine kinases and glycosylphosphatidylinositol-anchored proteins. The actual composition is highly heterogeneous, depending not only on the cell type and the state of the cell. Additionally, the presence of multiple mechanisms of exosome formation in one cell indicates an even higher variance. [90] [89] [68, 91, 92]

Tetraspanins

Tetraspanins are a family of transmembrane proteins, all of which share three essential features: (I) The four transmembrane domains, eponymous for the protein family. (II) The C- and N-terminal domains, which are short intracellular regions. (III) Two extracellular loops, that can be distinguished according to their size in a small and a large one. There are 33 known members of the tetraspanin family, including the markers CD9, CD63, and CD81, in the following referred to as TSPNs (often reported to be exosomal). [93] Most current analysis and characterization methods of extracellular vesicles rely heavily on these exosomal makers. [94] However, they are not expressed by all exosomes. Together with other markers like Alix, Flotillin, and Tsg101, the tetraspanins reveal the existence of exosomes – constantly ubiquitous makers are searched to get a more reliable overview. [95]

A comparison of TSPN expression on the surface of exosomes and in the cells of origin was performed. It has been demonstrated that if the expression of a specific TSPN is high for a specific cell type, these release vesicles also carry this protein with high abundance. This indicates that an enrichment based on the TSPN results in the negligence of EVs originating from cells with low expression levels. It has been shown that the TSPNs were enriched in the sEVs compared to the cells of origin, but they can also be found on the surface of other extracellular vesicle types, like microvesicles. [74]

CD9, motility-related protein 1, is involved in many cellular functions. As for other tetraspanins, CD9 contributes to motility, migration, proliferation, differentiation, and adhesion. [93]

CD63 is a reliable marker for extracellular vesicles and exosomes. The protein accumulates in the membrane of multivesicular bodies and is minimally expressed on the outer plasma membrane. CD63 is highly glycosylated and can be found in distinct tissues. Various interaction proteins, like CD82 and Major histocompatibility complex class 2 (MHCII) molecules, have been found. Due to the interaction with adaptor complexes and phosphatidylinositol 4-kinase an involvement in the protein-trafficking is hypothesized. [96–99]

CD81 is also described as Target for an Anti-Proliferative Antibody (TAPA1). The protein is widely expressed in various cell types and tissues and has been shown to form complexes with other tetraspanins, integrins, and immunoglobulins. [100]

Biogenesis

There are many reasons why a cell should expel substances into the surrounding extracellular space. On the one hand, degradation of all redundant components might be energy intensive and not always possible. On the other hand, the microenvironment of the cell can be adapted to the individual needs resulting in, e.g., cell or tissue growth, a defensive surrounding, or communication with other cells. [101]

Therefore, about 10 % of the human genome encodes proteins that get excreted by the cells into the extracellular environment. Deregulation of the underlying mechanisms often occurs under pathological conditions like cancer. There are different pathways of protein secretion: [102]

(I) The conventional secretory pathway or endoplasmic reticulum – Golgi secretory pathway: Here, proteins destined for secretion carry a signal peptide that initiates the sorting to the endoplasmic reticulum (ER). The protein gets shuttled via Coat Protein Complex II (COPII) coated vesicles to the Golgi apparatus. The proteins are transported within secretory vesicles from the Golgi apparatus to the cell membrane, where they fuse. The soluble cargo of the vesicle gets released into the extracellular space, whereas the membrane-bound constituents remain on the outer cell membrane. [103]

(II) Unconventional secretory pathways: This can be divided depending on if the secreted protein will be released into the extracellular space (a) or if it will stay encapsulated in a vesicular membrane (b) (see Figure 4).

(a) Proteins can be inserted into secretory lysosomes. The mechanism of translocation is still unclear, but when the lysosome fuses with the plasma membrane, soluble proteins get released. Further, a direct translocation of proteins from the cell membrane into the extracellular space has been reported. Another pathway enables proteins to be secreted independently from Golgi-apparatus. Proteins like HSP150 are packed into the ER, but the transfer to the cell surface is independent of Golgi-apparatus. The intraluminal vesicles that are formed are also COPII-coated; they fuse directly with the cell membrane and release the intraluminal cargo into the extracellular space. [103] [102]

    Another mechanism of trafficking proteins through the membrane is by pores. Since the mechanism has been shown for fibroblast growth factor 2, other proteins have shown a similar translocation mechanism. [104]

(b) The transfer via vesicle secretion – Many cytosolic substances like adenosine triphosphate function as a danger-associated molecular pattern in the extracellular space. Thus, the direct spillage of cytosol and its main constituents would lead to a severe condition for the surrounding tissue. Like in apoptosis, the way to securely secrete cytosolic components is to keep the enclosure intact and release them entrapped in vesicles. One option is the direct encapsulation on the outer cell membrane (Microvesicles); the other is described by a formation of vesicular structures within secretory lysosomes (Exosomes). [103, 105]

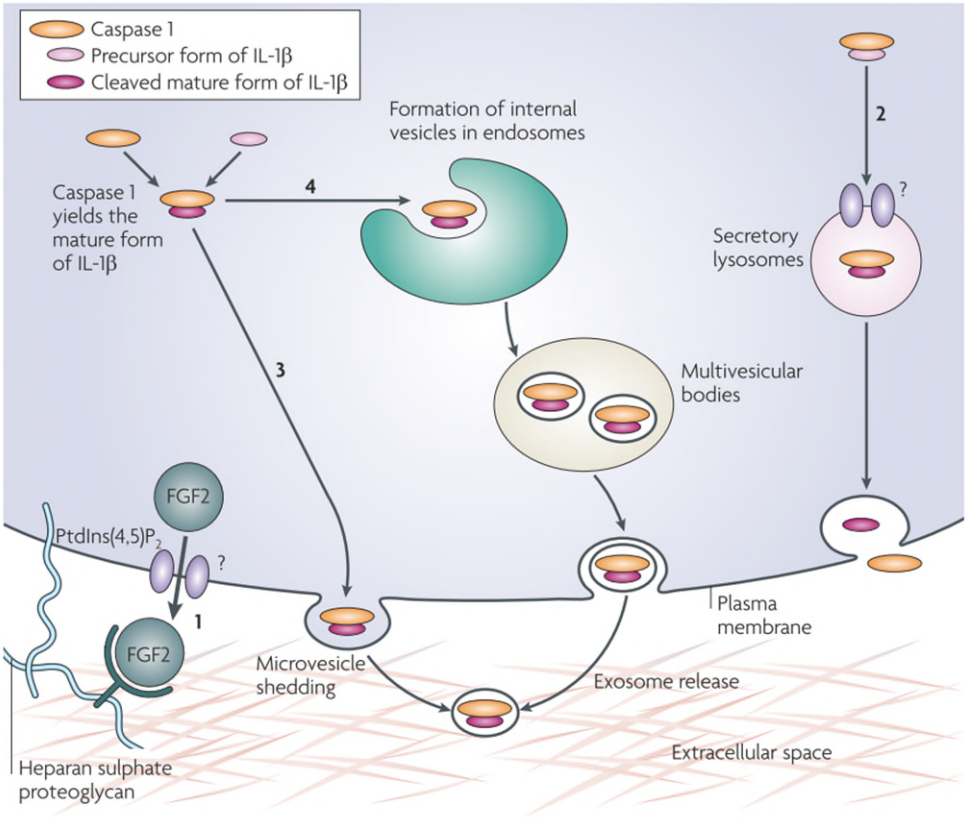

Figure 4 – Schematic overview of unconventional protein secretion exemplary for interleukin 1 beta (IL-1β) and fibroblast growth factor 2 (FGF2). Mechanisms 1 and 2 allow the direct release of free protein by pores (1) and by organelle fusion (2), whereas mechanisms 3 and 4 describe the vesicle secretion via microvesicle (3) and exosome (4) formation. [103]

In contrast to other extracellular vesicles, exosomes are formed in the endosomal compartment by inward budding of endosomal membrane forming multivesicular bodies (MVBs). MVBs are pre-lysosomal organs bound by a single outer membrane carrying multiple intraluminal vesicles (ILV). As such, MVBs can enter either the degradative pathway, where the luminal vesicles degrade by hydrolases or enter the secretory pathway by exocytosis. This process occurs through the fusion of the outer membrane of the MVBs with the plasma membrane – releasing the intraluminal vesicles into the extracellular space. [72, 78, 106, 107]

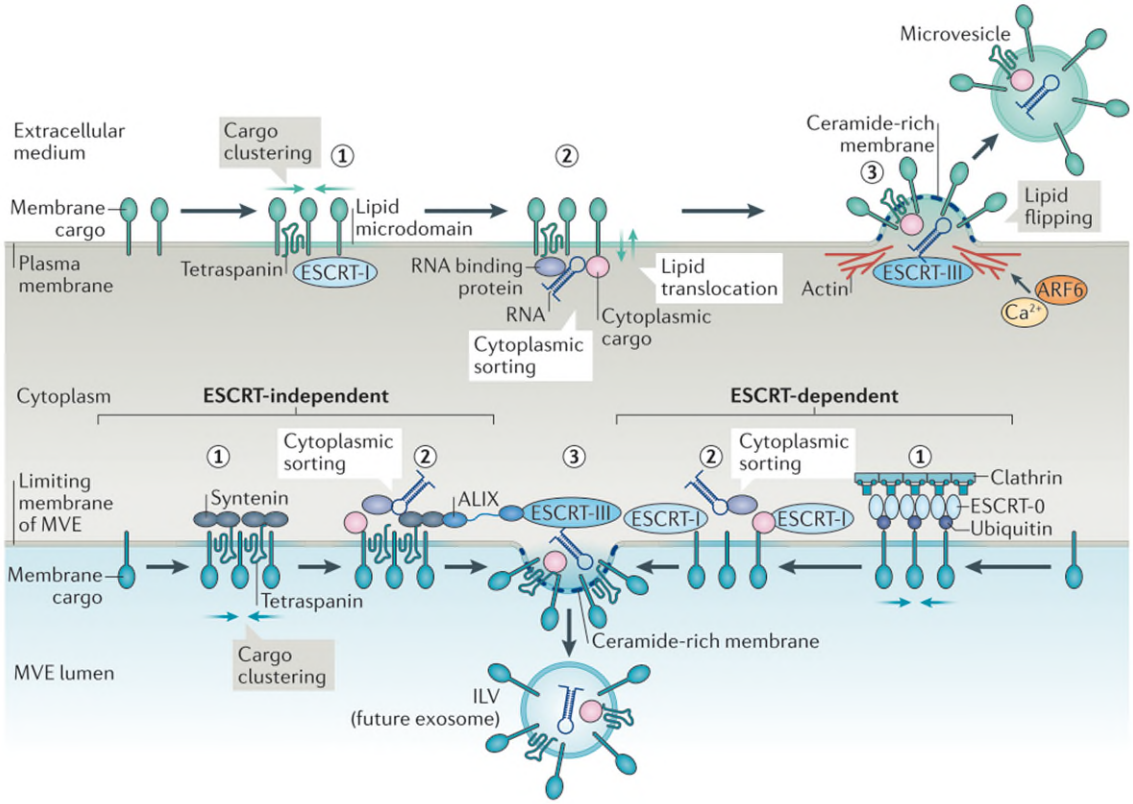

Figure 5 – Mechanisms of vesicle formation for microvesicles and intraluminal vesicles (ILVs) in an ESCRT-dependent and independent manner.[85]

As indicated in Figure 5 – Mechanisms of vesicle formation for microvesicles and intraluminal vesicles (ILVs) in an ESCRT-dependent and independent manner.[85] the ESCRT is deeply involved in loading, e.g., ubiquitinated membrane proteins into multivesicular bodies and exosome biogenesis. Therefore, exosomes carry proteins connected to the ESCRT machinery, like Tsg101, which has been proven to be ubiquitin-binding. Even though ubiquitinated proteins have been found in exosomes, it is hypothesized that the exosomal cargo gets de-ubiquitinated before vesicle formation. [102, 106] For specific cargoes like MHCII, a ubiquitin-independent sorting into the vesicles was described in antigen-presenting cells. Instead, the sorting is depended on CD9-containing membrane domains. For the recruitment of miRNA into exosomes released from human liver cells, the protein Alix is required. [108, 109]

A disruption of the ESCRT machinery does not stop the formation of MVBs and exosomes. Therefore, an ESCRT-independent pathway has been described that relies on sphingolipids, more specifically ceramides, which may promote vesicle formation due to its cone shape. A tetraspanin and ceramide-dependent packaging of the protein beta-

catenin and miRNAs has been reported. However, whether the ESCRT and the ceramide pathways are separated is still debatable, as they might also function in a single pathway. The exosomal excretion of Phospholipid Scramblase 3 (PLS3) and hepatitis virus RNA have been shown to rely on both ceramides and ESCRT. [110] [90] [108, 109]

Proteins from the Rab and Ral family are regulators of vesicular trafficking and are involved in exosome secretion. For example, MVBs require the presence of Rab27 to fuse to the plasma membrane and consequently for exosome release. Also, in oligodendrocytes, the recruitment of MVBs to the cell membrane is promoted by the presence of Rab35. At the same time, Ral1 seems to play a crucial role in the SNARE-related fusion of the MVB with the plasma membrane. The process of how the different players and hypothesized pathways interact, resulting in cargo recruitment and vesicle formation, is not yet fully understood. [80, 108, 109]

Function

After exosomes were thought to be part of a disposal system, it has been shown that they play a crucial role in intercellular communication. They are essential mediators under physiological and pathological conditions. [111]

As heterogeneous entities with a wide variety of cargo, exosomes are very versatile and have been researched for diverse functions. Physiologically, they have been shown to be involved in creating cell polarity during development. [112] Also, they appear to have immunogenic properties and can be involved in antigen presentation to immune effector cells. [113] In coagulation, platelets get activated, leading to increased secretion of exosomes and microvesicles, resulting in an enlargement of the surface for the prothrombinase complex. Exosomes are discussed to participate in inflammatory processes since they are also reported to incorporate prostaglandins. Furthermore, exosomes play a role in angiogenesis and cell death. During cell maturation, exosomes remove membrane-bound proteins and RNA and protein disposal, especially for cells that lack lysosomal degradation capabilities. Exosomes might also be involved in cell migration as they have been reported to transport chemo-attractant signals. [112] Also, exosomes are discussed to provide nutrients and signals, e.g., to sperms in the male and female

reproductive tract. Even a protective effect of EVs against Zika virus infections has been reported in seminal and saliva fluid. [114][115][68]

1.2.4. Limitations for using plasma sEV samples in clinical analysis

Since plasma EVs are influenced in quantity and composition by factors like age, sex, pregnancy, fasting, exercise, body mass index, and medication, there is a need to report the patient's status. This might also be why a biofluid sample's absolute amount of EVs was not yet connected to any disease. Besides the parameters that affect the patients' individual EV production and phenotype, there is a need to standardize the plasma collection, processing, and storage and the EV isolation procedure. The high abundance of potential biomarkers (e.g., RNA, protein) in cells or biofluids makes some assays susceptible to contamination. These contaminations might be brought in, but they can also originate from the non-sEV fraction of the sample itself. [116, 117]

The challenges of using plasma for sEV isolation have already been described; they might play a critical role in biomarker discovery. Due to the plasma composition, there is a high tendency to co-isolate lipoproteins, proteins, and protein aggregates found in high quantities in plasma. [118]

1.3. Aims

This work aims to identify isolation methods for sEVs originating from human plasma that show a high yield for EV markers and characteristics like particle concentration and size and a reduction of highly abundant proteins and lipoproteins from plasma, all evaluated based on multiple measurement techniques.

First, a broad range of isolation methods will be evaluated by the capability to be used in a clinical study analysis based on sEV yield and purity, throughput, and technical requirements. Also, the different characterization methods will be compared by their ability to detect and quantify EV markers and impurities and determine the particle size distribution and the concentration of the particles or EVs within the preparation.

Finally, in part one, three isolation methods will be chosen as superior and more thoroughly evaluated based on the analysis outcomes. Additionally, a toolbox for sEV characterization will be established, compared, and evaluated based on the specific readouts regarding their informative value and their advantages in biomarker analysis.

Second, the reproducibility of the chosen isolation methods will be evaluated. Five independent sEV isolations from one plasma pool, followed by EV characterization, should allow showing the variation brought in by the isolation method. For characterization, the streamlined workflow will be used to enable a comprehensive analysis of the single isolate.

One isolation method should be selected for further assessment in the third part of the experiment. Here, the method must prove if it can disclose the interindividual variation in sEV composition. As such, the method should be the best compromise between recovery and purity and adaptable to a wide variety of analytics. It should be capable of being used as a standard method for further experiments, followed by a flexible characterization workflow based on the needs of the individual scientific question.

In this part, the EV characterization methods should also reveal their advantages and disadvantages and can be compared in terms of their readout and informative value.

With this approach, this work aims to develop a robust technical basis for studying EV-based liquid biopsy strategies.

2. Materials & Methods

2.1. Equipment and software

2.1.1. *Table 1 – Chemicals and solutions*

Name	Item (#Cat)	Source (Manufacturer)
Dulbecco's Balanced Salt Solution (DPBS) (1X)	14190094	Gibco
Tween 20	P7949-100ML	Sigma-Aldrich
Fetal Bovine Serum (FBS), exosome-depleted	A2720801	Gibco
Triton X-100	BP151-100	Fisher Bioreagents
4x Laemmli Sample Buffer	1610747	Bio-Rad Laboratories
10x Tris/Glycine/SDS Buffer	1610772	Bio-Rad Laboratories
StartingBlock T20	WD322818	Thermo Scientific
20X Tris-buffered saline (TBS) Buffer	28358	Thermo Fisher Scientific
Blocker bovine serum albumin (BSA) in TBS (10X)	37520	Thermo Fisher Scientific
Development Substrate – Clarity Western ECL Substrate	170-5061	BioRad
SuperSignal Western Femto Maximum Sensitivity Substrate	34096	Thermo Scientific
Methanol for liquid chromatography LiChrosolv®	106018	Merck
Acetone ≥99,8%, SupraSolv®	1.00012.1000	Merck
Diluent 52	R52AA-1	MSD®
Diluent 53	R52AB-1	MSD®
MSD® Gold Read Buffer B	R60AM-1	MSD®
Diluent 100	R50AA-2	MSD®
1x TBS 1% Casein Blocker	1610782	BioRad

2.1.2. *Table 2 – Buffers*

Buffer/medium/solution	*Composition*
PBS-T	0.1% Tween 20 in DPBS
PBSF	2 % FBS in DPBS
Washing Buffer	25 mM Tris / HCl 150 mM sodium chloride (NaCl) Puffer 0.05% Tween 20, pH 7.5 + 1/100 Blocker BSA (10x)

2.2. Materials

2.2.1. Table 3 – Materials

Materials	Item (#Cat)	Source (Manufacturer)
Matrix 1,0 mL-Röhrchen mit Schraubverschluss	3740WHI	ThermoFisher Scientific
Eppendorf Conical Tubes 25 mL, snap cap	0030118405	Eppendorf
Protein LoBind Tubes 1.5 mL, snap cap	0030108442	Eppendorf
Microfuge Tube Polypropylene "Polyallomer "1.5 mL	357448	Beckman Coulter
Halt™ Protease Inhibitor Cocktail, Ethylenediaminetetraacetic acid (EDTA)-free (100X)	78425	ThermoFisher Scientific
Protein LoBind Conical Tubes 15 mL	0030122216	Eppendorf
Protein LoBind Tubes 5.0 mL	0030109302	Eppendorf
Microcentrifuge Tube 0.65 mL Prelubricated	3206	Costar
Thrombin	EXOQ5TM-1	System Biosciences
ExoQuick Ultra *ExoQuick Solution* *ExoQuick Buffer A* *ExoQuick Buffer B* *ExoQuick purification Columns*	EQULTRA-20A-1	System Biosciences
Protein LoBind Tube 2.0 mL Safe-Lock Tubes	022431102	Eppendorf
exoEasy Maxi Kit (20) *XE Buffer* *XBP Buffer* *XWP Buffer* *Collection Tubes (50 mL)* *Spin Column*	76064	Qiagen
Amicon Ultra – 0.5 mL Centrifugal Filter, 100 kDa Cutoff	UF510096	Merck Millipore
Exosome Isolation Kit Pan, human *Isolation Buffer* *Equilibration Buffer* *Exosome Isolation MicroBeads Pan, human*	130-110-912	Miltenyi Biotec
µColumns with plungers	130-110-905	Miltenyi Biotec
µ MACS MultiStand	130-042-303	Miltenyi Biotec
qEVsingle 35 nm	SP6	Izon
qEVsingle 70 nm	SP2	Izon
qEVoriginal Legacy 35 nm	SP5	Izon
qEVoriginal Legacy 70 nm	SP1	Izon
qEVoriginal 2. Generation 35 nm	ICO-35	Izon

qEVoriginal 2. Generation 70 nm	ICO-70	Izon
SmartSEC HT *SmartSEC Plate* *Collection plate* *Isolation Buffer*	SSEC096A-1	System Biosciences
ExoView Human Tetraspanin Plasma Kit *Incubation Buffer (10X)* *Solution A (10 X)* *Solution B (10X)* *Blocking Buffer* *Chips (16)* *Fluorescent labeled antibodies (Table 9)*	EV-TETRA-P	NanoView Biosciences
Nunc Zellkultur-Multischale, 24 wells	142475	ThermoFisher Scientific
Flat Tip Tweezer	72972-SP	Electron Microscopy Sciences
Strong Point Tweezer	16-100-124	FisherBrand
Fiber tip tweezer	78325-26	Electron Microscopy Sciences
96 Well Cell Culture Plate	3879	Costar
Criterion TGX Precast Gels, 26 Well comb, 15 µL, 1.0 mm	5671095	Bio-Rad Laboratories
Criterion TGX Stain-Free Precast Gels, 26 Well comb, 15 µL, 1.0 mm	5678095	Bio-Rad Laboratories
Trans-Blot Turbo, Midi Format, 0.2 µm PVDF Single Application	1704157	Bio-Rad Laboratories
Roller	1651279	Bio-Rad Laboratories
Development Folders	T2258	Applied Biosystems
Syringe 2 ml Inject Luer Solo	4606027	Braun
Nanosphere Size Standards (60 nm)	3060A	Thermo Fisher Scientific
Nanosphere Size Standard (100 nm)	3100A	Thermo Fisher Scientific
Nanosphere Size Standard (200 nm)	3200A	Thermo Fisher Scientific
Gold 96-well Streptavidin QuickPlex Plate	L55SA-2	*MSD®*
Round bottom plate	83.1837.500	*Sarstedt*

2.2.2. Antibodies

2.2.2.1. *Table 4 – Primary antibodies used in western blotting*

Antigen	Clone	Host species	Dilution	Source (Manufacturer)
GM130	EP892Y	Rabbit	1:500	Abcam
Calnexin	Polyclonal	Rabbit	1:1000	Abcam

Apolipoprotein A-I	EP1368Y	Rabbit	1:2000	Abcam
Apolipoprotein B	EPR2914	Rabbit	1:2000	Abcam
Flotillin 1	EPR6041	Rabbit	1:200	Abcam
CD9	HI9a	Mouse(/Biotin)	1:500	BioLegend
CD63	H5C6	Mouse(/Biotin)	1:500	BioLegend
TSG101	Polyclonal	Rabbit	1:500	Abcam
Albumin	15C7	Mouse	1:2000	Abcam

2.2.2.2. *Table 5 – Secondary Antibodies used in western blotting*

Host species	Target	Conjugate	Dilution	Cat. No.	Source (Manufacturer)
Mouse	Rabbit IgG	HRP	1:10000	211-032-171	Jackson Immuno Research
Goat	Mouse IgG	HRP	1:10000	715-035-150	Jackson Immuno Research
-	Biotin	Poly-HRP	1:10000	21140	Thermo Fisher Scientific

2.2.2.3. *Table 6 – Western Blot positive controls*

Name	Description	Catalog No.	Vendor	Dilution	Diluents
Cell Lysate Control	HEK-293 whole cell lysate	Ab7902	Abcam	1:40	Sample Buffer
	HeLa whole Cell lysate	Ab150035	Abcam	1:40	
Exo Standard	Exosome Standards Lyophilized exosomes from human plasma of healthy donors	HBM-PEP-100	HansaBioMed	1:30	Sample Buffer
Plasma Standard	Precleared human plasma pool	HMN623577-86 (pooled)	BioIVT	1:30	Sample Buffer

2.2.2.4. *Table 7 – Antibodies used in CellStream for single vesicle detection*

Antigen	Clone	Host species	Isotype	Source (Manufacturer)	Conjugate	Dilution
CD9	HI9a	Mouse	IgG1, κ	BioLegend	APC	1:160
CD63	H5C6	Mouse	IgG1, κ	BD Biosciences	Alexa Flour 647	1:40
CD81	JS-81	Mouse	IgG1, κ	BD Biosciences	APC	1:160
Isotype Control	MOPC-21	Mouse	IgG1, κ	BioLegend	APC	

2.2.2.5. *Table 8 – Capture antibodies included in the MACSPlex exosome human kit, Miltenyi*

Antigen	Isotype	Info
CD3	mIgG2a	
CD4	mIgG2a	
CD19	mIgG1	
CD8	mIgG2a	
HLA-DRDPDQ	recombinant human IgG1	MHC-class 2-complex
CD56	recombinant human IgG1	
CD105	recombinant human IgG1	
CD2	mIgG2b	
CD1c	mIgG2a	
CD25	mIgG1	
CD49e	recombinant human IgG1	
ROR1	mIgG1, κ	
CD209	mIgG1	
CD9	mIgG1	
SSEA-4	recombinant human IgG1	
HLA-ABC	recombinant human IgG1	MHC-class 1a-complex
CD63	mIgG1, κ	
CD40	mIgG1, κ	
CD62P	recombinant human IgG1	
CD11	mIgG2b	
CD81	recombinant human IgG1	
MCSP	mIgG1	
CD146	mIgG1	
CD41b	recombinant human IgG1	
CD41a	recombinant human IgG1	
CD24	mIgG1	
CD86	mIgG1	
CD44	mIgG1	
CD326	mIgG1	
CD133/1	mIgG1, κ	
CD29	mIgG1, κ	

CD69	mIgG1, κ
CD142	mIgG1, κ
CD45	mIgG2a
CD31	mIgG1
REA control	recombinant human IgG1
CD20	mIgG1
CD14	mIgG2a
mIgG1 control	mIgG1

2.2.2.6. *Table 9 – Capture and detection antibodies used in NanoView*

Antigen	Clone	Host species	Conjugate (Detection Ab)	Dilution	Source (Manufacturer)
CD9	HI9a	Mouse	Alexa Flour 488	1:1200	NanoView
CD63	H5C6	Mouse	Alexa Flour 647	1:1200	NanoView
CD81	JS-81	Mouse	Alexa Flour 555	1:1200	NanoView

2.2.2.7. *Table 10 – Devices*

Type	Name	Manufacturer
Centrifuge	Centrifuge 5424 R	Eppendorf
Shaker	ThermoMixer C (5382000015) SmartBlock Plate SmartBlock 2 mL SmartBlock 1.5 mL SmartBlock 0.5 mL	Eppendorf
Ultracentrifuge	Sorvall WX Ultra 80 Centrifuge	Thermo Scientific
Rotor	Kontron TFT 45.94 fix Angle	Kontron HermLe
Rotor Adapter	Adaptor for 4 Eppendorf 'Safe-Lock' or Beckman 'Microfuge' Polyallomer tubes each 1,5 mL, angle 45°	Beranek Laborgeräte
Rotator	Rotator SB2	Stuard
Centrifuge	Centrifuge 6910 R	Eppendorf
Rotor	S-4xUniversal Swing Bucket Rotor	Eppendorf
SEC Fraction Collector	Automated Fraction Collector	Izon
Centrifuge	Centrifuge 5810 R	Eppendorf
Rotor	Rotor A-2-DWP-AT (Swing Bucket)	Eppendorf
ExoView	ExoView R 100	NanoView

CellStream *488 nm Laser (200 mW)* *405 nm Laser (175 mW)* *642 nm Laser (150 mW)*	Amnis CellStream Flow Cytometer CS-100196 CS-200405 CS-200642	Luminex
Criterion Cell	1656001	Bio-Rad Laboratories
Power Supply	Model 1000/500 Power Supply	Bio-Rad Laboratories
Transfer System	Trans-Blot Turbo Transfer System	Bio-Rad Laboratories
Rocking table Kick II	Z640859	Sigma Aldrich
Two staged rocking platform	444-0145	VWR
ChemiDoc Touch Imaging System	17001401	Bio-Rad Laboratories
SpectraMax M2	M2	Molecular Devices
Exoid™	Exoid™	Izon
MACSQuant	MACSQuant 16	Miltenyi
MESO QuickPlex	SQ 120MM	Meso Scale Diagnostics
BioTek Washer	ELx405TS	Agilent
Centrifuge	Heraeus Pico 17 Centrifuge	Thermo Scientific

2.2.3. *Table 11 – Software*

Software	**Developer**
Image Lab 6.0	Bio-Rad Laboratories
ChemiDoc	Bio-Rad Laboratories
NanoViewer 3.1	Unchained Lab
NanoView Scanner 3.1	Unchained Lab
CellStream 1.3.384	Luminex
CellStream Analysis 1.3.384	Luminex
SoftMax Pro 5.4	Molecular Devices
Prism 9.1.0 (221)	GraphPad
Discovery Workbench 4.0	MSD®
NTA 3.4	Malvern Pananalytical
Excel Version 2209	Microsoft
Exoid™ Control Suite	IZON
MACSQuantify 2.13.3	Miltenyi

2.3. Methods

2.3.1. Plasma preparation

For the following experiments, commercial plasma was used individually and pooled. The individual samples were purchased from BioIVT, following data was provided by the company (Table 12):

Table 12 – Sample and donor information given by the vendor (BioIVT)

Sample ID	Lot#	Gender	Age	Ethnics	Collection date
IND01	HMN623577	Male	24	Hispanic	14. Mai 21
IND02	HMN623578	Male	25	Hispanic	15. Mai 21
IND03	HMN623579	Male	26	Hispanic	14. Mai 21
IND04	HMN623580	Male	30	Hispanic	06. Mai 21
IND05	HMN623581	Male	35	Hispanic	07. Mai 21
IND06	HMN623582	Male	51	Hispanic	05. Mai 21
IND07	HMN623583	Male	36	Hispanic	06. Mai 21
IND08	HMN623584	Female	55	Hispanic	06. Mai 21
IND09	HMN623585	Female	37	Hispanic	14. Mai 21
IND10	HMN623586	Female	27	Hispanic	15. Mai 21

All ten healthy human K3EDTA plasma samples (IND01-10) were thawed at room temperature and vortexed. Each individual sample was aliquoted into 96 1 mL matrix tubes, 750 µL each. 20 mL of the remaining sample was then merged to a total volume of 200 mL. The pooled plasma was aliquoted with 750 µL into 192 1 mL matrix tubes. The leftovers for each individual and the pooled plasma were transferred to a 25 mL Eppendorf tube. All the aliquots were stored at -80 °C until further use.

2.3.2. Plasma Preclearing

Before each isolation of EVs a pre-clearing step of the plasma was performed. The frozen plasma samples were thawed on the bench at room temperature until the samples were completely liquid. The samples were transferred to a centrifugation tube and centrifuged for 20 min at 4 °C with 2,000 x g. The supernatant was then

transferred to a fresh centrifugation tube, avoiding transferring the floating cloudiness, followed by a second centrifugation step at 10,000 x g and 4 °C for 30 min. The supernatants were collected and merged into a fresh 25 mL snap cap tube. The merged sample was vortexed and aliquoted according to the requirements of the isolation methods to 1.5 mL tubes. The aliquoted precleared plasma samples were stored at -80 °C until characterization or sEV isolation. In the following, the precleared plasma pool will be referred to as Plasma pool.

2.3.3. EV isolation methods

2.3.3.1. Ultracentrifugation

500 µL aliquots of precleared plasma were thawed at room temperature and mixed with the same volume of DPBS. The diluted samples were ultracentrifuged over night at 4 °C with ~100.000 x g [Sorvall WV Ultra 80 Centrifuge, Thermo Scientific] using an Adaptor for 1.5 mL Microfuge tubes, Kontron TFT 45.94 Fixed Angle, maximum of 106,500 x g. The pellet was resuspended in DPBS and on the shaker for 10 min at 2.000 rpm at 4 °C. A second ultracentrifugation washing step was performed and with ~100.000 x g at 4 °C for 3 h. Again, the supernatant was collected in a 15 mL tube and the pellet was resuspended in 100 µL of protease-/phosphatase inhibitor containing DPBS. For part 1, all samples were merged in a 5 mL tube and vortexed. All samples were aliquoted in 100 µL into 500 µL tubes. The aliquoted UC isolates were stored at -80 °C until characterization.

2.3.3.2. Precipitation – ExoQuick

The ExoQuick Ultra kit was used to isolate EVs according to the manufacturer's instructions. For this, 600 µL aliquots of the precleared plasma pool samples were thawed at room temperature. To each aliquot 4.8 µL of 611 U/mL Thrombin was added to obtain a 5 U/mL dilution. After 5 min on a spin rotor at room temperature the samples were centrifuged for 5 min with 10.000 x g at room temperature. 500 µL of supernatant was transferred to a fresh sample tube and 134 µL of ExoQuick solution was added. The tubes were repeatedly inverted and incubated at 4 °C for 30 min. The samples were centrifuged for 30 min at 4 °C with 3.000 x g and the supernatants were

separated and merged in a 15 mL tube. The pellet was resuspended in 200 µL of ExoQuick Buffer B and diluted in 200 µL of ExoQuick Buffer A. The ExoQuick purification columns were decapped and centrifuged (1.000 x g, 30 sec, RT, [Centrifuge 5424 R, Eppendorf]) to wash away the storage buffer. Two additional washing steps were performed with 500 µL of Buffer B followed by centrifugation (1.000 x g, 30 sec, RT, [Centrifuge 5424 R, Eppendorf]). For each wash the flowthrough was discarded. Then, the columns were capped at the bottom and 100 µL of Buffer B was added before the EV containing pellet resuspension was pipetted on the resin. The top cap was closed, and the columns were placed on the spin rotor at room temperature for 5 min. After removing the caps, the column was placed in a 2 mL tube and again centrifuged (1.000 x g, 30 sec, RT, [Centrifuge 5424 R, Eppendorf]) to obtain the EV isolate. The samples from were merged and protease-/phosphatase inhibitor solution was added to all samples. The samples were then aliquoted to 500 µL tubes and stored together with the supernatant at -80 °C until further characterization.

2.3.3.3. ExoEasy

The ExoEasy Maxi Kit was used to isolate EVs from precleared human plasma by membrane affinity. The plasma pool aliquots were thawed at room temperature, and the same volume of XBP Buffer was added to the sample. The tubes were inverted a few times and transferred to an ExoEasy spin column placed in a Collection tube. The columns were centrifuged with 500 x g at RT for 1 min [Centrifugation 5910 R, Eppendorf, S-4xUniversal Swing Bucket Rotor]. The flowthroughs were collected and merged in a 15 mL tube. 10 mL of XWP Buffer was added to the columns, followed by another centrifugation (500 x g, 5 min, RT [Centrifugation 5910 R, Eppendorf, S-4xUniversal Swing Bucket Rotor]). The flowthrough was discarded, and the column was placed in a fresh collection tube. 400 µL of XE Buffer was pipetted on the column before incubation for 1 min at RT. The sample was collected by centrifugation (500 x g, 5 min, RT [Centrifugation 5910 R, Eppendorf, S-4xUniversal Swing Bucket Rotor]) and re-applied to the column. After a second collection run, the buffer was exchanged to avoid the high salt concentration in the XE buffer for the EV characterization. For that, a 500 µL Amicon filter with a 100 kDa cutoff was placed in a centrifuge tube and

washed with 500 µL of DPBS, centrifuging with 14.000 x g for 20 min at RT [Centrifuge 5424 R, Eppendorf]. The flowthrough was discarded and the ExoEasy samples were pipetted on top of the Amicon filter. Another centrifugation run was performed followed by three washing steps with 500 µL of DPBS. The initial sample volume of 500 µL of protease-/phosphatase inhibitor solution containing DPBS was added to the filters and the filter was vortexed. After that the filter was placed upside down in a fresh Collection tube and centrifuged for 2 min, at 1.000 x g [Centrifuge 5424 R, Eppendorf] to collect the samples which were then merged. All samples were and aliquoted to100 µL in 500 µL tubes and stored at -80 °C.

2.3.3.4. Immuno-affinity capture

According to the manual of the Exosome Isolation Kit Pan, human, (Miltenyi Biotec) 500 µL of precleared plasma were thawed at room temperature. 50 µL of Exosome Isolation MicroBeads Pan, Human (anti-CD9, anti-CD63, anti-CD81) were added and incubated at room temperature for 1 h. The µColumns were placed on the magnet column holder, 100 µL of Equilibration Buffer was pipetted on the column, and it was rinsed three times with 200 µL of Isolation Buffer. The total volume of bead containing plasma was pipetted on the column and left to run through. The flowthrough was collected and merged in a 15 mL tube. Three more washing steps with 200 µL of Isolation Buffer were performed. After removing the µColumn from the magnetic column holder 100 µL of protease-/phosphatase inhibitor containing DPBS was added and the plunger was pushed into the column. The isolate was collected in 1.5 mL tubes before they were merged in a 5 mL tube. The samples were vortexed and aliquoted into 500 µL tubes to 100 µL each using a stepper pipette. The aliquoted samples and the flowthrough were stored at -80 °C until further characterization.

2.3.3.5. Size Exclusion Chromatography

qEVoriginal (Legacy/2. Generation) (35/70)

The thawed plasma samples were vortex and the SEC columns (qEVoriginal Legacy 35, qEVoriginal Legacy 70, qEVoriginal 2. Generation 35, qEVoriginal 2. Generation 70) were placed outside the fridge in an upright position to equilibrate to room

temperature. After the columns were placed in the SEC column rack the storage buffer was running through the column until the liquid surface reached the filter frit. A minimum of 10 mL of DPBS was used to flush the column before 500 µL of sample were pipetted to the frit. The void volume of 2.3 mL passed the column when the sample collection started. One EV containing fraction of 1.5 mL was collected in a 2 mL tube. 100X protease-/phosphatase inhibitor was added. The sample in part 1 – were merged. In all parts the sEV preparation was then aliquoted to 500 µL tubes which were then stored at -80 °C.

qEVsingle (35 Tween/35/70)

The precleared plasma pool was thawed at room temperature. The qEVsingle size exclusion columns were removed from 4 °C and equilibrated to room temperature. After removing the top and bottom caps, the columns (qEVsingle 35, qEVsingle 70) were placed upright into the SEC fraction collector. After the storage buffer ran to the filter, a minimum of 5 mL of DPBS was used to flush the SEC column before the sample application. 150 µL of precleared plasma was added once the buffer level reached the filter. 850 µL of DPBS was then added to collect a total void volume of 1 mL. Afterward, two 200 µL factions were collected in 1.5 mL tubes. The two fractions from all preparations were merged, and 100X protease-/phosphatase inhibitors was added before the EV preparation was vortexed, aliquoted to 100 µL in 500 µL tubes and stored at -80 °C for further characterization. For the implementation of the "qEVsingle 35 Tween" protocol PBS-T was used for rinsing, void, and sample collection.

SmartSEC

The precleared plasma pool samples were thawed at room temperature. The SmartSEC HT plate was removed from the plastic wrap and inverted about ten times before it was taped to the bench bottom down for the resin to settle. The bottom mat was removed before the SmartSEC HT plate was placed on a collection plate. After removing the top mat, the two plates were centrifuged at 500 x g for 1 min at room temperature [Centrifuge 5810 R, Eppendorf, Rotor: A-2-DWP-AT (Swing Bucket)]. The storage buffer was discarded from the collection plate, and the plate stack was

reassembled. 500 µL of SmartSEC Isolation Buffer was added per well, followed by second centrifugation to wash the columns. After a new collection plate was used to reassemble the plate stack, 500 µL of the sample was added to each well and was incubated on the column plate for 30 min at room temperature with a sealed SmartSEC plate to avoid contaminations. The stack was then centrifuged for 2 min with 500 x g at room temperature [Centrifuge 5810 R, Eppendorf, Rotor: A-2-DWP-AT (Swing Bucket)]. The flowthrough was collected and, for part 1 merged in a 5 mL tube. 500 µL of Isolation Buffer was added to each well after the stack has been reassembled with a new collection plate. To the EV preparation protease-/phosphatase inhibitor was added before the samples were vortexed. Both fractions were aliquoted to 500 µL tubes and stored at -80 °C until further characterization.

2.3.4. EV characterization methods

2.3.4.1. NanoView

For NanoView analysis the ExoView Human Tetraspanin Plasma Kit (NanoView Biosciences) was used. Prior to the experiment, the Incubation Buffer concentrate (10X) was diluted with Milli-Q water.

The samples were thawed and diluted according to Table 13 and incubated in Incubation Buffer (1X); for that, the samples (50 µL) were pipetted on the surface of the chips which were placed in the inner 8 wells of a 24-well plate. During the whole experiment, the chips were positioned so that the markings on the chips were facing upward and the wells did not touch the walls of the wells. To avoid scratching of the chips they were moved using a fiber tip tweezer. Only the eight inner wells were used whereas the outer wells and the space in between the wells were filled, each with 750 µL of Milli-Q water, to avoid evaporation of the sample. The lid was placed on top of the plate and covered with aluminum foil. The incubation was performed overnight at RT on the bench. After the incubation, 1 mL of Solution A was added into each well and the 24-well plate was then incubated on a shaker for 3 min at RT and 400 rpm. The chips were washed another two times with 750 µL of Solution A, where it was necessary to leave 250 µL on the chips after each washing step to avoid drying of the

chip. The same volumes of Blocking Buffer and Solution A were mixed, and the fluorescent-labeled antibodies included in the kit were added to obtain a dilution factor of 600. 750 µL of buffer was removed from each chip containing well, leaving approx. 250 µL of buffer in each well. 250 µL of antibody dilution were then added for a final staining dilution of 1200. The antibodies were left to incubate on the chips for 1 h, at room temperature again with the plate covered with aluminum foil to avoid the bleaching of the fluorophore. The wells were replenished to the initial volume of 1 mL with Solution A. Directly, 750 µL were removed from each well and replaced with fresh Solution A before the plate was placed on the shaker (400 rpm, RT, 3 min) again. The next washing step was performed, removing 750 µL from each well and replacing them with the same volume of Solution B. The plate was then put on the shaker for 3 min at RT with 400 rpm. This washing procedure was performed three times followed by another wash were Milli-Q water was used instead of Solution B. The chips were then transferred to a petri dish filled with Milli-Q water and from there to the petri dish lid, which was filled with Milli-Q water as well using a flat-tip tweezer. To avoid the drying of the chips during the transfer, the chips were kept horizontally. After the chips were washed in both dishes moving the chips vertically and horizontally, the strong point tweezers were used to slowly take the chips out of the petri dish in a 45 ° angle. The surface tension of the water has dried the surface of the chips immediately. The chips were then placed on the chip rack of the ExoView instrument and measured.

Table 13 – Dilution factor for NanoView assay.

Sample	NanoView dilution factor
Plasma pool	50
qEVsingle 35 Tween	5
qEVsingle 35	5
qEVoriginal 35	5
qEVoriginal 35 2GEN	5
qEVsingle 70	5
qEVoriginal 70	5
qEVoriginal 70 2GEN	5
ExoQuick	5
ExoEasy	5
Ultracentrifugation	10
SmartSEC	10

2.3.4.2.Flow cytometry – CellStream

The samples and the exosome-depleted fetal bovine serum (FBS) were thawed at RT. FBS was added to DPBS to obtain a 2 % dilution (PBSF). Antibodies were centrifuged [Centrifuge 5424 R, Eppendorf] at 4 °C for 5 min with 14.000 x g. The antibodies were then diluted in PBSF according to Tables 7. The same volumes of samples and antibodies were then pipetted to each assay plate well. The incubation was performed on a ThermoMixer C for 40 min at 37 °C at 400 rpm. To prepare a lysis control buffer PBSF was used to dilute Triton X-100 to a final concentration of 0.2 %. After antibody staining the sample was diluted 10-fold either with PBSF or Triton X-100 containing PBSF and was again incubated at 37 °C for 30 min at 400 rpm on the ThermoMixer C. 10 µL of sample from each well were then directly measured on the CellStream instrument in the small particle mode and with low flow rate (3.66 µL/min).

Table 14 – Luminex CellStream laser settings.

Laser	Intensity [%]
Side Scatter	20
Forward Scatter	10
647	100
488	100
405	100

2.3.4.3.Western Blotting

The samples were thawed and diluted in DPBS and sample buffer (4X) to normalize for plasma input or protein concentration. The centrifugation tubes were then transferred to the preheated ThermoMixer C and heated for 10 min at 70 °C and 800 rpm. The gels (either Criterion TGX Precast Gel or Criterion TGX Stain-Free) were unpacked, and the comb and adhesive strip removed. The gels were then gently washed with Milli-Q water before they were placed in the electrophoresis cell and covered with previously prepared running buffer. A 300 µL Eppendorf pipette was used to rinse the wells of the gel to avoid the rising of air bubbles during sample loading. 10 µL of the diluted sample, positive control, and 4 µL of protein ladder were loaded to the gel before the chamber was closed and connected to the power supply. The gels were run at 120-150 Volt for roughly 1:20 h. The gel box was then removed from the chamber and opened to take out the gel. The first part of the semi-dry PVDF membrane stack was placed in the transfer system cassette, followed by the gel. To avoid air bubbles, the gel was gently rolled out before the second part of the membrane stack was placed on top followed by another step of air bubble removal. The transfer system was used [Mixed Molecular weight, 2.5 A, 25 V, 7 min] to blot the protein to the membrane. The PVDF membrane was taken and transferred to a prepared MilliQ-water-containing membrane cassette. After making sure that no gel parts remained on the membrane, it was transferred to a blocking buffer-containing membrane cassette. After overnight incubation at 4 °C or 1 h at RT on a rocker, the blocking buffer was decanted and replaced by a blocking buffer containing primary antibody (Table 4).

Primary antibody incubation was performed overnight at 4 °C on a rocker. Using a Tween 20 and BSA containing washing buffer, the membranes were washed three times for 10 min at RT on a rocker. The secondary antibody (Table 5) was diluted 10.000-fold in washing buffer and incubated for one hour at RT on the membrane, followed by three more washing steps. The development substrate (Femto) was prepared right before the incubation of the membrane for 5 min at RT in the dark. The membrane was transferred to a development folder and measured on the ChemiDoc Imager:

First, a colorimetric image was taken for faint band visualization before the chemiluminescence 3x3 images were taken. Six images were recorded starting from 10 sec to 120 sec in "Configure Signal Accumulation Mode."

2.3.4.3.1. Fixation Protocol A (FixA)

The fixation of the proteins on the PVDF membrane was performed during the Western Blot protocol right after the semi-dry blotting of the proteins. Instead of directly transferring the blot to the blocking buffer, it was placed in an acetone-resistant plastic box placed on ice filled with precooled acetone. The membrane was incubated for 30 min while gentle shaking on a rocker. The acetone-treated membrane was then dried on air for a few seconds. For rehydration, the PVDF membrane was transferred to a 50 % methanol-water-mixture before the western blot protocol was continued with blocking the membrane.

2.3.4.3.2. Fixation Protocol B (FixB)

For fixation protocol B the steps of fixation protocol A are followed. After the rehydration of the membrane in a 50 % methanol-water mixture, it was transferred to a pneumatic trough placed on a hot plate and filled with DPBS. A thermometer and a magnetic stirrer were placed in the DPBS. For 30 min, the DPBS was kept at 50 °C and gently stirred while the membrane floated upside down on the surface. The membrane was then quickly transferred to the blocking buffer to prevent drying, and the western blot protocol was continued.

2.3.4.4.MSD® TSPN (CD9/CD63/CD81) ECL

The relative quantification of the tetraspanins, as well as the colocalization, was performed in an Electrochemiluminescence (ECL) assay. Thus, the assay format was symmetric, meaning that the capture and detection antibody used was the exact clone, binding to the same epitope. In the case of the colocalization analysis, different target proteins were bound by capture and detection antibodies (e.g., CD9 (Capture) and CD63 (Detection)). Therefore, the assay should not detect single molecules but only physically connected molecules by, e.g., membrane. For this experiment, the MSD® assay plate was first blocked with 150 µL of 1% casein-blocking buffer for 1 h at room temperature. Afterward, the blocking buffer was discarded, and the plate was washed three times using a Biotek washer (TTBS, 150 µ). The biotinylated antibody was diluted in Diluent 100 1/30, and 50 µL was added to each well and left to incubate for 1 h at room temperature while shaking with 700 rpm. After three steps of washing with TTBS, the samples and calibrators diluted in assay Diluent 52 were prepared. 25 µL of the same assay diluent were pipetted to each well, followed by 25 µL of the diluted sample (Table 15) and calibrator. The plate was sealed with an adhesive strip and incubated for 1 h at room temperature on a shaker set to 700 rpm. Three washing steps were performed, and the detection antibody was diluted 100-fold in antibody Diluent 53. 25 µL of the diluted antibody were pipetted to each well before the plate was sealed and incubated for again 1 h at RT with 700 rpm. After another three-fold wash, the wells were filled with 150 µL of Read Buffer and analyzed on the MSD® Quickplex instrument.

Table 15 – Dilution factor for human TSPN (CD9/CD63/CD81) ECL

Sample	CD9 ECL dilution factor	CD63 ECL dilution factor	CD81 ECL dilution factor
Plasma pool	32	2	2
qEVsingle 35 Tween	8	2	2
qEVsingle 35	4	2	2
qEVoriginal 35	8	2	2
qEVoriginal 35 2GEN	8	2	2
qEVsingle 70	2	1	1
qEVoriginal 70	2	1	2
qEVoriginal 70 2GEN	2	2	2
ExoQuick	2	2	2
ExoEasy	8	2	2
Ultracentrifugation	16	2	2
SmartSEC	16	2	2

2.3.4.5.Apolipoprotein A1 and Apolipoprotein B100 ELISA

For the detection of Apolipoprotein A1 and B100 (ApoA1, ApoB100), ELISA kits were used. All included reagents were left on the bench to adapt to room temperature, excluding TMB, which was used cold later in the assay. The reagents were diluted in MilliQ-water as indicated by the manufacturer to obtain working solutions. The samples were diluted to the required dilutions using the Apo ELISA Buffer (Table 15). A pre-dilution in Triton-X 100 was performed in the case of the ApoB100. Each well of the plate was filled with 300 µL of washing buffer and aspirated again. This procedure was repeated 5 times in total for one washing circle. 100 µL of diluted sample and standard were then transferred to the wells, and the plate was covered with an adhesive strip. The plate was incubated for 2 h at room temperature or 4 °C overnight. At the end of the incubation, the Detection Antibody was diluted in Apo ELISA Buffer 2000-fold before 100 µL were pipetted to each well of the plate. The plate was covered with an adhesive strip and left at room temperature for 1 h for incubation. After another 5 washing steps, 100 µL of the

Streptavidin-HRP – diluted 1:1000 in Streptavidin-HRP diluent – was added. 100 µL of TMB was added after another 5 washes and after 15 min of incubation at room temperature in the dark 100 µL of stop dilution was added and the plate was measured in the microplate reader at a wavelength of 450 and 570 nm.

Table 16 – Dilution factors for human apolipoprotein A1 and apolipoprotein B100 ELISA.

Sample	ApoA1 ELISA dilution factor	ApoB100 ELISA dilution factor
Plasma pool	200000	5000
qEVsingle 35 Tween	10	200
qEVsingle 35	100	100
qEVoriginal 35	100	100
qEVoriginal 35 2GEN	100	100
qEVsingle 70	10	10
qEVoriginal 70	10	10
qEVoriginal 70 2Gen	100	10
ExoQuick	100	10
ExoEasy	1000	100
Miltenyi Pan Bead	1000	10
Ultracentrifugation	5000	10
SmartSEC	1000	500

2.3.4.6.Human IgG and human Albumin ELISA

All reagents within the kit except the TMB were removed from the refrigerator and left to adapt to room temperature. The washing buffer (25X) was diluted with MilliQ water, whereas the Biotin-Antibody (100X) and the HRP-Avidin (100X) were diluted in the belonging buffers. The standard was centrifuged with 10.000 rpm at RT. The sample diluent was mixed with 10X Blocker BSA before the samples and standards were diluted as required (Table 17). 100 µL of standards and samples were transferred in duplicates to the plate. The plate was covered with an adhesive foil and left at 37 °C for 2 h on the ThermoMixer C. Each well was aspirated, and 100 µL of prediluted Biotin-antibody (1X) was added, followed by another sealing and incubation for 1 h at 37 °C. After the incubation, the plate was mixed manually, followed by three washing steps with 200 µL of Washing Buffer each. After the last washing buffer was aspirated, the plate was blotted on a paper towel to remove the leftover buffer. 100 µL of HRP-Avidin solution was added, and another 1-hour incubation at 37 °C. Five washing steps were performed before adding 100 µL of cold TMB Substrate. Sealed and protected from light, the plates were

left to incubate at 37 °C for 30 min. 50 µL of stop solution was added to each well, and the measurement took place with a SpectraMax M5 at a wavelength of 570 and 450 nm.

Table 17 – Dilution factor for human IgG and human albumin ELISA.

Sample	IgG ELISA dilution factor	Albumin ELISA dilution factor
Plasma pool	2500000	2500000
qEVsingle 35 Tween	250	100
qEVsingle 35	250	100
qEVoriginal 35	250	100
qEVoriginal 35 2GEN	250	100
qEVsingle 70	10	10
qEVoriginal 70	10	10
qEVoriginal 70 2GEN	10	10
ExoQuick	1000	1000
ExoEasy	10000	5000
Miltenyi Pan Bead	1000	1000
Ultracentrifugation	50000	5000
SmartSEC	500000	50000

2.3.4.7.Bead-based flow cytometry – MACSPlex Exosome Kit

For the MACSPlex assay the 1.5 mL tube protocol was used. 120 µL of buffer, plasma pool, and EV isolations from human plasma were used undiluted. The MACSPlex capture beads were vortexed for more than 30 seconds before 15 µL were added to each tube. An overnight incubation was performed while gently shaking the sample on the rocker, protected from light. After the incubation a washing step was performed. For that, 500 µL of MACSPlex Buffer was added and the sample was centrifuged [Heraeus Pico 17 Centrifuge, Thermo Scientific] at 3.000 x g for 5 min. 500 µL of supernatant were aspirated before 15 µL of the detection antibody mix (CD9/CD63/CD81 – APC labeled) were added. Another incubation step was performed for 1 h on the rocker. Two further washing steps were performed by adding 500 µL of MACSPlex Buffer, centrifugating (3.000 x g for 5 minutes), and aspirating the supernatant. During the second washing step the sample was again incubated for 15 min after adding the MACSPlex Buffer. The residual volume (~130 µL) was resuspended and transferred to a 96-well round bottom plate before the measurement with the MACSQuant Analyzer.

2.3.4.8.Tunable Resistive Pulse Sensing– Exoid™

For the instrument setup the nanopore (NP80) was installed and wetted using the wetting solution followed by the wetting program. The upper and bottom chamber were cleaned properly by removing the wetting solution first and take up the remnant solution with a lint free tissue. After reinstalling the nanopore 75 µL of measurement electrolyte solution was added at the bottom and 35 µL to the top chamber. Again, the solution was removed, and same volumes of blocking solution were added to both chambers and the coating procedure was performed. After removing the blocking solution, top and bottom chamber were again filled with measurement electrolyte and optimization was performed. Calibration particles were added to the top chamber as the electrolyte solution was removed. These 60 nm particles with a known concentration were measured diluted 4.000-fold in measurement electrolyte solution using a pore stretch of 47 mm, and measurement pressures of 550, 750, and 1150 Pa as well as a potential difference of 600 mV. After another cleaning step the analysis of the samples was performed, if possible, with the same instrument settings. The dilution of the samples in 2X PBS was optimized to have 500 to 2.000 particles measured per minute (Table 18). If the settings were changed for sample measurement the calibration beads were measured with the adapted settings again to assure that for each instrument setting a corresponding calibration run was performed.

Table 18 – Sample dilution and instrument settings for Exoid™ particle size and concentration measurement.

Sample	***Dilution factor***	***Pressure 1 [Pa]***	***Pressure 2 [Pa]***	***Pressure 3 [Pa]***	***Electric tension [mV]***	***Stretch [mm]***
ExoQuick	2	1800	2000	2400	450	47
SmartSEC	100	550	750	1150	450	47
ExoEasy	2	550	750	1150	450	47
Ultracentrifugation	4	300	500	900	250	50
qEVsingle 70	2	1300	1500	1900	450	47
qEVsingle 35	10	550	750	1150	600	47
qEVsingle 35 Tween	10	550	750	1150	600	47
qEVoriginal 70	2	550	750	1150	600	47
qEVoriginal 35	5	550	750	1150	600	47
qEVoriginal 70 2GEN	10	550	750	1150	600	47
qEVoriginal 35 2GEN	10	550	750	1150	600	47
Plasma pool	100	550	750	1150	600	47

2.3.4.9.Total protein – BCA

The samples were thawed at room temperature and vortexed properly. The BSA standard with a concentration of 2 mg/mL was diluted in a dilution series ten times according to Table 19. The plasma pool, SmartSEC and Ultracentrifugation samples were diluted in water to a final volume of 100 µL whereas the other samples were measured undiluted. 25 µL of the prepared samples, standards, and blanks were transferred to a 96-well plate. After all samples and replicates were pipetted into the wells, 25 mL of reagents A and 500 µL of reagent B were combined and 200 µL of the prepared reagent mix were added to each well. The plate was sealed with an adhesive foil and placed in a ThermoMixer C which was preheated to 36 °C. The plate was shaken for 30 s at 400 rpm before it was incubated for 30 min without shaking. The plate was then measured on a plate reader at a wavelength of 562 nm.

Table 19 – Prepared bovine serum albumin standards for BCA total protein quantification.

Standard	BSA concentration [µg/ml]
STD 1	2000
STD 2	1500
STD 3	1000
STD 4	500
STD 5	250
STD 6	150
STD 7	100
STD 8	50
STD 9	25
STD 10	10
STD 11	5

2.3.4.10. Nanoparticle Tracking Analysis

The NS300 (NanoSight) was set up according to the manufacturer's instructions. The instrument settings were selected so that the size measurement of 60-, 100-, and 200 nm beads was possible individually in water. The chosen settings and focus remained unchanged during the sample measurements (Table 20). The dilutions of the samples were adapted so that 40-60 particles per frame were measured – referred to in Table 21.

The dilutions were performed with PBS in 13 mL tubes right before the measurement. After the sample was diluted and vortexed it was transferred to a 2 mL syringe and injected into the flow cell of the instrument. After each measurement the syringe was pushed manually until another sample section was visible until three videos were recorded.

Table 20 – NanoSight instrument and measurement settings

Instrument	NS300
Software	NanoSight NTA 3.4 – Sample Assistant
Camera	sCMOS
Laser	405 nm (violet)
Camera level	10
Screen Gain	1
Target temperature	25 °C
Syringe speed	-
Capture duration	30 sec
Measurements per sample	3

Table 21 – Dilution factors of sample types for NanoSight measurement of particle size and quantity.

Sample type	Dilution factor in PBS
Plasma pool	500
qEVsingle 35 Tween	100
qEVsingle 35	20
qEVsingle 70	20 (<40 particles per frame)
qEVoriginal 35	50
qEVoriginal 35 2GEN	40
qEVoriginal 70	20
qEVoriginal 70 2GEN	20
Ultracentrifugation	10
SmartSEC	320
ExoQuick	80
Miltenyi Pan Bead	10

2.3.5. Data analysis

2.3.5.1. BCA/ELISA/ECL

The SoftMax and Discovery Workbench 4.0 data were collected without setting blank wells and exported in .txt-file format and pasted to Excel. The mean blank values were subtracted from all values before they were sorted, and the standard curve nominal values were assigned. The curve fitting was performed using GraphPad Prism by setting up a xy table with two replicate values in side-by-side subcolumns. The nominal values were set as x-values, and the RFU values were entered as y-values. The x-values were then transformed into the decadic logarithm. A nonlinear regression curve fit was performed using the equation "asymmetric Sigmoidal, 5PL, X is log (concentration)". The samples with an unknown concentration were interpolated from the standard curve without any confidence interval. As the weighting method, 1/Y^2 was chosen. The other settings were kept at default values. The interpolated values were transformed back (X=10^X). The Data were then transferred to Excel for further analysis, including dilution factor back calculation and initial plasma input normalization.

2.3.5.2.Western Blotting

The images from the ChemiDoc were analyzed using the Image Lab software. The chemiluminescence and the colorimetric images were transformed for optimal band visualization. For optimized illustration of the results, the images were rotated and cropped before they were saved and exported as .tiff-files. For relative quantification, one positive control band was set as the reference band (Table 22). The relative evaluation of the bands allows a semi-quantitative statement about the occurrence of the corresponding proteins.

Table 22 – Positive control reference band

Protein	Positive Ctrl
Apolipoprotein A-I	Plasma Control
Apolipoprotein B	Plasma Control
Albumin	Plasma Control
GM130	Cell lysate Control
Calnexin	Cell lysate Control
CD9	Exosome Control
CD63	Exosome Control
Flotillin 1	Exosome Control

2.3.5.3.NanoView

The NanoView data were analyzed using the NanoViewer software. As the detection threshold, the default values of 500 were used for the three fluorescence channels (488 nm, 647 nm, 555 nm). For all chips, the files for interferometry and fluorescence were exported to .csv-files. The size distribution data from the TSPN spots were weighted based on the maximum peak height for normalization.

2.3.5.4.CellStream

The gating strategy for TSPN positive vesicles was performed according to the following figure (Figure 6). All antibodies used were detected within the same channel (B6) and thus the readout is for all analytes the same. As experimental control the lysis was performed as well as isotope control in plasma and PBSF control. Here the antibody was diluted in PBSF only to observe the signals originating from antibody aggregates. The gaiting strategy is based on two steps: First, the expected size range of exosomes is not measurable with neither the side scatter not the forward scatter. Second, this population is tested for fluorophore positivity in the B6 channel of the CellStream Instrument. The sample only was also tested but did not give any fluorophore positive results. The B6-population areas (EV-positive) were set to be minimal in the controls. The readout was exported from the CellStream analysis software as events per mL, the dilution factors were included and the results normalized for plasma input.

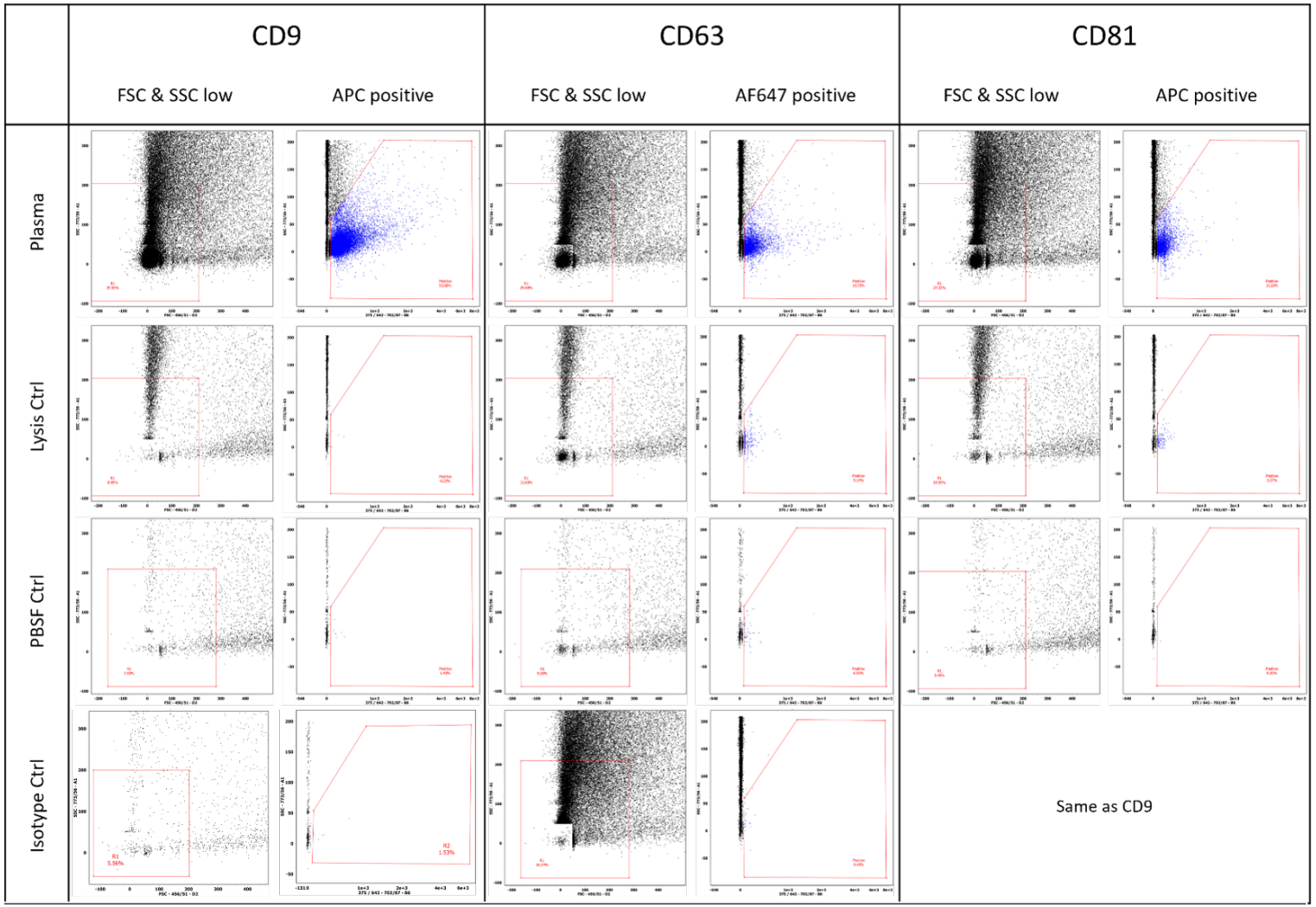

Figure 6 – Gating strategy for CD9, CD63, and CD81 positive exosomes measured on the CellStream instrument. The gaiting was performed based on scatter negativity for both forward scatter (FSC) and side scatter (SSC) including only events with less than 200 for both. The B6 channel was used to detect Allophycocyanin (APC) and Alexa Fluor 647 (AF647) labeled EVs within the FSC & SSC low-population. Gating is illustrated based on a plasma sample including the corresponding lysis control (lysis Ctrl), Buffer Control (PBSF Ctrl), and isotype Control (isotype Ctrl).

2.3.5.5.MACSPlex

The blank sample's median intensity values were subtracted from the values for each analyte bead. Samples with high values (>1) for the negative control beads (mIgG1 control, REA control) were excluded from the analysis. Negative or low values (<1) were not reported.

2.3.5.6.Tunable Resistive Pulse Sensing – Exoid™

Within the Exoid™ Control Suite, each sample was compared to the corresponding calibration run to ensure accurate quantification. The sizing and concentration data were then extracted in a .csv- and .pdf-format and merged from the .csv-files into an Excel file. Dilution factor was included to the quantification data and normalization for plasma input was performed.

2.3.5.7.Nanoparticle Tracking analysis – NanoSight

The NanoSight results were gathered with a detection threshold of 5 and exported into an .csv-file. The data from the .csv-files were merged in one Excel file and then back calculated for dilution factor and normalized for protein input (particle quantification) or maximum peak height (particle size distribution)

2.3.5.8.Correlation analysis

The correlation analysis was performed with GraphPad Prism. Here, the data were analyzed either as a correlation matrix (heatmap – Figure 23, Figure 42) or the direct comparison between two datasets. To identify the linear correlation, a Spearman correlation coefficient has been calculated and reported. All other settings were left in the default setting. Exceptionally, in Figure 12 R-squared was reported.

3. Results and discussion

This study aims to evaluate different sEV isolation methods in terms of feasibility, yield, and purity (Part 1 – Isolation method feasibility), reproducibility (Part 2 – Reproducibility of superior EV isolation methods), and interindividual variation (Part 3 – Interindividual variation of qEVsingle 35 Tween EV isolation). To this end, the plasma of 10 healthy donors was analyzed as a plasma pool (part 2) and individually (part 3).

3.1. Part 1 – Isolation method feasibility

3.1.1. Results

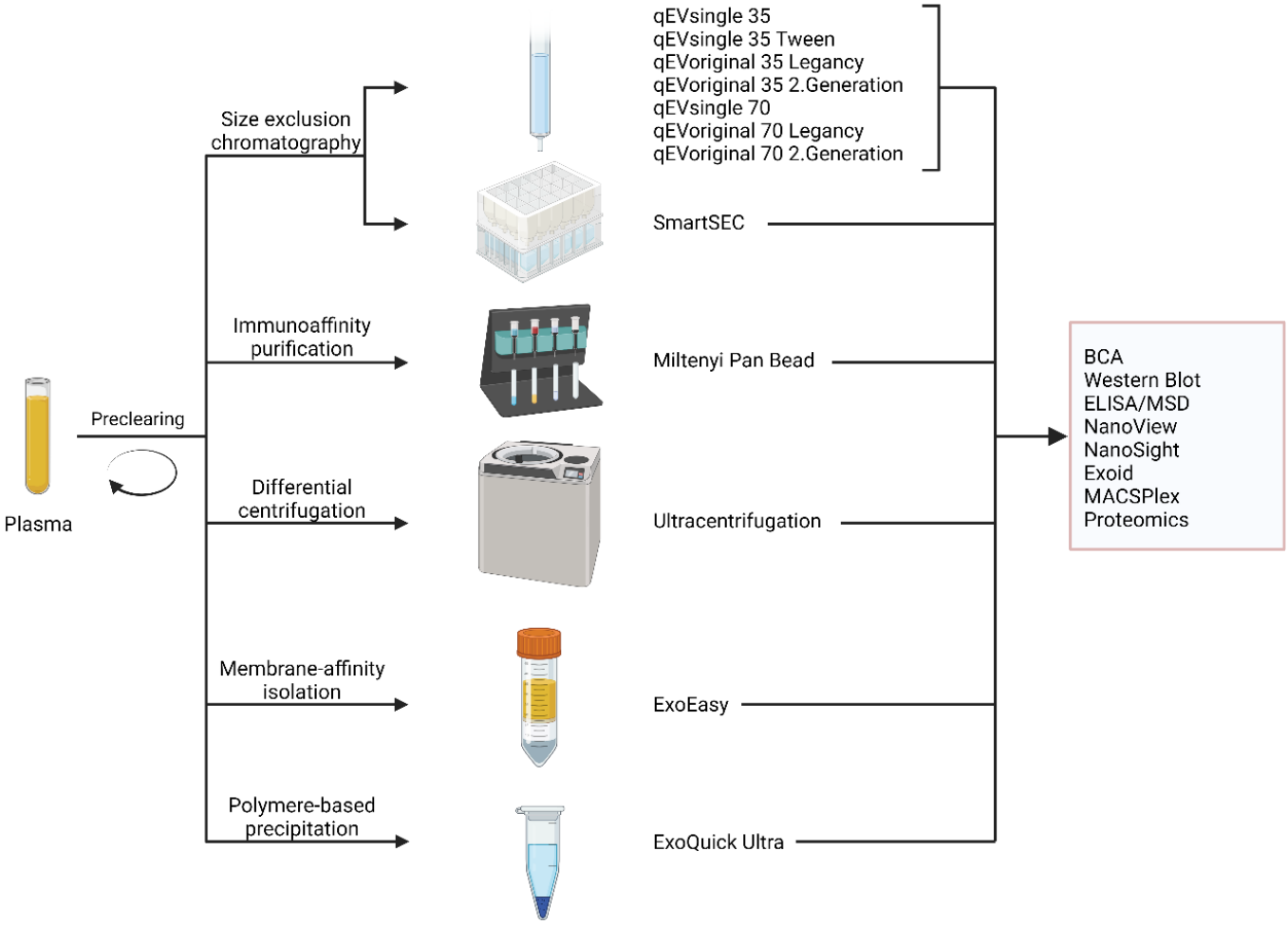

Figure 7 – Overview of the experimental workflow for the evaluation of the feasibility of different sEV isolation methods. A plasma pool was prepared and precleared from cells, cell debris, and microvesicles by a two step centrifugation protocol. Hereafter, the precleared plasma pool was further purified by differenet separation methods. The characterization methods used are stated in the box on the right.

Part 1 of this thesis aims to identify three methods that provide a high EV yield next to low co-purification of non-EV particles and the possibility for high-throughput sample analysis. Thus, twelve divergent EV isolation approaches were compared using methods characterizing EV size, protein content, surface protein markers, colocalization of EV markers, and co-purified non-EV material (Figure 7).

3.1.1.1. Particle size distribution

3.1.1.2. Particle quantification

3.1.1.3. TSPN based quantification

Summary of TSPN based EV characterization

3.1.1.4. Evaluation of EV purity using proteins and markers for non-EV particles

3.1.1.1.Particle size distribution

Three methods give us data about the particle size distribution in the prepared sEV isolations. First, the **NanoView** determines the particle size of the bound EVs based on the interferometric measurement. The reported data represent the particles on the TSPN spots (CD9, CD63, CD81). The measured particle size is uniformly distributed for all the isolation methods used (Table 23). Most of the particles detected are close to 50 nm in diameter, which is the instrument's detection limit. This is not only true for the TSPN capturing spots but also for the MIgG-"negative control"-spot. Although the particle numbers bound on the TSPN spots are higher, the size distribution is almost identical. Maybe the particles that tend to attach unspecifically to the spot surface are also particles in the same size range, like lipoproteins. Another reason might be that a great majority of the particles are within the measured size range. The presence of bigger particles would therefore be negligible. Even the plasma sample shows a similar size distribution to most of the sEV isolations, with its maximum peak at 55 nm in diameter. Even though the measured peak maximum is for all the samples, either 50 or 55 nm in diameter, the mean particle size reaches up to 81.5 nm in diameter (ExoQuick).

Of note, in the case of the qEVsingle 35, a negative number of particles was detected in the 50 nm size range and were excluded. This can be explained by the way the NanoView

gathers the data. The chips are scanned twice, once before and after the sample incubation. If, for any reason, the number of particles in a specific size range is lower after the incubation, a negative value will be output. If a sample is not measurable or the result is not valid, N/A is given.

The data acquired by **Exoid™** measurement mostly gives a homogenous picture of the different isolation methods (Table 23). The detection limit is 40 nm in diameter since an NP80 pore was used for the measurement. Like the size distribution obtained by the NanoView, the Exoid™ gives a unimodal peak skewed to the detection limit. In contrast, the Ultracentrifugation results show a bimodal distribution, where the secondary peak is between 70 and 75 nm. This is due to the measurement of the same sample with two different pressures. Here one measure at 1150 Pa pressure resulted in a unimodal peak at 50 to 55 nm in diameter. The measurement at 500 Pa also showed a unimodal peak shifted to bigger particle diameter. The highest mean particle size (85.9 nm) can be found in the qEVsingle 70 sample, and the remaining qEV-size exclusion columns (70) reveal a mean particle size above 60 nm. The same is true for the ultracentrifuged sample with the second highest particle size (mean particle diameter = 73.3 nm). All the other isolation methods and the plasma pool showed a mean particle size between 64.0 and 59.2 nm. Some samples were not measurable since the nanopore was blocked, which led to a constant drop in currency. This might be caused by bigger particles, aggregates, or precipitates within the samples. For the ExoQuick EV preparation, the number of particles detected in the undiluted sample was too low.

In contrast to Exoid™ and NanoView, the **NanoSight** shows a much broader size distribution. The data displayed focuses on the interval where most of the particles were represented. However, in theory, the NanoSight can measure particles with a diameter between 10 and 1000 nm. Often particle size distribution has multimodal peaks without a clear maximum. Nevertheless, most particles are between 50 and 200 nm for all isolation methods and the plasma pool (Table 23). The smallest particle size was measured in the qEVsingle 35 Tween sample with a peak maximum of 79.7 nm and a mean particle size of 96.0 nm. The remaining samples exhibit peak maxima between 103.6 (Miltenyi Pan Beads) and 170.2 nm (SmartSEC).

When **comparing** the data from the three measurement technics, there is a clear shift in the measured particle sizes in the case of the NanoSight (Figure 8). The mean particle size is more than 100 nm bigger (> factor 2) compared to the Exoid™ and NanoView data. The same is true for the peak maximum. Whereas NanoView and Exoid™ measure the peak to be about 50 nm for all samples, NanoSight determines values above 100 nm for every isolate but qEVsingle 35 Tween. Initial experiments with the NanoSight showed that a measurement of beads with different particle sizes results in a single peak, even though the individual assessment gives good results (data not shown). From these results, there is no doubt that a high number of small particles is present in most of the samples. In a more complex environment, the instrument neglects the presence of smaller particles. Weather Exoid™ and NanoSight neglect the presence of larger vesicles cannot be judged. For this, there is a lack of controls and experiments.

Another question is if the particles analyzed by the different methods are sEVs. The NanoView captures vesicles or particles based on the presence of the TSPNs. Besides the interferometric measurement, it can detect labeled particles with fluorescent markers. However, more than 90 % of the particles analyzed fluorescent-based are not measurable by interferometry. This suggests that the majority of the sEVs are reported to be below 50 nm.

Interestingly, the Exoid™ indicates similar results. Since we measure the particles close to the detection limit, the concern that the sEVs are even smaller is justified. Exoid™ and NanoSight give no additional information that would help clarify whether the measured particles are vesicular. Lysis experiments performed with the NanoSight led to no significant change in the size distribution (data not shown). Consequently, almost all particles detected by NanoSight are most likely not EVs. The same setup has been tested on the NanoView, where the amount of double TSPN positive particles dropped significantly when adding Triton X-100. These tests have not yet been performed on the Exoid™, but the device can resolve two different-sized bead populations. The instrument is set up based on an assumption of the particle size within a sample. Here the pore size used for the analysis plays a pivotal role in the measurement. Since we expected an sEV typical size distribution, we chose the NP80, which covers a range from 40 to 225 nm, according to the manufacturer.

In summary, all sizing methods show a size distribution confirming that the isolated particles are within the expected size range of sEVs, though the actual peak position varies depending on the particle sizing methods. However, the data indicates that a considerable amount of EVs is smaller than the detection limit of the presented sizing methods or not measurable in a complex sample. Additionally, particle sizing by NanoSight is biased by non-EV particles.

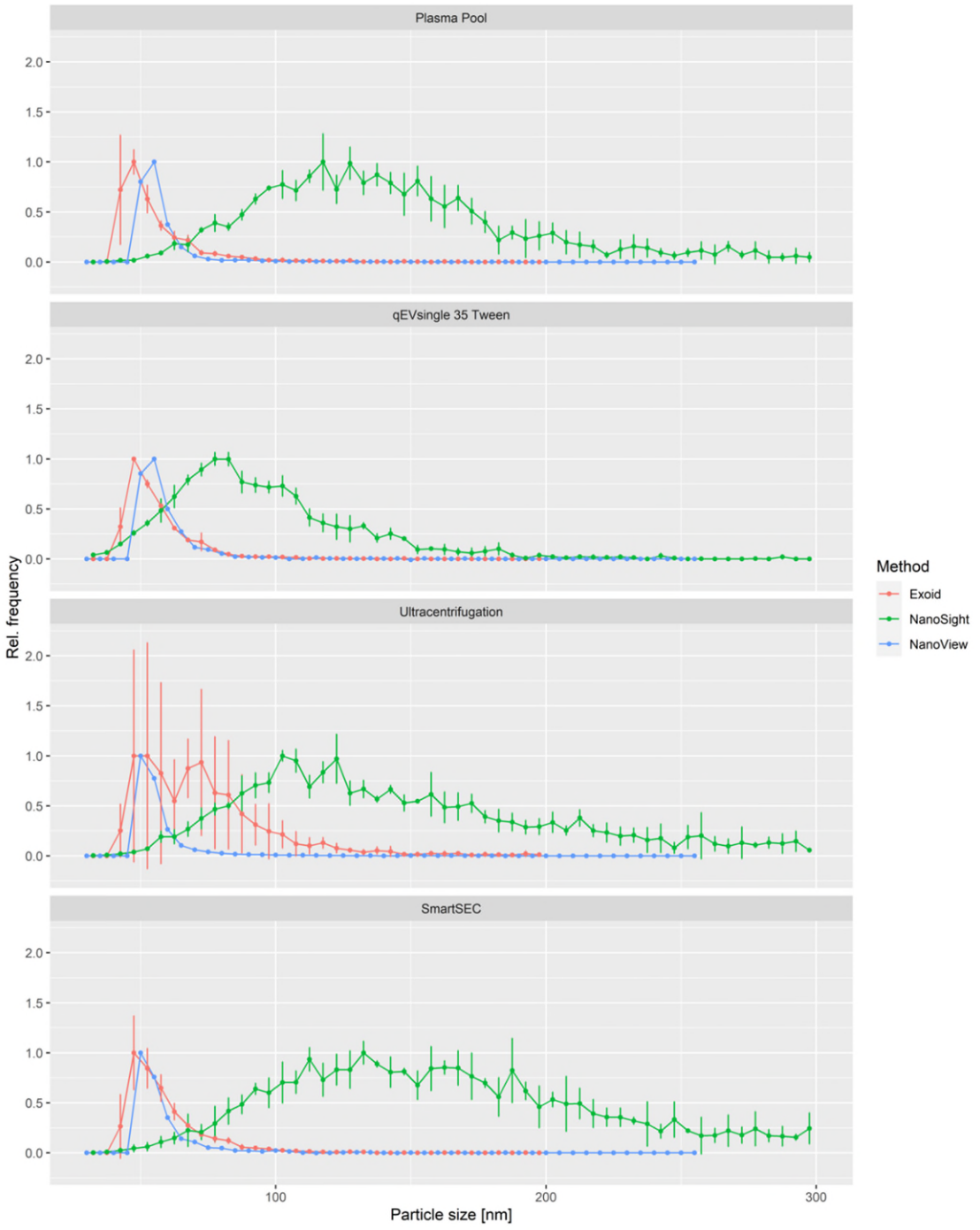

Figure 8 – Normalized size distribution of a human plasma (healthy) pool and three extracellular vesicle (EV) isolates (qEVsingle 35 Tween, Ultracentrifugation, and SmartSEC) origination from the plasma pool. The normalization was performed for maximum peak height. The size distribution was measured using three methods, namely Exoid™ (red), NanoSight (green), and NanoView (blue). The particle size was determined as the diameter in nanometers. The NanoView measurement, including the interferometry signals from the tetraspanins (TSPN) CD9, CD64, and CD81, were all measured three times. Due to the analysis, the size distribution results were merged without analyzing the individual TSPN difference, and no error was given. The error bars for the NanoSight indicate the standard error for each reported size bin after three repeated measurements were performed. The error bars of the Exoid™ report the standard deviation of each reported particle size bin measured under three different pressures (Table 18).

Table 23 – Comparison of the determined particle size mean and mode in the different isolation methods(qEVsingle 35 Tween, qEVsingle 35, qEVoriginal 35 2GEN, qEVsingle 70, qEVoriginal 70, qEVoriginal 70 2GEN, ExoQuick, ExoEasy, Ultracentrifugation, and SmartSEC) and the origination healthy human plasma pool. The measurement was performed using three different sizing methods: NanoSight, Exoid™, and NanoView. The Miltenyi Pan Bead isolation was excluded from sizing because the vesicles were lysed during the isolation method. If the measurement was not able to perform or the concentration was too low to be measured, no values (NA) were reported

	NanoSight		**Exoid™**		**NanoView**	
	Mean [nm]	Mode [nm]	Mean [nm]	Mode [nm]	Mean [nm]	Mode [nm]
Plasma Pool	155.1	120.6	56	47.5	57.6	55
qEVsingle 35 Tween	96	79.7	56.6	47.5	58.7	55
qEVsingle 35	197.5	138.9	58.8	47.5	67.1	55
qEVoriginal 35	186.1	129.5	59.2	47.5	58.6	55
qEVoriginal 35 2GEN	179.3	124.6	56.2	47.5	60	55
qEVsingle 70	174.7	139.3	85.9	67.5	44.8	50
qEVoriginal 70 2GEN	168.6	130.1	64	47.5	61	55
qEVoriginal 70	186.2	148.1	68.9	52.5	N/A	N/A
ExoQuick	167.5	116.2	N/A	N/A	55.8	50
ExoEasy	213.7	154.3	59	52.5	81.5	55
Ultracentrifugation	173.3	110.3	73.3	52.5	57.1	50
SmartSEC	180.7	170.2	59.2	47.5	57.8	50

3.1.1.2.Particle quantification

The same methods used to evaluate the particle size distribution allow quantifying the number of particles or EVs. Especially NanoSight and Exoid™ are built to quantify the particle measured in an absolute way. The NanoView gives two values that can be used as an indirect EV quantification. One is the label-free detection method, where interferometry is used to evaluate the number of particles bound to the antibody-labeled chip. The fluorescence method evaluates the number of EVs based on the presence of TSPN bound by specific antibodies. The difference in the detection modes has already been indicated in the particle size distribution section. The numbers determined by NanoSight are consistently higher compared to Exoid™ (Table 24). The differences reach from a factor of 136x (Ultracentrifugation) to 6944x (qEVsingle 70). Even though correlation analysis shows an excellent R-squared value of 0.97, this is nearly exclusively based on the outliers Plasma pool and SmartSEC. By excluding these results, correlation is no longer detectable.

Still, the two methods share some commonalities. Both show that about 90 % (88 % – NanoSight, 94 % – Exoid™) of particles detected in the plasma pool were found after SmartSEC. Further, the qEV 35 columns show a higher particle concentration than the qEV 70 columns. The qEVsingle 35 Tween method showed the highest concentration and lowest in the qEVsingle 70. ExoEasy and Ultracentrifugation isolation can be classified in between.

The results from the NanoView can be distinguished between the interferometric and the fluorescence measurement. Both data should reflect the TSPN particles, but the correlation is low ($r = 0.72$). Overall, the Plasma Pool sample had in both cases the highest particle count. Ultracentrifugation and qEVsingle 35 Tween samples were the EV isolations with the highest counts, in both measurement the qEV methods showed slightly higher readouts. There is a big divergence between the fluorescence count and the interferometric measurement. This together with the low overall count of particles detected by interferometric readout limits the informative value of the interferometric readout.

Table 24 – Particle concentration and TSPN positive particles per spot based on three different characterization methods. NanoSight, Exoid™, and NanoView give absolute or relative particle concentrations where the NanoView data can be evaluated based on the interferometric measurement (particles >50 nm, single positive for TSPN) and the fluorescence-based measurement (double positive for TSPN). The characterization has been performed on all prepared isolation methods, but the samples indicated with "N/A" were either not measurable or did not give valid results)

	NanoSight	**Exoid™**	**NanoView**	
	Particle Conc./mL	Particle Conc./mL	TSPN pos. particles per spot Interferometry	TSPN pos. particles per spot Fluorescence
qEVsingle 35 Tween	1.08E+11	2.08E+08	1333.4	522705
qEVsingle 35	2.21E+10	8.07E+07	621.6	99650
Ultracentrifugation	9.73E+09	7.18E+07	1265.5	513873
SmartSEC	3.18E+11	1.91E+09	910.7	384396
qEVsingle 70	7.43E+09	1.07E+06	770.4	3580
qEVoriginal 70 2GEN	2.21E+10	2.58E+07	1574.4	45400
qEVoriginal 70	1.13E+10	1.51E+07	589.9	21750
qEVoriginal 35 2GEN	4.57E+10	1.83E+07	557.6	155175
qEVoriginal 35	3.47E+10	1.02E+08	1484.0	199045
Plasma Pool	3.63E+11	2.03E+09	88491.3	854216
Miltenyi Pan Bead	N/A	N/A	N/A	N/A
ExoQuick	7.83E+10	N/A	625.1	109316
ExoEasy	1.07E+10	2.99E+06	481.7	36841

3.1.1.3.TSPN based analysis

Single Vesicle characterization – NanoView

The fluorescence mode of the NanoView gives additional insight into the characteristics of the EVs. The staining of the TSPN with different fluorophores allows #the detection and interpretation of TSPN colocalization. The data can be simplified when focusing on the symmetric assay results – gathered using the same antibody for capturing and detecting (CD9/CD9, CD63/CD63, CD81/CD81). The plotted data in Figure 9 show the yield of each isolation method based on the plasma pool sample EV count. The Ultracentrifugation and SmartSEC method show a high overall yield (52.1 % and 41.2 %), whereas the qEVsingle 35 Tween shows a relatively high abundance of CD9-positive vesicles. Compared with the results from the other Izon columns, CD63 and CD81 are still more enriched. Thus, the qEVsingle 35 Tween shows the methods' second-highest overall EV yield (49.3 %).

The EV distribution in the different column factions has been evaluated in initial experiments (data not shown): It has been demonstrated by western blot analysis that the qEV35 columns lead to a better enrichment of the EVs in early fractions, whereas the qEV70 columns lead to a separation of the EVs in different fractions. Interestingly, the qEV35 column again exceeds the results from the qEV70 columns. The separation of different-sized EVs into different fractions might be of interest for further analysis, but since we are aiming for a high sEV yield without bias, the separation and further dilution of the EV-fractions is not beneficial.

The ExoQuick isolation results in a high CD63 count, but the overall yield is comparable to the qEVoriginal 35 2GEN samples (both ~15 %). The membrane affinity method ExoEasy leads to a low yield comparable to the qEVoriginal 70 2GEN results.

The colocalization data, shown in Figure 10, give an insight into the quality of the data. The number of vesicles bound to the MIgG control spot is negligibly low. Moreover, the overall error between the triplicates turns out to be low even in samples with poor EV concentrations like qEVsingle 70.

Since the data can be gathered and analyzed in a standardized way, the comparability with published data is good, even though the resulting fluorescent signal is not

compared to any standard, which would enable an absolute quantification. The colocalization data is extremely helpful when new markers need to be established. By simply using fluorophore-labeled antibodies against the target of interest, other EV populations can be visualized and counted, but also the distribution of biomarkers on the surface of the EVs can be quantified relatively.

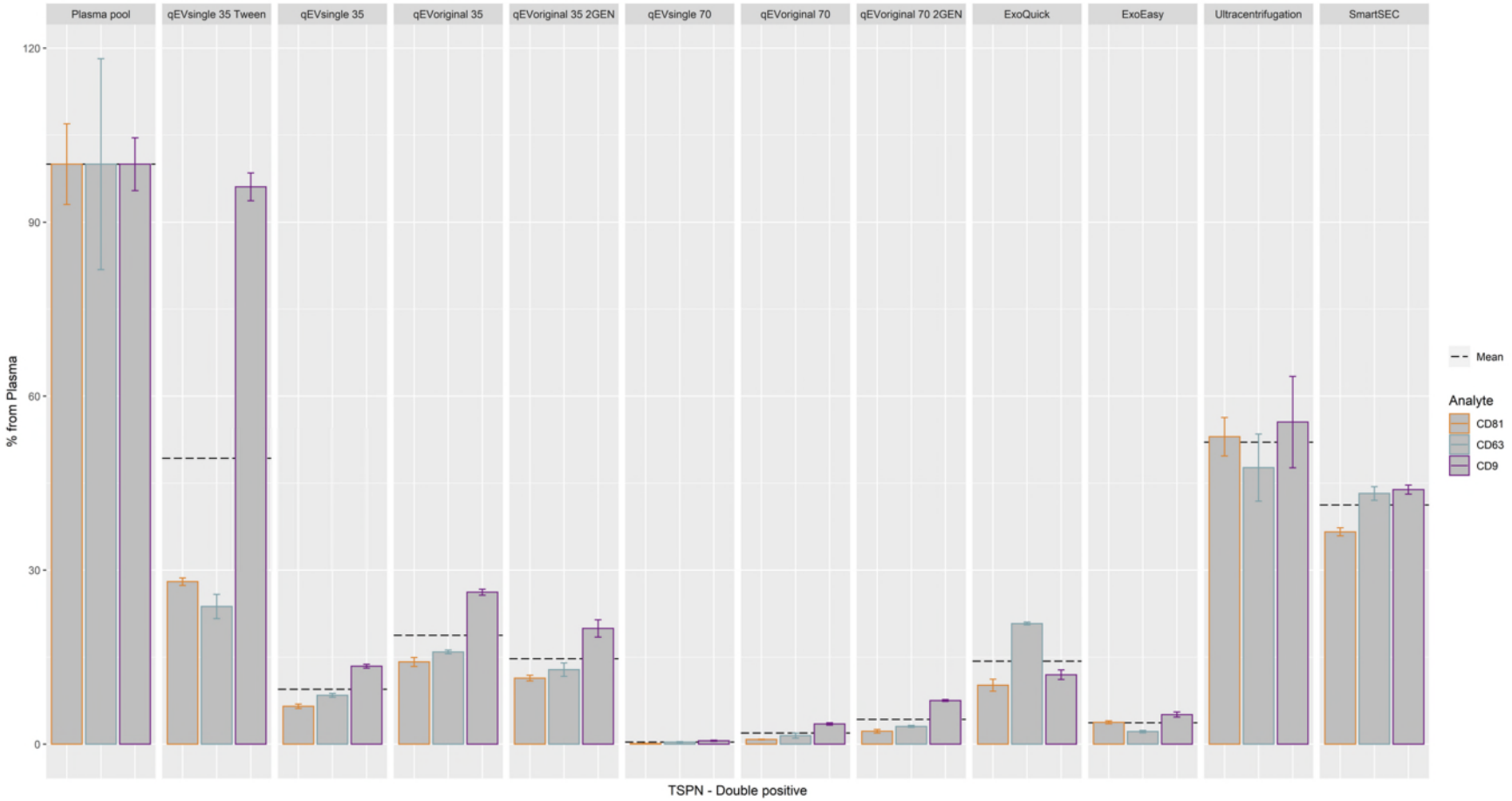

Figure 9 – Extracellular vesicle yield investigated with the NanoView assay. in the isolation methods qEVsingle 35 Tween, qEVsingle 35, qEVoriginal 35 2GEN, qEVsingle 70, qEVoriginal 70, qEVoriginal 70 2GEN, ExoQuick, ExoEasy, Ultracentrifugation, and SmartSEC. For the analysis, the dataset is reduced to the vesicles that are double positive for the different tetraspanins (CD9, CD63, and CD81). The normalization is based on the plasma volume from which the EV isolates originate. For the assay, the Instrument analyses three spots, and their normalized mean is indicated by the bar height, where their normalized standard error is represented by the error bars. The dashed line indicated the mean yield based on the three TSPNs.

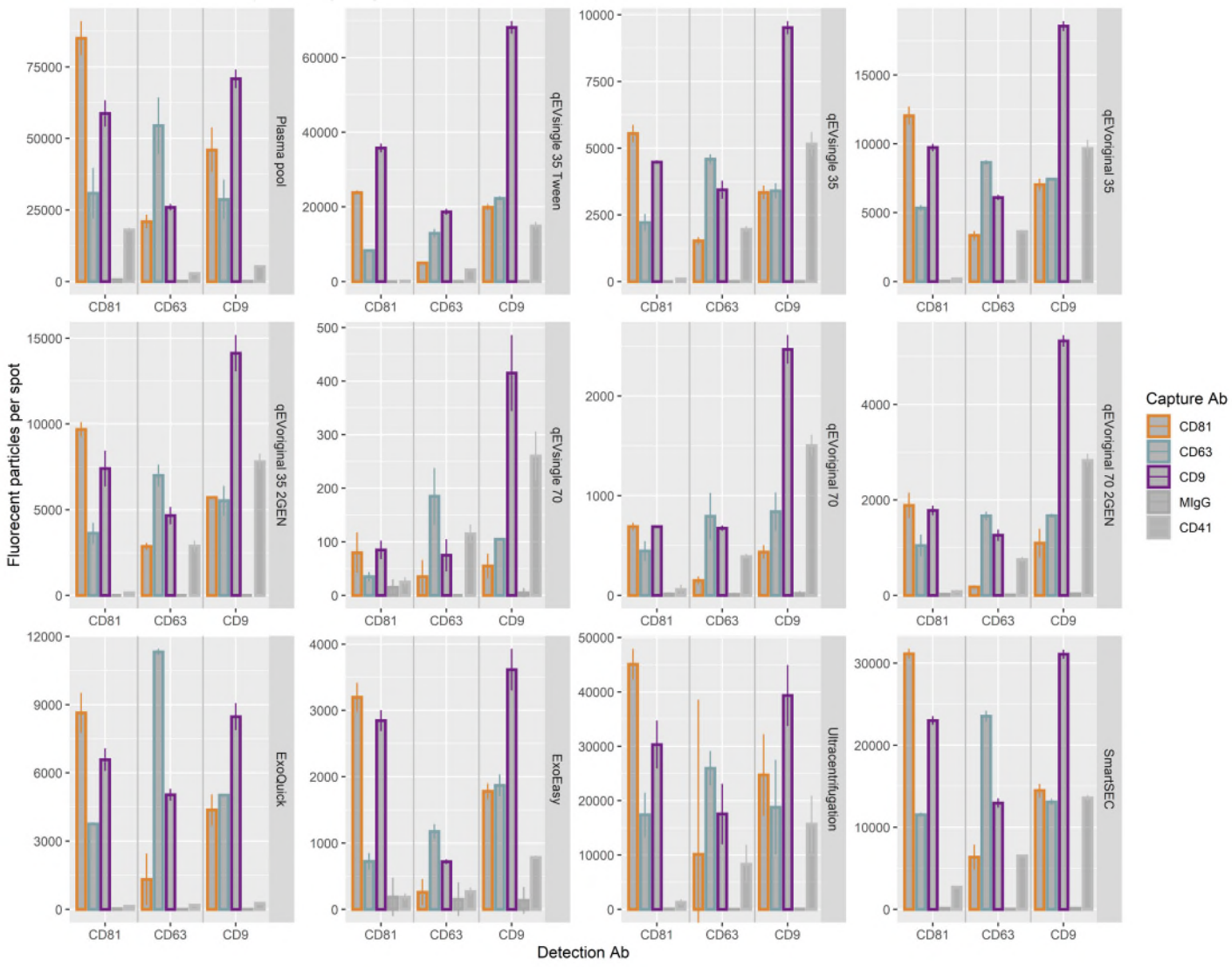

Figure 10 – NanoView based colocalization analysis of the different extracellular vesicle isolates. (methods qEVsingle 35 Tween, qEVsingle 35, qEVoriginal 35 2GEN, qEVsingle 70, qEVoriginal 70, qEVoriginal 70 2GEN, ExoQuick, ExoEasy, Ultracentrifugation, and SmartSEC) and the origination healthy human plasma pool. The colocalization analysis was performed on the NanoView instrument and the reported data is particles per spot, where the analyzed spot surface is alsways the same area. The flourecently labeled detection antibodies (CD9, CD63, CD81) are indicated on the x-axis whereas the capture antibodies (CD9 [orange], CD63 [green], CD81 [violet], nonbinding isotype control (MIgG) [darkred], and CD41 [grey]) are indicated by the colors. The data is normalized for plasma input.

MSD – Electrochemiluminescence detection-based immunoassay for bulk EV detection and quantification

An electrochemiluminescence detection-based immunoassay, MSD, was used for bulk EV characterization. Figure 11 summarizes the results from three MSD experiments with the differentially isolated EVs. A symmetric assay for one of the TSPNs has been performed in each plate. Ultracentrifugation and SmartSEC reveal a good yield (61.5 % and 64.7 %) with homogeneous TSPN specificity. For the Izon qEV-columns, we can see a preference for CD9-positive EVs, which is also true for the ExoEasy method. ExoQuick again shows a comparable yield pattern with higher enrichment of CD63 positive EVs compared to CD9 and CD81. Comparing the mean values, we can see that the order of the isolation methods is different compared to the NanoView results. Based on the MSD results the SmartSEC method outperforms the Ultracentrifugation isolation, while qEVsingle 35 Tween is in the third rank.

The results confirm mostly the results gathered by NanoView. The similarity of the data is notable since the principle of the detection differs between the methods. In NanoView analysis the individual vesicles are counted by analyzing the images taken by a microscope while different lasers excite the fluorophores. The MSD signal is generated by an electrically induced redox reaction of the antibody tags, followed by a light-emitting reaction that is then measured and relatively quantified to an EV standard. The captured vesicles remain intact, and the binding of the detection antibody is due to the presence of multiple epitopes on the surface of one vesicle. The signal intensity per vesicle plays a crucial role in the MSD setup, whereas the NanoView will report the signal intensity per vesicle separately.

Additionally, for the NanoView, capturing all TSPN takes place on one chip. Consequently, the antibodies compete for the EV binding – that is double positive in many cases. In the MSD measurement, the individual ligand binding assays occur in different wells. Thus, there is no competition between the capturing antibodies.

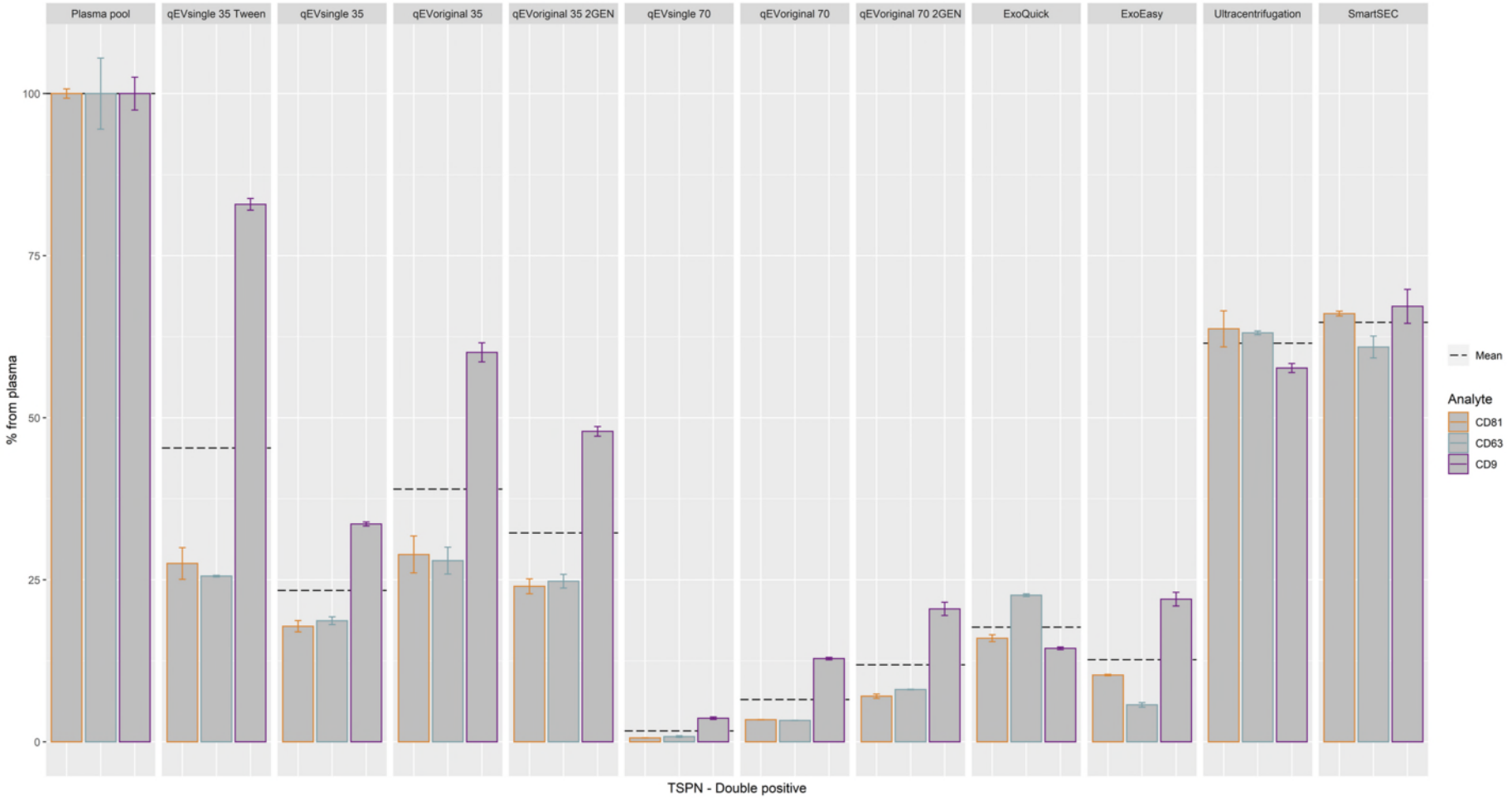

Figure 11 – Extracellular vesicle yield investigated with the MSD assay. in the isolation methods qEVsingle 35 Tween, qEVsingle 35, qEVoriginal 35 2GEN, qEVsingle 70, qEVoriginal 70, qEVoriginal 70 2GEN, ExoQuick, ExoEasy, Ultracentrifugation, and SmartSEC. For the analysis, the dataset reflects the vesicles that are double positive for the different tetraspanins (CD9, CD63, and CD81). The normalization is based on the plasma volume from which the EV isolates originate. For the assay, the Instrument analyses three spots, and their normalized mean is indicated by the bar height, where their normalized standard error is represented by the error bars. The dashed line indicated the mean yield based on the three TSPNs.

MSD – Colocalization analysis

The fact that the MSD platform and the NanoView gave similar results intensified our interest in testing the measurement of colocalization data that can be gathered on the MSD platform. The initial experiment can easily be performed on the NanoView, where the detection antibody against the biomarker protein reveals the colocalization with the TSPN and enables decision-making regarding the actual readout (e.g., anti-CD81 as capturing and anti-biomarker as detection). Once established, the assay could be transferred to the MSD platform, where a higher throughput and more quantitative readout can be achieved. Like this, we aim to measure, e.g., membrane-bound biomarkers on the surface of vesicles in the future.

For testing this colocalization measurement, we transferred the capturing and detection options equivalent to the NanoView to the MSD. The correlation between the two methods is plotted in Figure 12. The correlation of the symmetric assay format showed a correlation coefficient (R squared) above 90 percent – indicated in light orange. In contrast, the combinations of CD81 and CD9 for both capture and detection demonstrated a poorer correlation (R squared = 0.66 (CD81 – CD9) and 0.71 (CD9 – CD63), the R squared values of the remaining antibody combinations are 0.77 and above. The interpretation of the data is challenging because different isolation methods are compared with high variability in protein, lipoprotein, and EV concentration. Nevertheless, the data show a good correlation, resulting in higher confidence in the individual methods data. This will be further evaluated in the later sections focusing on interindividual variability (Part 3 – Interindividual variation of qEVsingle 35 Tween EV isolation).

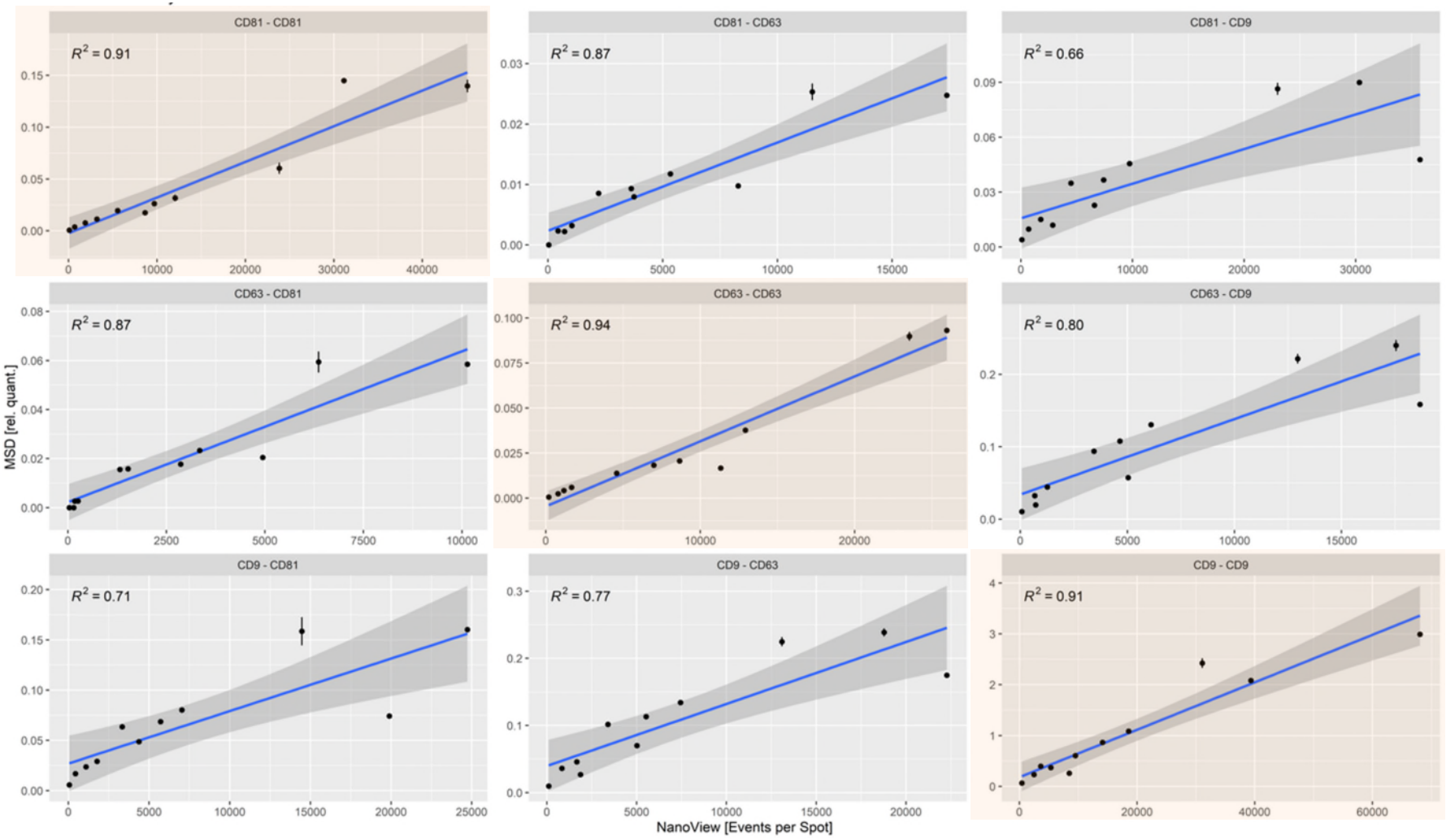

Figure 12 – MSD and NanoView result correlation analysis of the colocalization of the tetraspanins (CD9, CD63, CD81) on the surface of extracellular vesicles (EVs). The values of the different EV isolation methods qEVsingle 35 Tween, qEVsingle 35, qEVoriginal 35 2GEN, qEVsingle 70, qEVoriginal 70, qEVoriginal 70 2GEN, ExoQuick, ExoEasy, Ultracentrifugation, and SmartSEC were plotted after they were analyzed by NanoView and an electrochemiluminescence assay (MSD). Both of which give relative or semiquantitative readouts and were normalized by the plasma input. For each colocalization analysis the detection (D) and capture (C) antibody were stated above (D – C).

Multiplexed bead-based flow cytometry – MACSPlex

The MACSPlex assay analyzes EV surface markers with 39 different bead populations coated with different antibodies against a variety of membrane proteins (see Table 8) including two negative control antibodies. First, the EVs bind to the antibody coated beads. Then, for the fluorescence staining of the vesicles APC conjugated antibodies against CD9, CD63, and CD81 bind to the EVs/Bead complex. The readout is based on flow cytometry and requires the colocalization of the TSPNs, which are detected by APC-labeled antibodies. The sample analysis has been performed without initial normalization per total protein as recommended in the user manual as the samples are very heterogeneous and we could not perform the analysis with different dilutions for each sample, thus, the quantitative readout must be considered with care. Also, the kit does not come with a positive control or standard that would help to put the results in context. Nevertheless, the observed results allow a few conclusions to be drawn. First, the ExoQuick sample gave a high value of unspecific signals in the flow cytometer that gave high positive results for all the beads, including the isotype control antibody coated ones (not shown). Second, the highest results for the TSPNs can again be seen for the qEVsingle 35 Tween, Ultracentrifugation, SmartSEC, and qEVoriginal 35 methods (Figure 13). However, the distribution does not reflect earlier results by other methods. Third, the highest intensity can be found on the CD9 beads in qEVsingle 35 Tween.

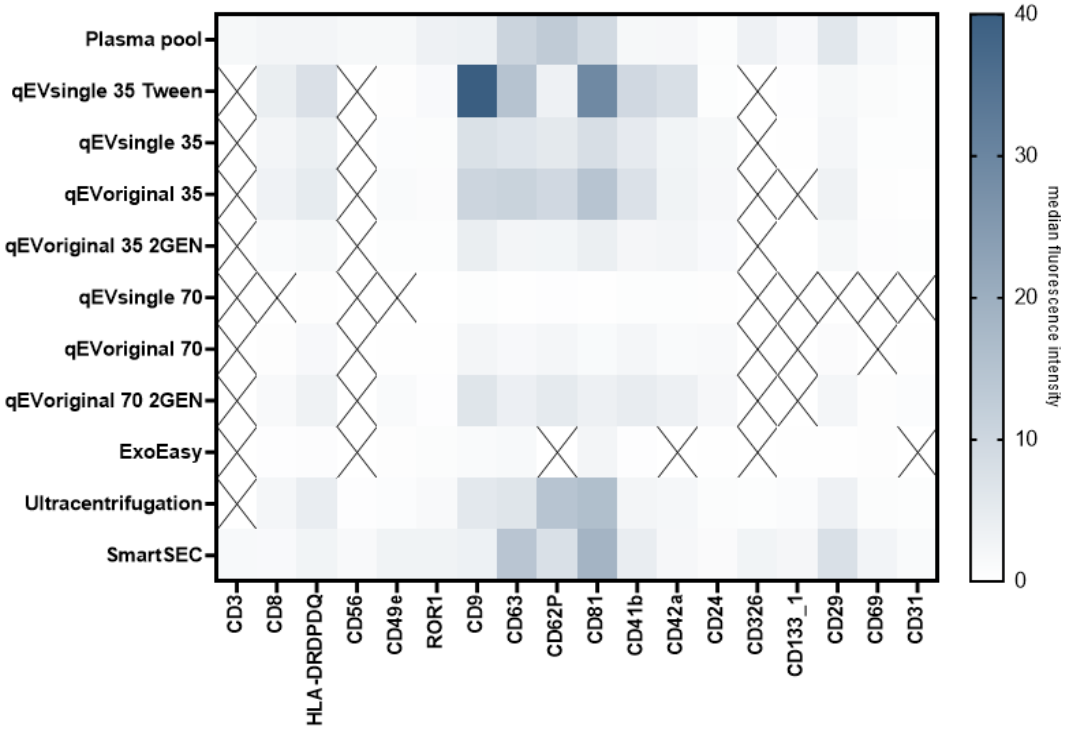

Figure 13 – Heatmap of the median fluorescence intensity of the MACSPlex beads after labeling the extracellular vesicles bound to the beads with CD9, CD63, and CD81 antibodies. The values were normalized for plasma input. The analysis was performed with plasma EVs isolated by qEVsingle 35 Tween, qEVsingle 35, qEVoriginal 35 2GEN, qEVsingle 70, qEVoriginal 70, qEVoriginal 70 2GEN, ExoQuick, ExoEasym Ultracentrifugation, and SmartSEC. Overall 39 bead populations were analyzed, all coated with different antibodies (Table 8). Two antibodies were negative controls – indicating samples with high background – and only 18 of the residual 37 were positive (>1) for at least one sample.

Western Blotting

The Western blot analysis of the different isolation methods shows the abundance of CD9 and Flotillin-1 (Flot1) in all the methods (Figure 14). In contrast, the detectability in the case of CD81 seems lower since the methods with low intensity for CD9 and Flot1 demonstrate faint bands for CD81. Interestingly, the Miltenyi Pan Bead method shows only low or no signals for TSPN. The enrichment for the specific markers was thought to result in a high readout. In contrast, the SEC methods SmartSEC, qEVsingle 35 Tween, qEVoriginal 35, and qEVoriginal 35 2GEN demonstrate high EV yield that all measured positive markers can confirm. The qEV70 columns constantly show lower yield compared to their corresponding 35 version. The qEV 35 samples also show higher signals for the lipoprotein marker Apolipoprotein B100 (ApoB), which will be discussed in the following

sections. Ultracentrifugation also reveals high signals for positive markers and demonstrates a good depletion of ApoB100.

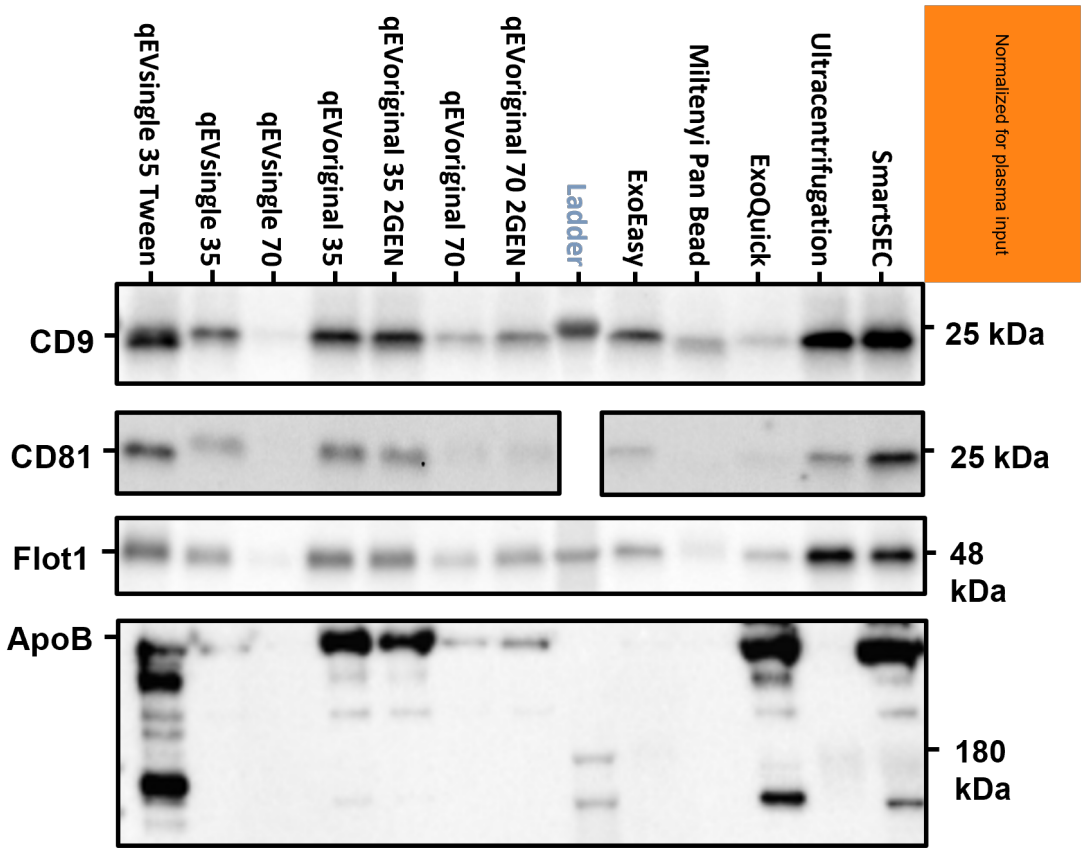

Figure 14 – Western blot images for the analysis of the markers of extracellular vesicles (EVs) CD9, CD81, and Flotillin-1 (Flot1), and the low-density lipoprotein marker apolipoprotein B (ApoB). The analytes were detected and relatively quantified in isolations of extracellular vesicles (EVs) originating from healthy human plasma. The methods investigated are qEVsingle 35 Tween, qEVsingle 35, qEVoriginal 35 2GEN, qEVsingle 70, qEVoriginal 70, qEVoriginal 70 2GEN, ExoQuick, ExoEasy, Ultracentrifugation, SmartSEC, and Miltenyi Pan Bead. The input per pocket was normalized for plasma input. The band height is indicated on the right based on the ladder and the manufacturer's declarations.

Western blot sensitivity optimization by fixation

Initial experiments showed weak bands for CD81 with western blot analysis using the standard protocol. Two fixation protocols were used and directly compared to the standard protocol to enhance the sensitivity. The fixation method A (FixA) includes a 30 min acetone incubation at 0 °C of the PVDF (Polyvinylidene fluoride) membrane after blotting. After the acetone treatment, the membrane was dried in air and rehydrated with methanol and water (50 % each) before transferring the blot to Blocking Buffer. The fixation method B (FixB) contains the same steps as FixA. Instead of directly blocking the membrane, another heating at 50 °C for 30 min in DPSB was inserted.

In the WB-fixation experiment, the positive control HBM-Exosomes, and the SEC sample qEVsg35T were analyzed using the standard protocol (nonFix) and the fixation protocols (FixA/B).

The FixA protocol increased the signal of the CD81 band at ~22 kDa by a factor of 4.4 – 5.7x based on a relative quantification. The FixB protocol did not bring further advantages in sensitivity for CD81. The increase in signal intensity compared to the nonFix protocol was 3.8 – 5.2-fold, thus resulting in a comparable intensity as the fixation protocol without additional heating. The unspecific binding band at ~34 kDa was not affected or showed a slight reduction in signal intensity to 0.6-fold. The total lane backgrounds were identical with and without acetone treatment. The maximum increase was 1.4x for FixA and 1.1-fold for the FixB protocol.

A comparison of the different isolation methods with and without acetone fixation was performed to confirm the positive effects on the quantification also in correlation to other CD81 quantification methods shown in Figure 14.

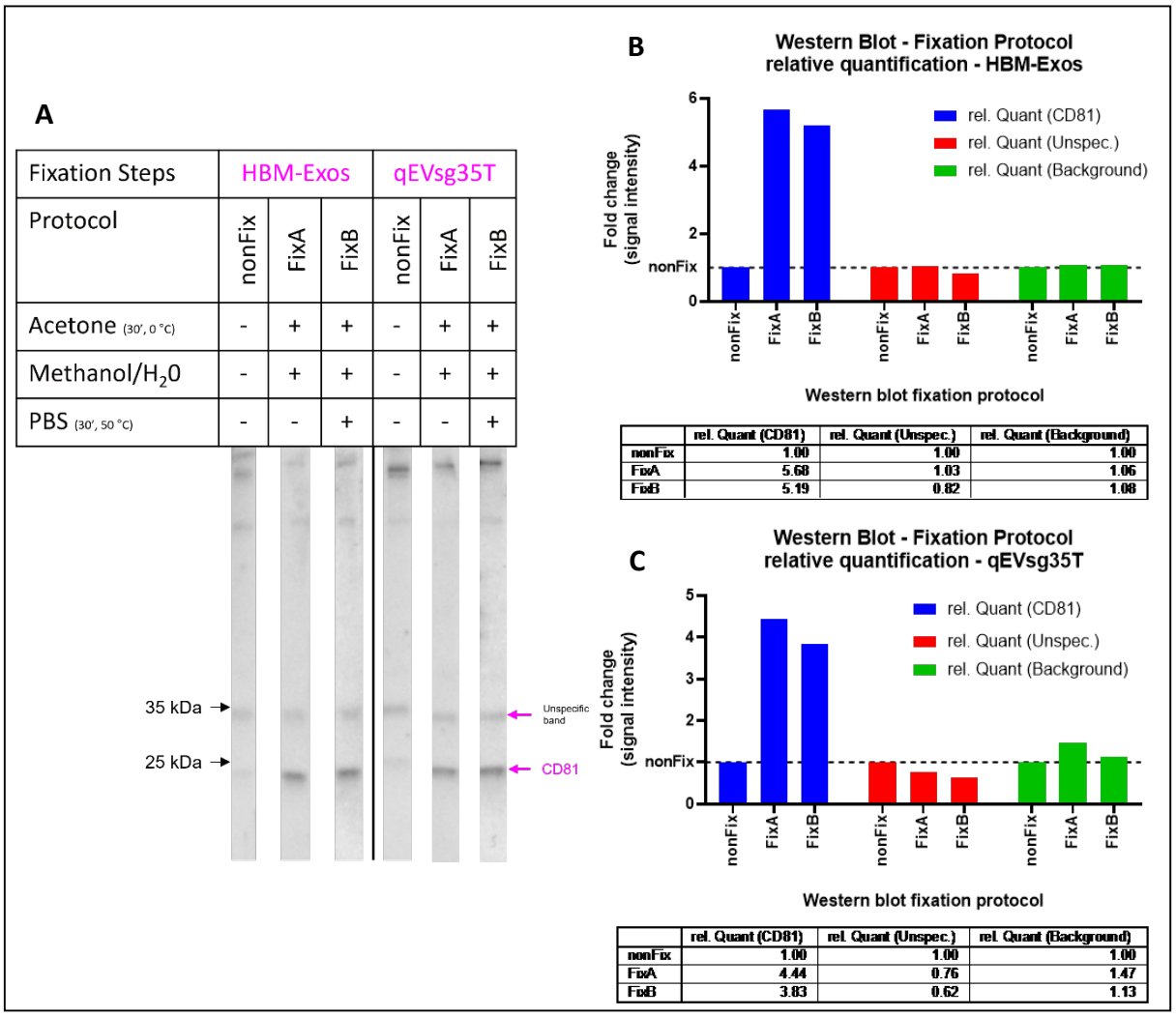

Figure 15 – Comparison of western blot protocols for CD81 quantification. (A) Western blot lanes from Hansa BioMed Exosome Standard Lyophilized exosomes from human plasma of healthy donors (HMB-Exos) and qEVsingle 35 Tween isolated plasma exosomes (qEVsg35T) with acetone treatment (FixA), a combination of acetone treatment and heating (FixB), and a western blot protocol without a protein fixation strategy (nonFix). Size standard band height is indicated on the left and the height of an unspecific band and a CD81 specific band were noted on the right. (B) Relative quantification (rel. Quant) for HBM-Exos of the CD81 band (CD81), the unspecific band (Unspec.), and the total background for the three protocols normalized to nonFix. (C) Relative quantification for qEVsg35T bands and background normalized to nonFix.

Summary of TSPN-based EV characterization

To identify the superior EV isolation methods in terms of EV yield using TSPN-based EV characterization, the date was accumulated in Figure 16 using z-score normalization. Z-scores, the normalization of the data by the mean (set as zero) and the standard deviation (set as one), allows the visualization of the merged positive marker readouts gathered from Western blotting, MSD, NanoView, and MACSPlex assay. The summarized data in

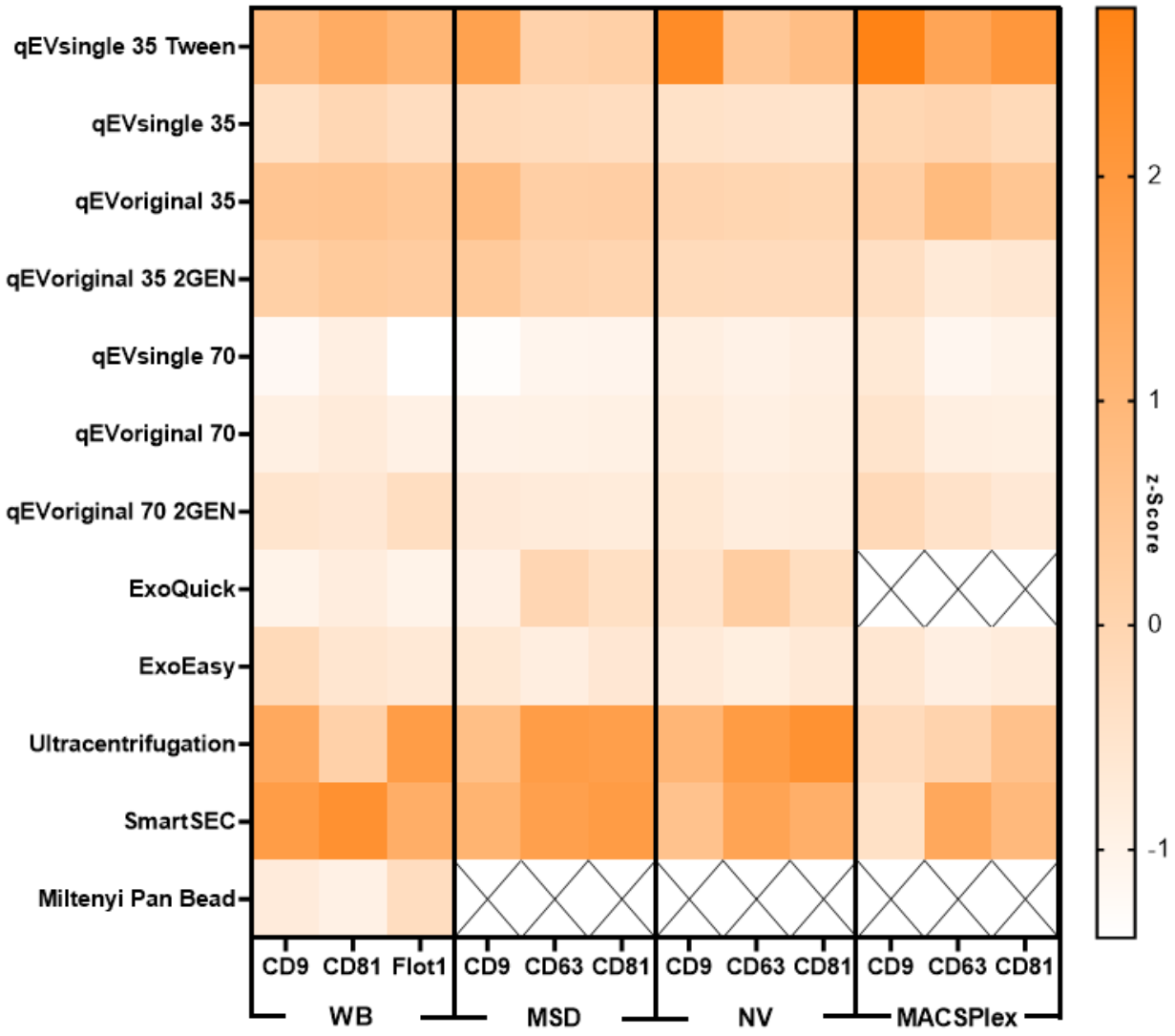

Figure 16 – Heatmap of the z-scores of markers of extracellular vesicles detected by Western Blot (WB), electrochemiluminescence (MSD), NanoView (NV), and MACSPlex. The standardization was based on plasma input on the variation of the different isolation methods for each analyte and platform. Here the mean of all methods represents the z-score value of 0 as one standard deviation is normalized to be 1. The measurements where the results were invalid are marked by an "X".

Figure 16 reveals the methods with a high sEV yield. Notably, most of the methods allow to draw the same conclusions. The methods with the highest readout are Ultracentrifugation, SmartSEC, and qEVsingle 35 Tween, followed by the other qEV 35 columns.

3.1.1.4. Evaluation of EV purity using proteins and markers for non-EV particles

BCA

The total protein quantification via BCA indicated that the protein of the precleared plasma gets considerably decreased with each isolation method (Figure 17). Nevertheless, the level of decrease varies a lot between the different methods. Whereas 7,3 % of the protein remains in the isolated EVs after SmartSEC, only 0,06 % can still be found in the Miltenyi Pan Bead isolated EVs. Depending on which Izon SEC column was used for the purification of EV preparations, they still include between 0.11 % (qEVsingle 70) to 0.42 % (qEVsingle 35 Tween). Again, the type 35 columns show higher values than the 70 columns.

Interestingly, the protein concentration increases in the qEVsingle 35 columns by 69.4 % by adding Tween compared to the non-Tween method. Ultracentrifugation, the isolation method with the second highest protein concentration, contains 3.19 % of the total plasma proteins. ExoQuick and ExoEasy line up between Ultracentrifugation and the qEV-methods having values of 0.98 % and 0.57 %. As indicated in Figure 17, the depletion of the ten highest abundant proteins alone would decrease protein by approximately 90 %. All the methods used are below that theoretical threshold that would indicate high remaining protein contamination.

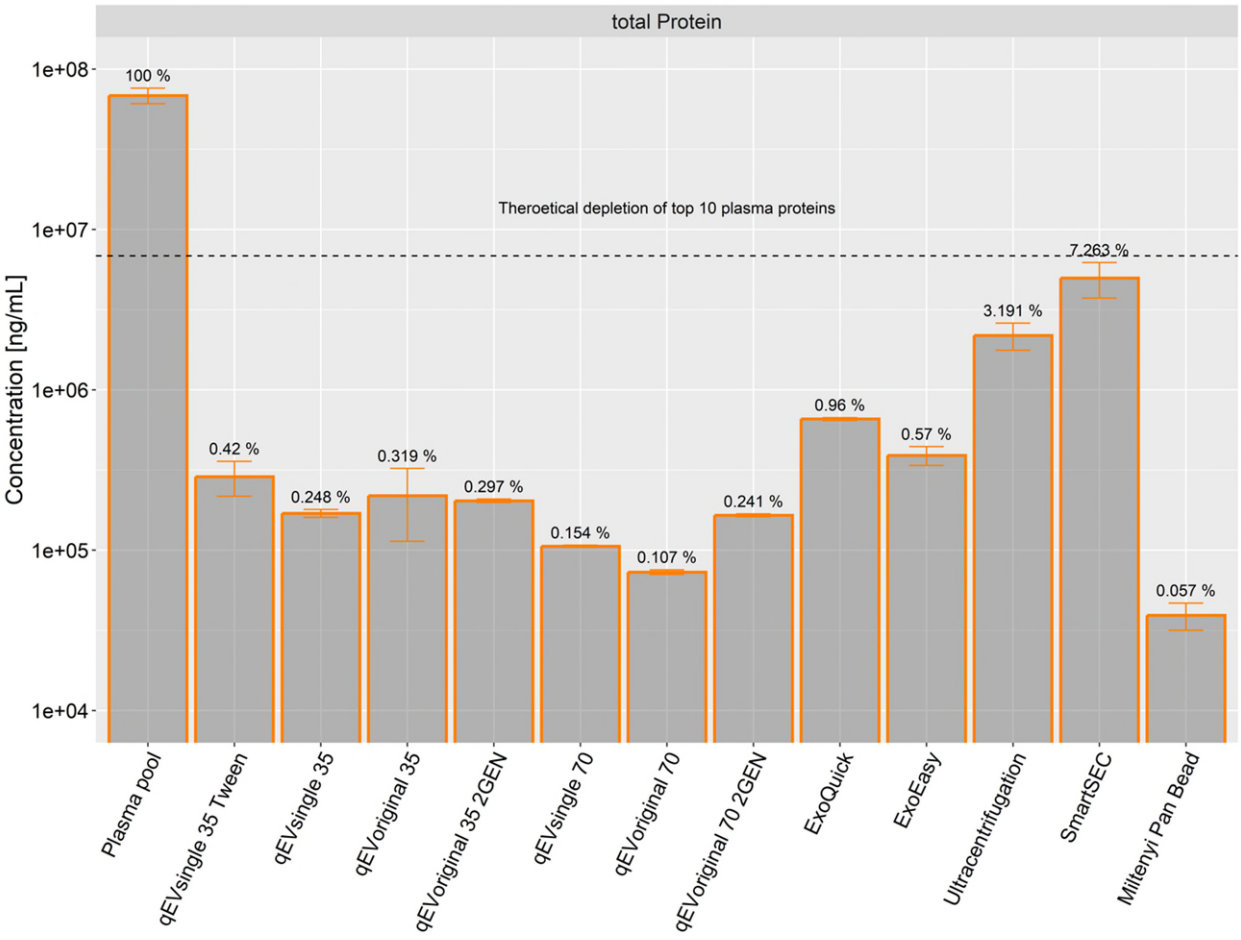

Figure 17 – BCA based total protein quantification in plasma pool as well as isolates of extracellular vesicles (EVs) based on the methods qEVsingle 35 Tween, qEVsingle 35, qEVoriginal 35 2GEN, qEVsingle 70, qEVoriginal 70, qEVoriginal 70 2GEN, ExoQuick, ExoEasy, Ultracentrifugation, SmartSEC, and Miltenyi Pan Bead. The concentration is normalized to the plasma input volume. The samples measurement was repeated twice, and the bar height indicates their mean as the standard deviation is represented by the error bars. The dashed lane stands for the protein concentration after the theoretical depletion of the ten most abundant proteins in plasma.

Human Albumin

Albumin is the most predominant protein in human blood. As visualized in Figure 18, it shows a similar distribution in the different EV isolates, like the total protein. The SmartSEC method has the highest residual albumin, followed by Ultracentrifugation. The qEV columns show an excellent depletion of albumin compared to all other methods. The qEVoriginal 35 method reveals the highest values for all the qEV columns with only 0.0006 %. Interestingly, compared to the total protein quantification, the albumin levels are below the one from the Miltenyi Pan Bead isolation method. This could be due to the

contamination by unspecific binding for the bead-based isolation, whereas the proteins most likely to contaminate the SEC samples are the proteins with high molecular weight or a higher order structure.

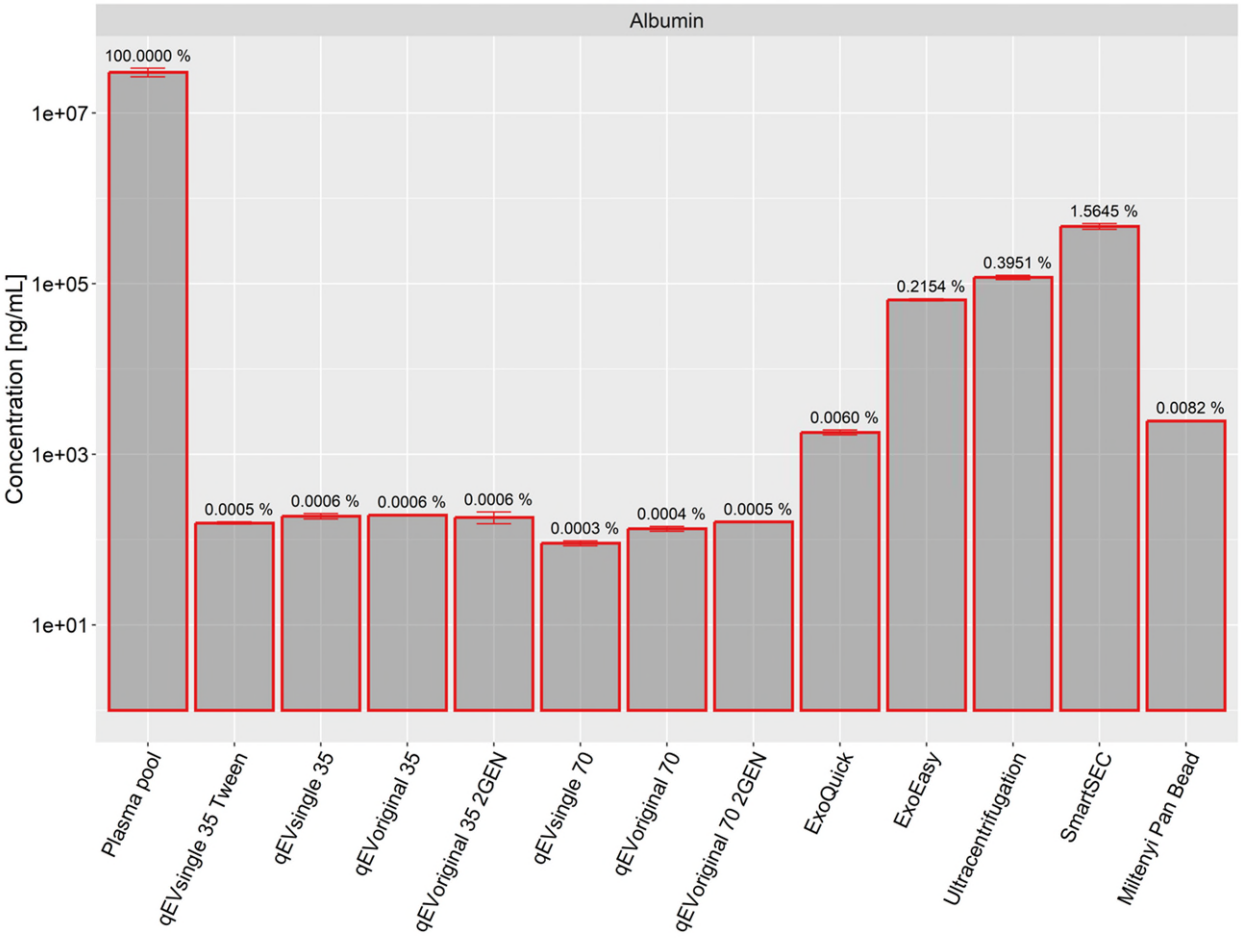

Figure 18 – Enzyme-linked immunosorbent assay (ELISA) based quantification of human albumin in plasma pool as well as isolates of extracellular vesicles (EVs) based on the methods qEVsingle 35 Tween, qEVsingle 35, qEVoriginal 35 2GEN, qEVsingle 70, qEVoriginal 70, qEVoriginal 70 2GEN, ExoQuick, ExoEasy, Ultracentrifugation, SmartSEC, and Miltenyi Pan Bead. The concentration is normalized to the plasma input volume. The sample measurement was repeated twice; the bar height indicates their mean, and the error bars represent the standard deviation.

Human Immunoglobulin G

With approximately 150 kDa, immunoglobulin G is one of the higher molecular representatives of the highly abundant plasma proteins. As such, the remaining concentration in the short SEC column SmartSEC is prominently high and represents 13 % of the precleared plasma IgG (Figure 19). The concentration in the precleared plasma sample is 4.45 mg/mL. qEVsingle 70 is the sample with the lowest concentration,

representing only 0.001 % of the IgG input. Overall, the qEV 70 columns show the lowest remaining IgG (original: 0.003 %; original 2Gen: 0.007 %), followed by the qEV 35 columns (single Tween: 0.011 %; single: 0.016 %; original 2GEN: 0.019 %; original: 0.025 %) and Miltenyi Pan Bead isolation (0.014 %). ExoEasy and ExoQuick are with values of 0.24 % and 0.098 % again in the mid-range.

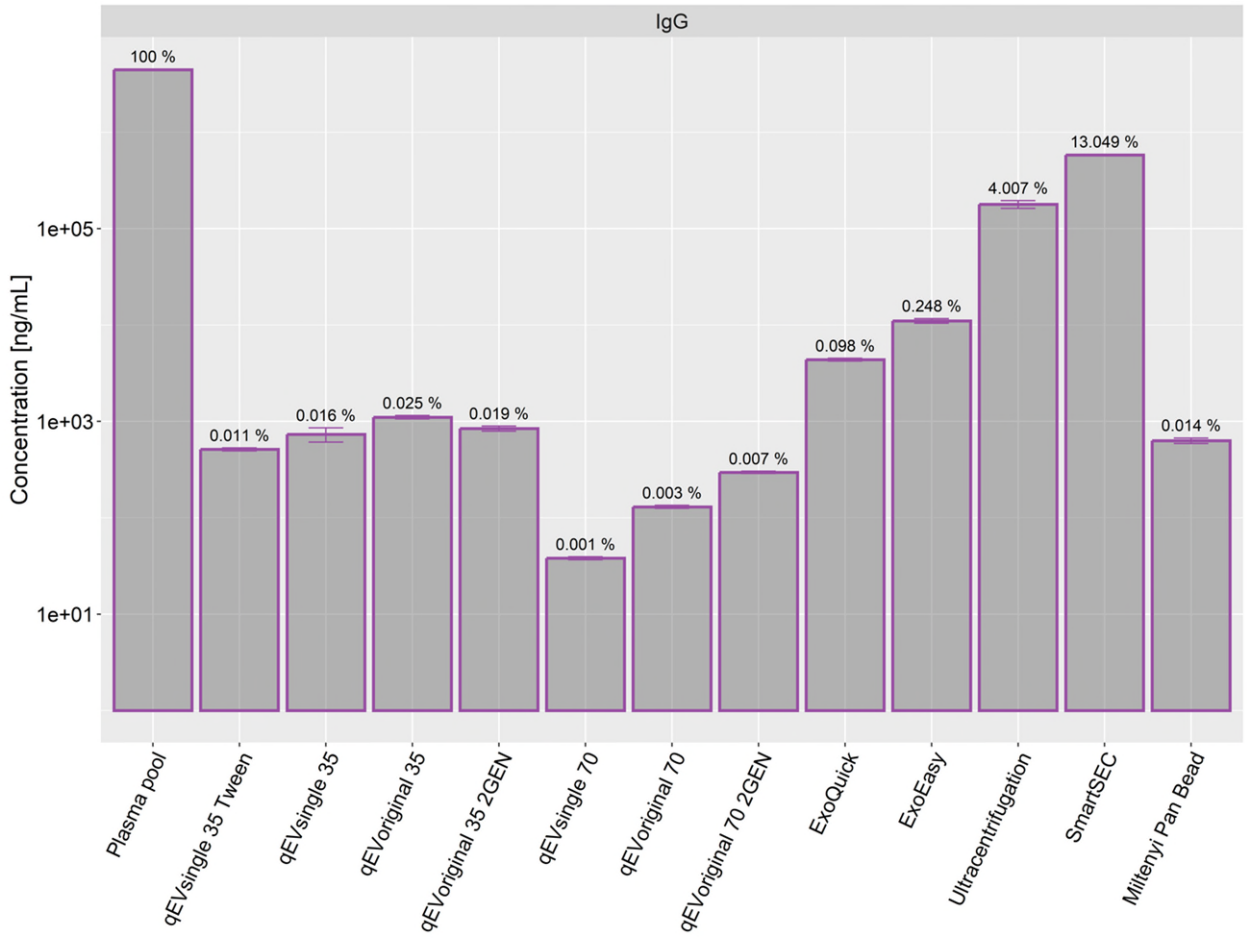

Figure 19 – Enzyme-linked immunosorbent assay (ELISA) based quantification of human immunoglobulin G (IgG) in plasma pool as well as isolates of extracellular vesicles (EVs) based on the methods qEVsingle 35 Tween, qEVsingle 35, qEVoriginal 35 2GEN, qEVsingle 70, qEVoriginal 70, qEVoriginal 70 2GEN, ExoQuick, ExoEasy, Ultracentrifugation, SmartSEC, and Miltenyi Pan Bead. The concentration is normalized to the plasma input volume. The measurement of the samples was repeated twice. The bar height indicates the mean as the error bars represent the standard deviation.

Apolipoprotein A1

Human apolipoprotein A1 can be found in high amounts in the Ultracentrifugation sample. Approximately 1.3 % of the plasma ApoA1 remains after the EV isolation. The concentration in plasma is at 1.24 mg/mL. The other EV isolations contain less than 1%, ExoEasy and ExoQuick 0.87 and 0.84 %, followed by the Izon columns and Miltenyi Pan Bead isolation (Figure 20). The ExoQuick was above the limit of quantification measured in a 1:100 dilution and though not reported. A concentration of 4914.8 ng/mL plasma was measured in previous experiments originating from the same sample. That would rank the sample slightly above the qEVoriginal 35 2 GEN sample but below the qEVoriginal 35 sample, which is the qEV column showing the highest amount of HDL contamination. The

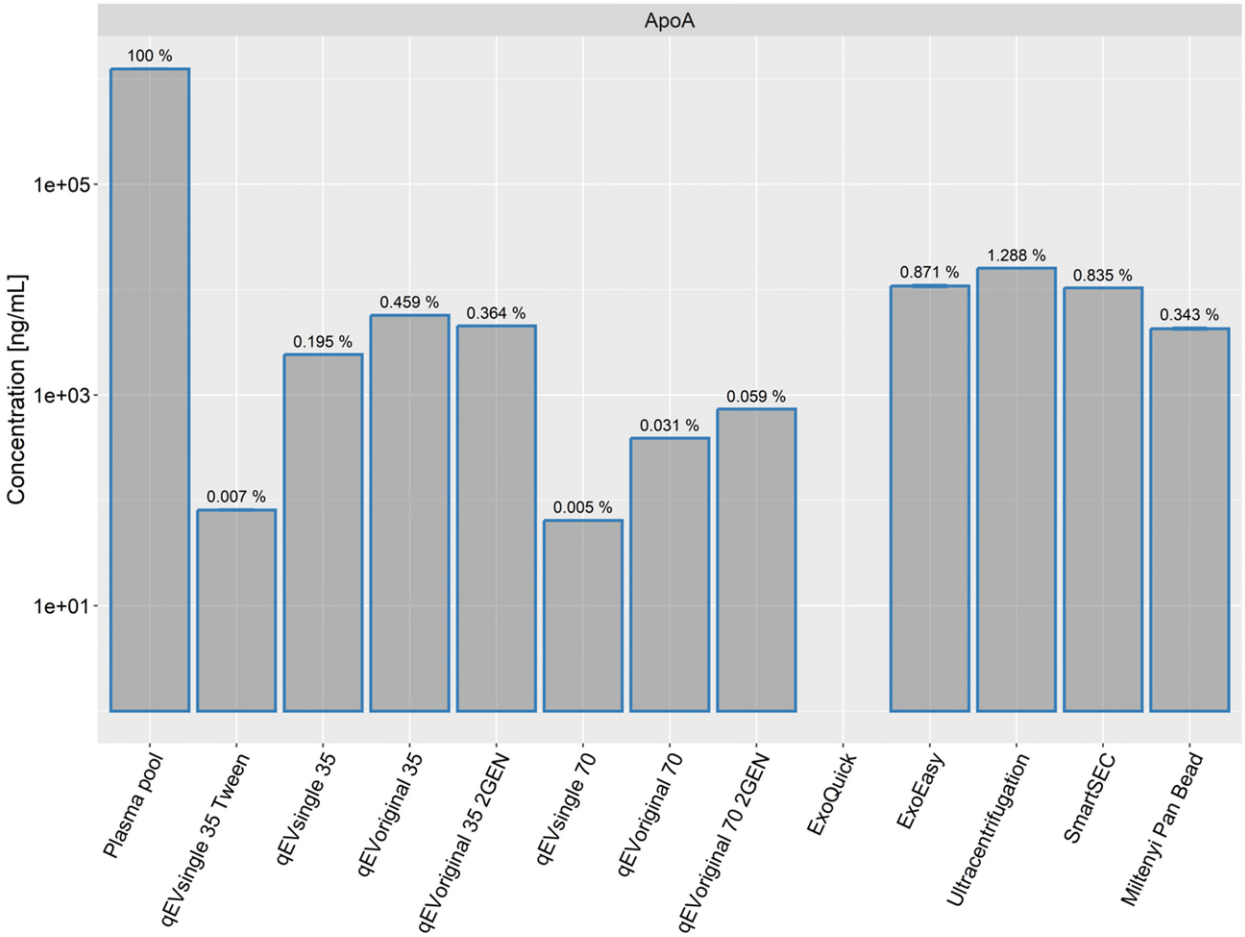

Figure 20 – Enzyme-linked immunosorbent assay (ELISA) based quantification of apolipoprotein A1 (ApoA) in plasma pool as well as isolates of extracellular vesicles (EVs) based on the methods qEVsingle 35 Tween, qEVsingle 35, qEVoriginal 35 2GEN, qEVsingle 70, qEVoriginal 70, qEVoriginal 70 2GEN, ExoQuick, ExoEasy, Ultracentrifugation, SmartSEC, and Miltenyi Pan Bead. The concentration is normalized to the plasma input volume. The sample measurement was repeated twice, and their mean is indicated by the bar height, as the standard deviation is

levels of qEVsingle 35 Tween and qEVsingle 70 are low (81.0 and 64.5 ng/mL plasma) and would indicate a depletion factor of more than 15,000-fold. Again, the Miltenyi Pan Bead isolation is not as pure as the qEV 70 columns and depletes 99.66 % of the HDL.

Apolipoprotein B100

Low-density lipoproteins have been indirectly quantified by the presence of its backbone protein apolipoprotein B100 by ELISA (Figure 21). The concentration in the precleared plasma sample was at 1.27 µg/mL. The data from the isolated EVs indicate a high co-purification of LDL when using size exclusion-based methods. The EV sample with the highest contamination is SmartSEC with 30 % residual ApoB100. The qEV-35 column also co-purifies between 2 and 8 % of the ApoB. The 2 % remnant protein can be found in the

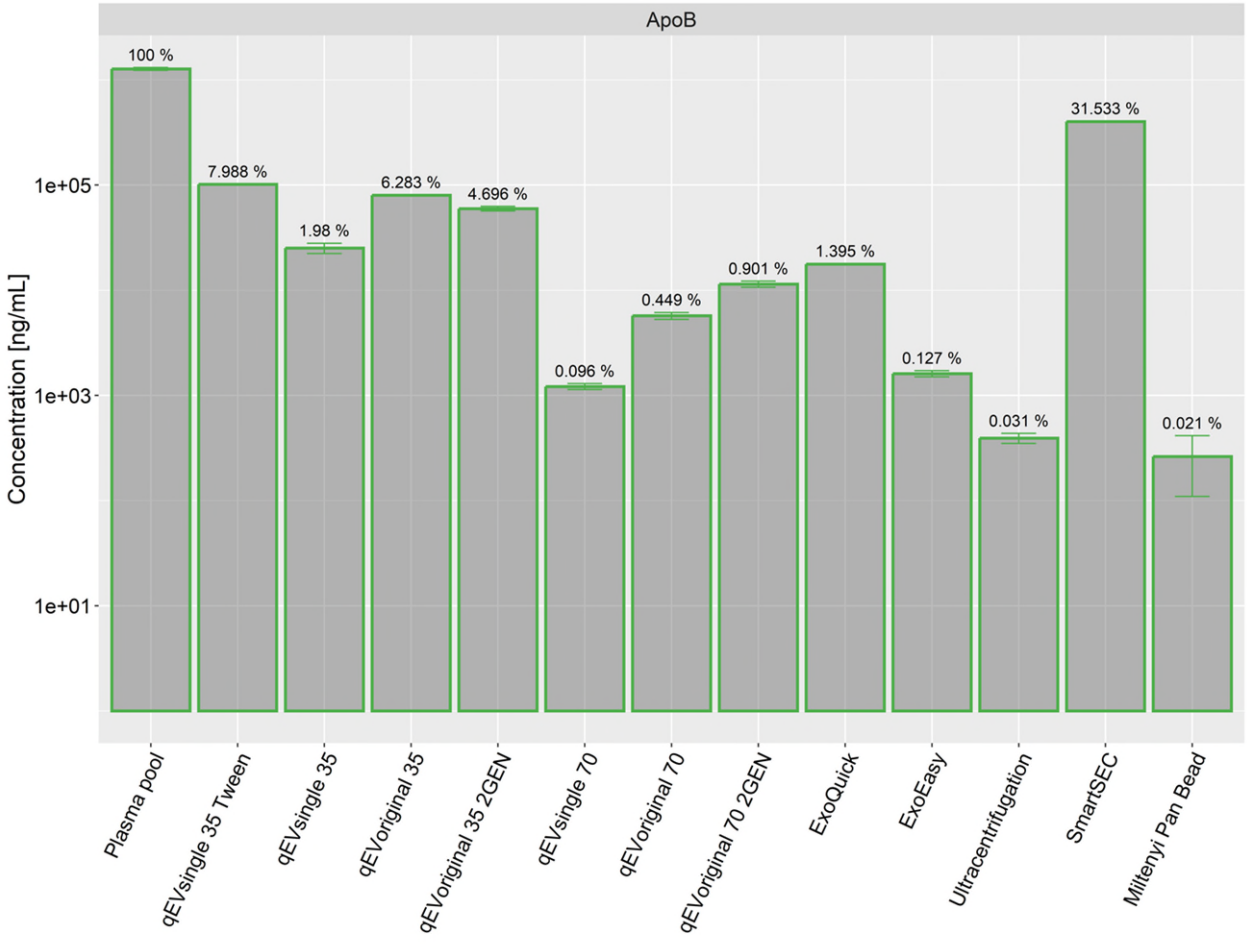

Figure 21 – Enzyme-linked immunosorbent assay (ELISA) based quantification of apolipoprotein B100 (ApoB) in plasma pool as well as isolates of extracellular vesicles (EVs) based on the methods qEVsingle 35 Tween, qEVsingle 35, qEVoriginal 35 2GEN, qEVsingle 70, qEVoriginal 70, qEVoriginal 70 2GEN, ExoQuick, ExoEasy, Ultracentrifugation, SmartSEC, and Miltenyi Pan Bead. The concentration is normalized to the plasma input volume. The samples measurement was repeated twice, and their mean is indicated by the bar height as the standard deviation is

qEVsingle 35 method, whereas the addition of Tween-20 leads to an enhanced co-purification with 8 %. The ExoQuick method contains 17.7 µg/mL plasma, which is still 1.4 % of the plasma LDL. In contrast to the other methods, the ExoEasy, Ultracentrifugation, and Miltenyi Pan Bead method are good in depleting HDL with residual protein of 0.12, 0.03 and 0.02 % from plasma.

Western Blot negative marker

The appearance of common negative markers was analyzed by western blot analysis (Figure 22). First, impurities originating from other cellular components than EVs like GM130 and Calnexin could not be identified in any of the purified plasma samples. The same is true for the plasma sample itself, indicating that these contaminants do not play a critical role in the case of plasma EVs. Second, the highly abundant plasma proteins ApoA and ApoB already quantified by ELISA have been proven in high relative quantities in some of the purified samples. Due to the low protein concentration, the amount of

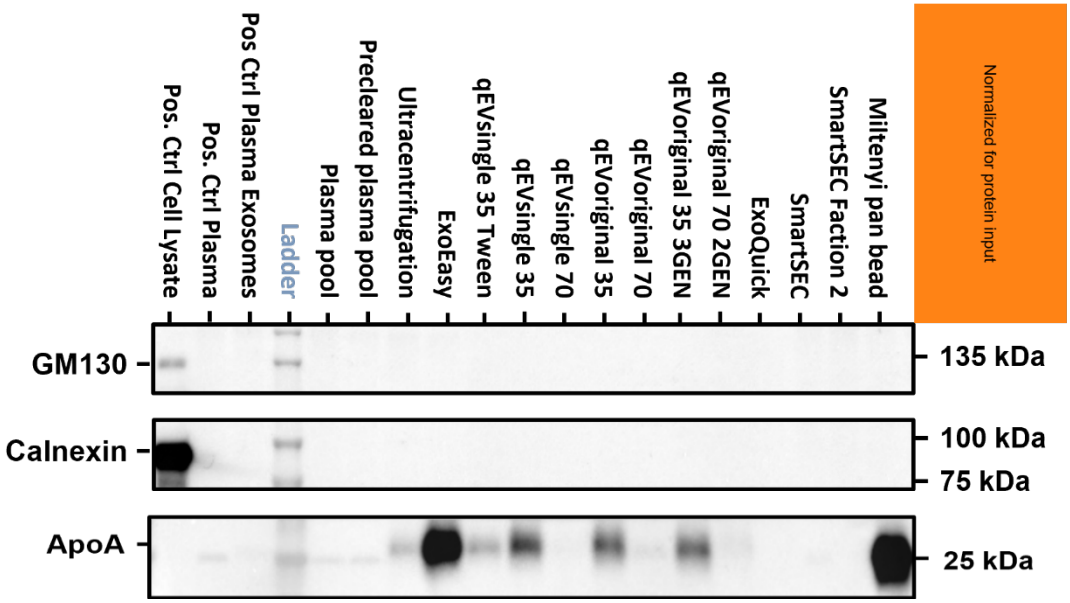

Figure 22 – Western blot images from the analysis of impurities in different extracellular vesicle (EV) isolates originating from healthy human plasma. The positive controls were further defined in Table 6. The sample input for the plasma, precleared plasma, and plasma EV isolates (Ultracentrifugation, ExoEasy, qEVsingle 35 Tween, qEVsingle 35, qEVsingle 70, qEVoriginal 35, qEVoriginal 70, qEVoriginal 35 2GEN, qEVoriginal 70 2GEN ExoQuick, SmartSEC, SmartSEC Fraction 2 and Miltenyi Pan Bead were normalized for total protein input. The markers Golgi matrix protein 130 (GM130), calnexin, and apolipoprotein A (ApoA) were investigated.

loaded Miltenyi Pan Bead sample was very high. Here, a high relative ApoA level can be observed.

3.1.1.5.Summary co-purification of non-EV material

Assessing co-isolation of plasma proteins and lipoproteins offers evaluation of the co-purification of non-EV material and, thus, purity of the implemented EV isolation methods.

When comparing the ELISA results from the different measured impurities, there is a constant trend for the non-lipoprotein analytes. The correlation analysis (Figure 23) reveals the measurement of the total protein concentration already reveals the same trend as the quantification of IgG and albumin. Thus, their quantification does not favor the decision of which isolation methods performs best.

In contrast, the measurement of the different lipoproteins indicates a co-purification of specific subtypes dependent on the isolation method.

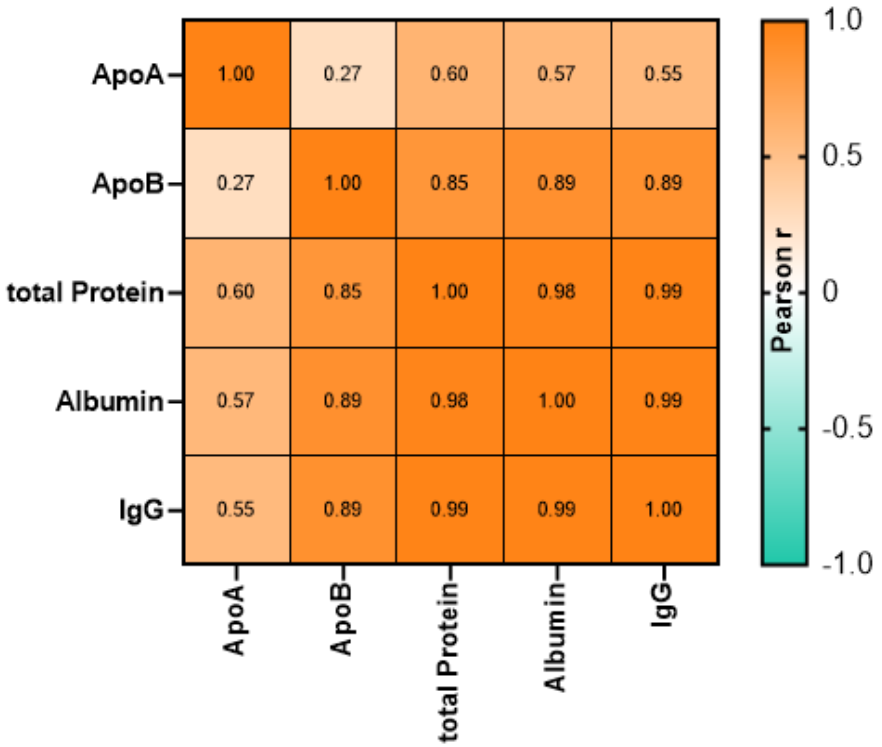

Figure 23 – Correlation matrix based on the quantification of apolipoprotein A1 (ApoA), apolipoprotein B100 (ApoB), total protein, Albumin, and Immunoglobulin G in the different plasma extracellular vesicle (EV) isolations. Pearson R was calculated based on the mean values of each quantification method and the EV isolation method.

Next, the markers summarized in *Summary of TSPN-based EV characterization* are normalized to total protein (BCA) to improve the comparability of the different readouts of the EV characterizing methods taking the detected impurities into account (Figure 24). This helps with the selection of the superior sEV isolation methods and allows the visualization including one source of impurities. Here, we again see a high yield and good purity in the qEV35 columns. Interestingly, with the western blot results, the Miltenyi Pan Bead isolation outperforms the other Isolation methods by the appearance of CD9 and Flotillin-1, whereas CD81 is relatively low. That might be an artifact of enrichment methods that allows the lysis of EVs but not the detachment of the captured proteins from the antibodies. Since the immunoaffinity-based isolation does not allow the later characterization of the intact EVs, the other characterization methods are either not feasible or do not give accurate readouts. Ultracentrifugation and SmartSEC have been shown to give high yields of EVs that lack purity. Consequently, the normalized results are comparably weak in contrast to the qEV 35 SEC columns. Especially on the NanoView and on the MACSPlex assay, the qEVsingle 35 Tween outperforms the other methods, especially in the determined CD9 positive and CD81 positive vesicle count.

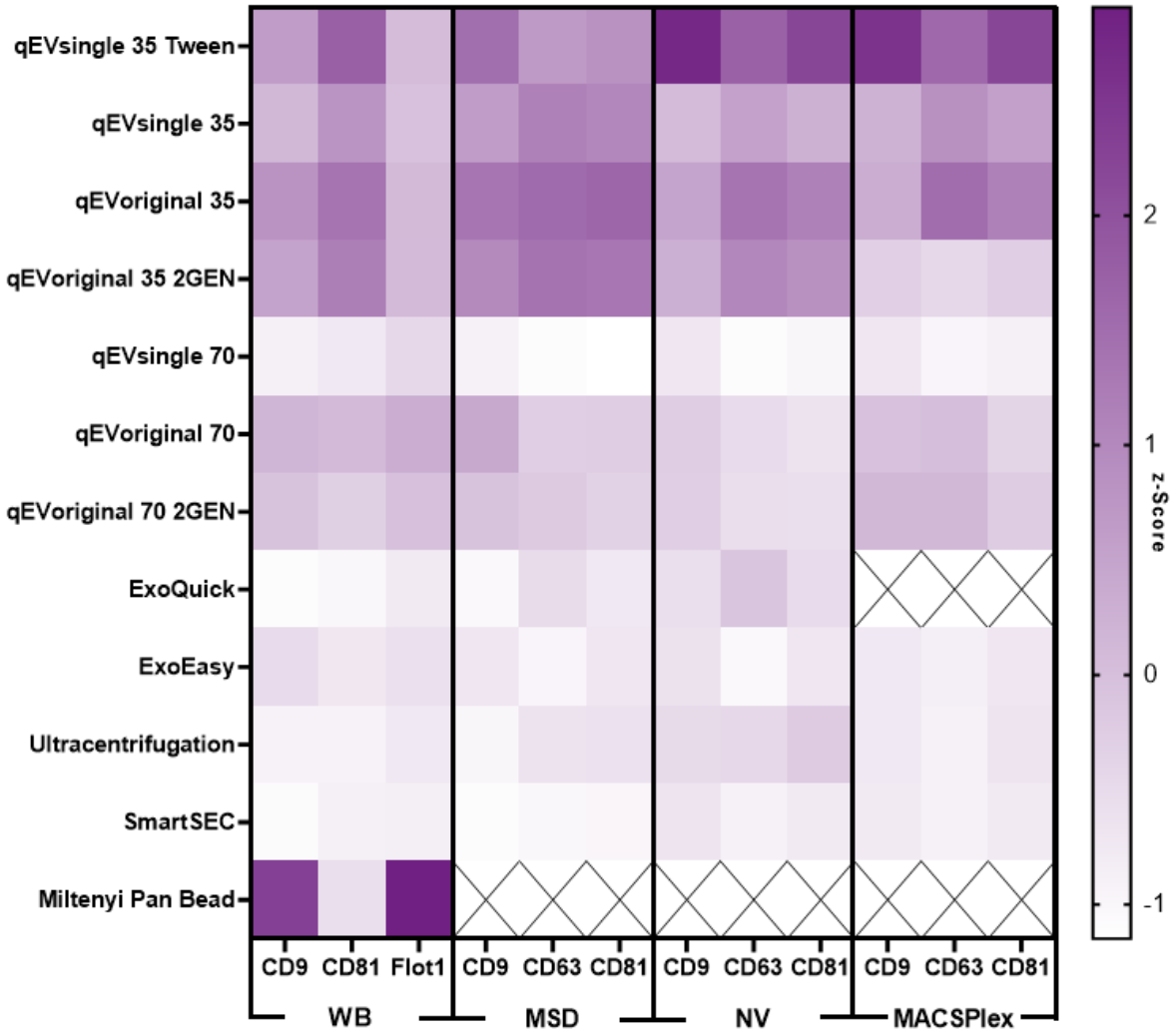

Figure 24 – Heatmap of the z-scored of different quantification methods for normalized EV-marker positive EVs (CD9, CD63, CD81, Flotillin-1 (Flot1)). The analysis is based on Western Blot (WB), Electrochemiluminescence (MSD), NanoView (NV), and MACSPlex. The values were normalized for total protein concentration. The z-score represents for each analyte and method the mean of all the tested methods (z-score = 0) and the number of standard deviations from the mean (+1 standard deviation from mean ≙ z-score = 1) and is indicated by coloration (purple). Invalid or missing results are indicated by an "X".

3.1.2. Discussion

The comprehensive analysis of different isolation methods should help to identify those with high throughput, purity, and yield. These requirements should be weighed against each other to define the methods with a beneficial compromise that can be used to analyze clinical samples. Three tested methods should be selected to further evaluate and test for reproducibility. Additionally, the characterization methods should be compared to evaluate their significance, throughput, and applicability. Since the sample volume for

experiments in the second and third parts of the experiment is limited (450 – 500 µL per sample), the sample input volume should still be sufficient for an extensive characterization. The three sEV isolation methods that outperformed the others, especially in yield, are Ultracentrifugation, SmartSEC, and qEVsingle 35 Tween.

3.1.2.1. Particle size distribution – *Major difference between size determination methods and minor difference between isolation methods*

The size determination of the particle isolated is performed by default mostly with the NanoSight, ZetaView (both nanoparticle tracking analysis), or Exoid™ (tunable resisitve pulse sensing) instruments or by dynamic light scattering and by electron microscopy. It should confirm the presence of particles in the expected size range. [119–121]

In this experiment, the particle size distribution was measured using three different methods NanoView, Exoid™, and NanoSight. Even though the data given by the different methods give unequal sizes, all methods indicate a mode in particle size between 47 and 170 nm in diameter. That indicates the presence of small extracellular vesicles [<200 nm] in all the preparations. [121] Since the NanoSight and Exoid™ are not exclusively investigating the size of TSPN-positive vesicular structures but all particles, possible co-isolations of lipoproteins might also fall into the size range. Especially VLDL (very low-density lipoproteins) have been shown to exhibit a size range between 35 to 200 nm. [122] Hence these lipoproteins are prone to be co-isolated by methods like size-exclusion chromatography. To minimize the contamination of the plasma samples with chylomicrons and VLDL, collection from fasted subjects is highly recommended in a clinical setup. [123] Interestingly, our data suggest that the precleared plasma pool samples demonstrate a similar size distribution to the EV isolates in all three methods. This can be explained by the 10 k x g centrifugation (preclearing) that effectively removed bigger particles and vesicles. However, the plasma sample still contains the vast majority of lipoprotein indicating that the size distribution does not provide information about the purity of the analyzed sample.

For the NanoSight methods, the same has already been shown in human serum samples. [74] There, the larger median size of the isolated EVs compared to the raw sample was

explained by a lower number of protein aggregates, LDL, and VLDL that are represented by particles <60 nm.

Similar effects have been seen after the immunoaffinity depletion of ApoB-positive lipoproteins. [124] The sample showing the smallest particle size in the NanoSight measurement is the qEVsingle 35 Tween isolated plasma. Here, the difference to the qEVsingle 35 samples is noticeable. Even though the same column was used, the mean particle size for the Tween method is about 50 % lower, which could be explained by the substitution of loosely associated proteins on the surface of the vesicles by tween. These associated proteins are often referred to as corona. Together with the hydration shell, this alone could explain a shift in diameter up to 40 nm. [125] Since our observed effect is even bigger, other or additional effects might play a role. As a surface-active substance, tween could also interact with the surface of the size exclusion columns. This interaction could potentially reduce pore size and, consequently, lead to an earlier elution of smaller particles. Even though this shift was observable in the NanoSight instrument, the Exoid™ and NanoView show much lower differences between qEVsingle 35 and qEVsingle 35 Tween.

The ExoEasy shows the highest mean diameter in the NanoSight measurement. The abundance of highly heterogeneous-sized particles in the ExoEasy has already been shown by other groups using NTA. [126] While Exoid™ was not able to confirm these findings, NanoView showed a similar shift.

Since the results were very homogeneous within a particle size determination method, none of the isolation methods proved superior. ExoEasy showed comparably big particles in NanoSight and Exoid™ compared to the other isolation methods raising doubt about the method to be used as an sEV isolation method. The NanoSight measurement indicated that the qEVsingle 35 Tween method results in smaller, more uniform particles with a low variation between the three measurements compared to the other isolation methods.

3.1.2.2. Particle quantification – *Inconclusive data due to non-EV particles*

The measurement of the particle concentration can be performed with most methods that are used for size determination. This includes particle tracking analysis and tunable

resistive pulse sensing, which were compared to the EV quantification method NanoView. They should reflect the number of EVs per volume and thus allow further characterization of the isolate. [121, 127] The disadvantages of particle quantification have already been stated in literature. In complex matrices that include aggregates and other structures within a comparable size range, particle quantification might lead to false conclusions. In that case, measuring EVs labeled with genuine EV markers removes the limitations since the read-out should exclude protein aggregates and lipoproteins. [128]

Accordingly, the particle concentration given by the different methods does not benefit the selection of superior isolation methods. The raw plasma sample and the SmartSEC isolation method show the highest number of particles. The impurity of the raw plasma sample and the presence of particles like lipoproteins have been shown. Thus the differences in particle concentration measured by NTA and Exoid™ can not be directly linked to the appearance of vesicles. The NanoView instead shows the number of TSPN-positive particles, but since most of the particles are measured to be smaller than 50 nm in diameter, they are not quantified in the interferometric measurement. Nevertheless, the number of particles measured varies greatly between the different isolation methods, indicating that the chosen method significantly impacts the EV yield and purity. In plasma EV preparations, the measurement of particle quantity is not conclusive.

None of the particle quantification methods help to determine superior isolation methods; still, there might be an informative value in combination with other methods. Nevertheless, SmartSEC shows an overall high particle count in all methods used.

3.1.2.1. TSPN based analysis – *Distinct differences in EV marker profile reveals the yield of the different isolation methods*

The **expression of EV markers** like the TSPNs is used to indicate the presence of sEVs. Since the detection alone is not a reliable read-out, combined with other characterization methods, they are highly informative. Most of the methods used do not quantify the presence of a protein alone but investigate the co-occurrence of multiple molecules. This creates another level of confidence as the expression of soluble proteins or disrupted vesicles is neglected. However, the presence of the EV markers still allows a high level of contamination. [129] The TSPNs, as a commonly used sEV marker, can also be present on

the surface of larger vesicle populations. In contrast to other membrane markers, some TSPNs show a low tissue specificity. [65] Even though none of the TSPNs is present on all sEVs, the measurement of all three TSPNs should reflect the total sEV abundance. [128] In the data analysis, the TSPN are treated equally, although, e.g., CD63 is more specific to exosomes – and thus sEVs – than CD9. [69]

Depending on the characterization method, detecting sEV-markers was possible in all sEV isolations and enabled identification differences between the EV isolation methods. Especially three methods showed an overall increase in the TSPN compared to the other isolation methods. Namely, qEVsingle 35 Tween, Ultracentrifugation, and SmartSEC revealed the presence of EV-markers in various characterization methods.

qEVsingle 35 Tween showed similar results to other qEV 35 columns but higher detectability of CD9, indicating a higher yield for that subpopulation or a better detectability of CD9 in the presence of Tween-20, e.g., by reducing the unspecific binding of proteins (corona) to the vesicles. [130] This effect of tween-20 has not yet been described in the literature and needs to be evaluated further.

The fact that the qEV 35 columns, in general, lead to a higher yield compared to the qEV 70 column is already mentioned in the manufacturer's user manual. They claim an increased yield by a factor of up to three, but with our protocol, the differences were higher, especially for qEVsingle columns. [131] The manufacturer's recommendation to use >5 mL of plasma and an additional concentration step of the isolated sEVs seems exaggerated since we were able to detect EV-markers starting with only 150 µl of plasma with a wide variety of methods, including standard methods like a western blot. Nevertheless, the concentration of the EV preparation might lead to a better detectability of other EV markers like TSG101, CD63, ALIX, and Syntenin via western blot and other ligand-binding assays. These markers were tested in the western blot but did not give a valid signal without additional concentration for any of the isolation methods analyzed.

Comparing the 2nd generation (2GEN) columns to the conventional counterpart (now legacy) did not show an increased yield for the qEVoriginal 35. In contrast, the qEVoriginal 70 2GEN method shows a higher EV yield than the qEVoriginal 70 column.

Besides the yield of the TSPN, isolation method selection is also based on whether the further characterization of EVs can be performed. For example, the **Miltenyi Pan Bead** isolation does not allow the analysis of unbound intact vesicles. Due to that, all characterization methods that require the presence of intact vesicles can not be performed. It also prevents the study of the colocalization of two or more markers and particle size and concentration measurement. Once isolated by immunoaffinity and lysed, the analysis of sEVs is restricted to conventional protein quantification. All other isolation methods give intact vesicles that can be detected in different characterization methods. Conclusively, Miltenyi Pan Beads is not feasible with our established EV characterization workflow.

The **ExoQuick** isolation gave a high false positive signal in the MACSPlex assay. The isotype control beads showed high values. Overall, a high background was observed in the flow cytometer, which might be due to the polymers that were not thoroughly cleaned. Besides this, the overall yield was not as high as the qEV 35 columns. Even in less complex matrices like cell supernatant, the yield of the ExoQuick method has been shown to be low. [132] However, the isolation method comparison by Ter-Ovanesyan et al. found the highest EV yield when using cerebrospinal fluid as an EV source. [128] This shows the immense impact of the biofluid on the isolation strategy.

The **ExoEasy** isolation of plasma EVs results in a low sEV yield, indicated by several EV-marker quantification methods. The filter material itself consists of layers with hydrophilic and hydrophobic properties. [133] The mild interaction of the vesicles with these layers might not be sufficient for a general remaining in the filter. As specified by the manufacturer, the flowthrough was reapplied, but the low yield indicates a high EV loss in that step. Additionally, a buffer exchange was required to reduce the interference of the XE buffer. During this additional filtration step, EVs might have an unspecific binding to the filter unit. According to Vergauwen et al., applying a filter unit with a 10 kDa cutoff might lead to a higher recovery during buffer exchange. [134] These minor variations in the protocol could maybe increase the overall yield, but since a buffer exchange is required for further characterization the manual work per sample is increased a lot. Still, maybe the buffer is compatible with other readout methods reducing the hands-on time

and increasing the yield. Thus, the relevance for clinical sample analysis would be improved. With our EV marker quantification workflow the ExoEasy is not favorable.

Overall, the different EV-characterization methods based on surface markers showed good discrimination between the different isolation methods. The data of the different characterization methods correlated and thus confirmed each other. Like that, the methods helped to evaluate the superior sEV isolation methods. The isolation methods giving the highest EV yield are qEVsingle 35 Tween, Ultracentrifugation, and SmartSEC.

3.1.2.2.Purity of sEV-isolations – *High purity comes with low yield*

The EV yield must be balanced with the amount of non-EV constituents of the plasma that can still be found in the isolated EVs. The concentration of total protein, albumin, IgG, ApoA, and ApoB has been investigated to reflect a subset of possible impurities. Overall, the **SEC columns by IZON** show a good separation of proteins, including albumin and IgG. HDL can also be depleted largely, whereas LDL gets co-isolated. That can be explained by an overlap in the size of the sEVs and LDL, respectively VLDL, particles [135][118]

The separation of sEVs from LDL can be performed by **Ultracentrifugation**, which was nicely demonstrated. [136] The difference in density between EVs (1.06-1.21 g/mL) and LDL (<1.063 g/mL) enables a good separation. Nevertheless, the density of EVs and HDL is widely overlapping, leading to a high co-isolation and, thus, a high concentration of ApoA in the sEV isolated by ultracentrifugation. [74][137] The Ultracentrifugation method also revealed a high concentration of remaining proteins, including albumin and IgG. This trend has also been observed in other ultracentrifugation-based isolation protocols of circulating EVs. [138]

Interestingly the protein impurity was even higher in the **SmartSEC** method. This short size exclusion column was not long enough to separate the EVs from the protein-rich fraction. Even though this method tends to be high in impurities, the method can isolate 96 different samples simultaneously. The yield has been shown to be high, and the technical requirements and hands-on times are low.

Even though the yield of the **Miltenyi Pan Bead** isolation method seems low, the concentration of the remaining total proteins is also deficient. In contrast to the SEC-

based methods, the reduction of the proteins is not specific to their size. Thus, the albumin as the main constituent of the human plasma is more abundant in the bead-based isolation compared to the IZON SEC columns. Simultaneously, the amount of ApoB is much lower compared to all the other methods. This is important to keep in mind if a specific protein is picked for estimating the purity. Even if albumin and total protein correlate well, the normalization to albumin favors SEC-based methods, whereas the normalization by total protein reveals a higher purity of the Miltenyi Pan Bead isolation. The same misconception can arise by normalizing the presence of HDL or LDL. An SEC-based approach favors the co-isolation of low molecular weight proteins and particles like protein aggregates and lipoproteins.

In general, the error source in biomarker concentration determination increases with more protein appearance. Thus, the normalization can be performed by the total protein quantification. In that case, the Miltenyi Pan Bead isolation, and the IZON qEV columns show their full potential. Ultracentrifugation and SmartSEC, which show a high yield, get in the background.

Besides the Miltenyi Pan Bead isolation, qEVsingle 35 Tween gives the highest yield for EV-markers with low protein contamination. This method, which relied on a plasma input of only 150 µL, exceeds the other qEVsingle methods and the qEVoriginal that have a higher plasma input.

Compared with the qEVsingle 35, the Tween method shows a much higher LDL contamination shown by western blot and ELISA. Here a similar explanation as in the EV marker increase can be applied since the LDL particles overlap in size range. The decreased HDL content makes higher total contamination with later eluting proteins unlikely.

The quantification of plasma impurities helps evaluate the quality of the sEV preparation. Even though the results overlap for the highly abundant proteins albumin and IgG with the total protein quantification, evaluating different proteins individually and their depletion is highly interesting. Since many of the methods investigated rely on size, the additional measurement of alpha-2-Macroglobulin as a high molecular plasma glycoprotein (~720 kDa) would have shown the efficiency and limitations of size-based separation. [139]

All qEV 35 columns show an advantage when normalizing for the total protein. Miltenyi Pan Bead isolation also shows superior results in the western blot analysis. Nevertheless, the readout also revealed the co-isolation of lipoproteins for the isolation methods with a high yield. If a very pure EV isolate is required a Miltenyi Pan Bead enrichment might be superior. It depends on the biomarker and the assay if the impurities effect the readout.

3.1.2.3. Summary Isolation methods comparison

The methods that should be further investigated are the ones with the highest EV yield, namely Ultracentrifugation, SmartSEC, and qEVsingle 35 Tween.

Since **qEVsingle 35 Tween** shows the best compromise between yield and purity and is expected to have similar errors and pitfalls to other qEV-based methods, this method was further characterized. It shows a high sample throughput and does not require expensive instruments or a high level of experience and practice from the operator.

Ultracentrifugation yielded a high presence of EV markers, but there are some doubts about the method. This includes the appearance of impurities and whether ultracentrifugation generates aggregates or even disrupts the vesicles by the applied force. [123, 140] Still, this method is quite commonly used in the field and can be of interest on many occasions. Thus, if this method is reliable and reproducible it should be further investigated.

The **SmartSEC** is the fastest method enabling a much higher sample throughput than other methods. The interest in reproducibility and robustness is high since the columns are very short, so slight variations in handling might lead to considerable deviations in the composition and yield. If the method is capable of further analysis of biomarkers depends on the biomarker. If, for example, a biomarker is present in a soluble form in human plasma, there is a need to deplete the majority of the proteins that are non-EV bound. In this case, the SmartSEC method will be detrimental since the soluble form will likely be included in the EV preparation. If this is not the case, there might be a need for a fast method with high EV yield and high but not relevant impurities.

A comprehensive analysis of the vesicle isolates with many standard methods, and a comparison with new approaches for EV characterization have been performed.

Nevertheless, the analytical workflow misses methods like electron microscopy. Even though the method is barely quantitative, it is still considered the gold standard for verifying the presence of EVs and determining their size and morphology. [141, 142] It would give additional insight into the size determination methods used and which is more reliable. A systematic analysis of different isolation methods performed by Bachaurski et al. (2019) included transition electron microscopy in their evaluation and the NanoView, NanoSight, and ZetaView. Their analysis shows the same deviation in median size between the NanoSight and the NanoView results in serum EV preparations by ultracentrifugation. Here, the electron microscopy data show greater similarity with the NanoView results with a peak maximum close to 50 nm. [127] The results presented in this publication are nicely confirmed in this study. Still, the great variety of the EV preparations analyzed, concerning, e.g., protein and EV concentration and viscosity, could also lead to variability in the visualization of the EVs by electron microscopy [91]. Another disadvantage of electron microscopy is the low throughput and the elaborate analysis, which prohibits its use in a clinical setting.

The selection of markers analyzed by western blot in detail and presented was performed by the feasibility. Additional EV markers, including CD63, ALIX, TSG101, and Syntenin were tested, but the read-out was inconclusive in plasma EV preparations. Since the sample volume was one of the limiting factors of the analysis, a concentration of the sample to enhance the detectability was not possible. Also, the EV loss during the enrichment step would have been detrimental to the interpretation of the Western Blot data.
Nevertheless, the characterization is primarily based on the TSPNs as analyzed by Western Blot, MACSPlex, NanoView, and MSD. The focus on these markers is reasonable since they are widely expressed and commonly characterized. [128] Still, the read-out might favor the isolation methods that specifically enrich these TSPNs, namely Miltenyi Pan Bead isolation. As the other methods focus on other common properties of the EVs, the TSPN read-out is a reliable source for the comparison of isolations from the same origin. Here, the determination of the yield should in theory, be transferable to other EV markers.

3.2. Part 2 – Reproducibility of superior EV isolation methods

3.2.1. Results

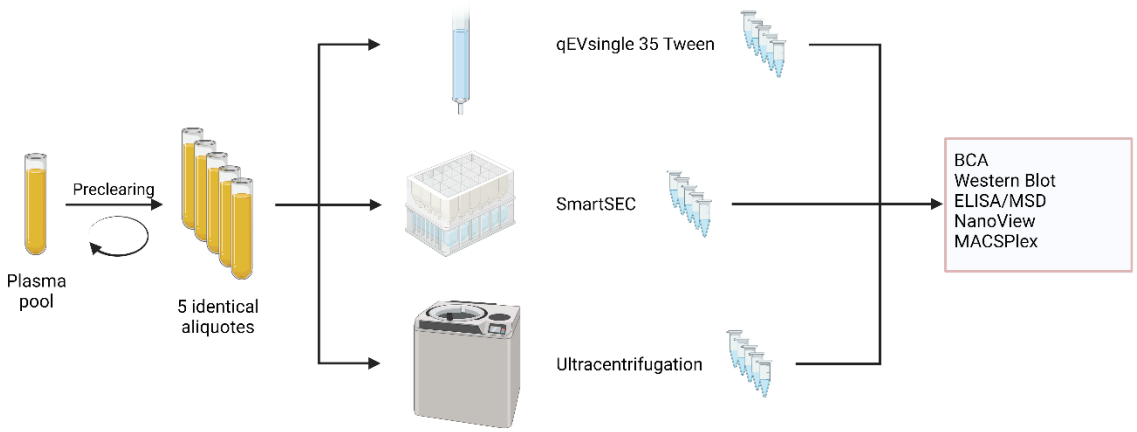

Figure 25 – Schematic workflow for analyzing the reproducibility of the methods qEVsingle 35 Tween, SmartSEC, and Ultracentrifugation. The samples originate from the same healthy human plasma pool precleared by sequential centrifugation and aliquoted prior to extracellular vesicle isolation. For each method, five aliquots were isolated. The isolated samples were analyzed based on the listed characterization methods.

Aim of Part 2 – Reproducibility of superior EV isolation methodsis to test the reproducibility of the superior EV isolation methods. Therefore, the methods chosen in part 1 were performed five times in a row. The sample material originates from the same plasma pool as in *Part 1 – Isolation method feasibility.* Several aliquots have been used to perform the plasma pre-clearing. The aliquots were merged again to have an original uniform sample. After a mixing step, the sample was aliquoted and frozen at -80 °C until the sample was processed further. The five isolations have been performed for each isolation method according to the protocols. After the individual samples were aliquoted to 100 µL each, they were frozen until they were thawed for characterization. For further analysis, we decided to perform MSD, Western blotting, NanoView, and MACSPlex analysis for EV marker- or EV-qualification and quantification. BCA for total protein quantification and ELISAs for ApoA and ApoB were used to evaluate lipoprotein contamination. Based on our in-house criteria for experimental assay validation, the acceptance criteria were defined as the following:

> **At least 2/3 of the samples must be within an acceptance interval of ±30 % from the mean of all measured aliquots.**

By the nature of the different characterization methods, we defined the MSD as the most quantitative method based on two significant characteristics. First, the ligand binding assay principle is well-established and has been proven to fulfill the highest criteria in other settings. Second, despite the other methods, the MSD kits come with a EV standard that allows the setup of a standard dilution series and, consequently, a relative quantification with a wide range of linearity for the one marker evaluated.

To distinguish the replicated isolation and the replicated measurement of the same aliquot in the upcoming section, the replicated isolation will be named technical replicate, whereas the measurement of the same aliquot is called repeated measurement.

3.2.1.1. MSD

3.2.1.2. NanoView

3.2.1.3. Western Blot

3.2.1.4. Impurities

total Protein

High density lipoprotein

Low density lipoprotein

3.2.1.5. MACSPlex

3.2.1.6. Summary

3.2.1.1. MSD

The reproducibility data were collected by the MSD assay using the symmetric assays for TSPN detection. Two repeated measurements have been performed to enable the calculation of the variance of the assay alone. The data presented in Figure 26 shows that all three methods were able to demonstrate reproducibility within the preset criteria. All isolations of specific methods were measured within a ±30 % interval from the mean. The most reproducible method is the SmartSEC, which shows a relative standard deviation of only 3.1 % for the CD9-positive EVs. At the same time, the mean relative standard deviation of the measured duplicates is higher in the SmartSEC samples (4.5 %) compared to the other isolation methods (qEVsingle 35 Tween: 1.1 %; Ultracentrifugation: 1 %). The maximum relative deviation for SmartSEC was detected in preparation four at 4.6 %, and

three of the preparations had a deviation from the mean below 1 %. For Ultracentrifugation and qEVsingle 35 Tween, the relative standard deviation is almost equal to 14.2 % for both methods. Nevertheless, the maximum deviation from the mean is 23.5 % for the qEV method, which is higher than the 13.2 % for the Ultracentrifugation. In the case of the CD63 positive EV, the relative standard deviation is 0.6 % for SmartSEC, and all the technical replicates are within a ±1 % error range from the mean. For Ultracentrifugation, the standard variation is 7.5 % with a maximum error of 10.8 % (technical replicate 5). In the case of CD63, the variation from the mean is much higher for the qEVsingle 35 Tween method (CV% = 19.5 %) compared with the Ultracentrifugation method. The qEV method has its maximum error from mean in the technical replicate 5 with 27.1 %, while the rest of the replicates is within the ±20 % range. CD81 showed the highest variation between the technical replicates in the qEVsingle 35 Tween samples with a relative standard deviation of 22.8 %. Ultracentrifugation and SmartSEC replicates show considerably lower standard deviations of 6.6 and 4 %.

Overall, the SmartSEC method shows the lowest variability, followed by the Ultracentrifugation. The least reproducible method is the qEVsingle 35 Tween method based on the MSD-EV-assay. Nevertheless, all methods fit our criteria, meaning that less than two-thirds of the measured technical replicates showed a variation from the mean of less than 30 %. None of the methods showed technical replicates with more than a 30 % deviation. The minimal variation of the characterization method alone gave high confidence that the measured variation of the replicates is not an artifact of the MSD assay variance.

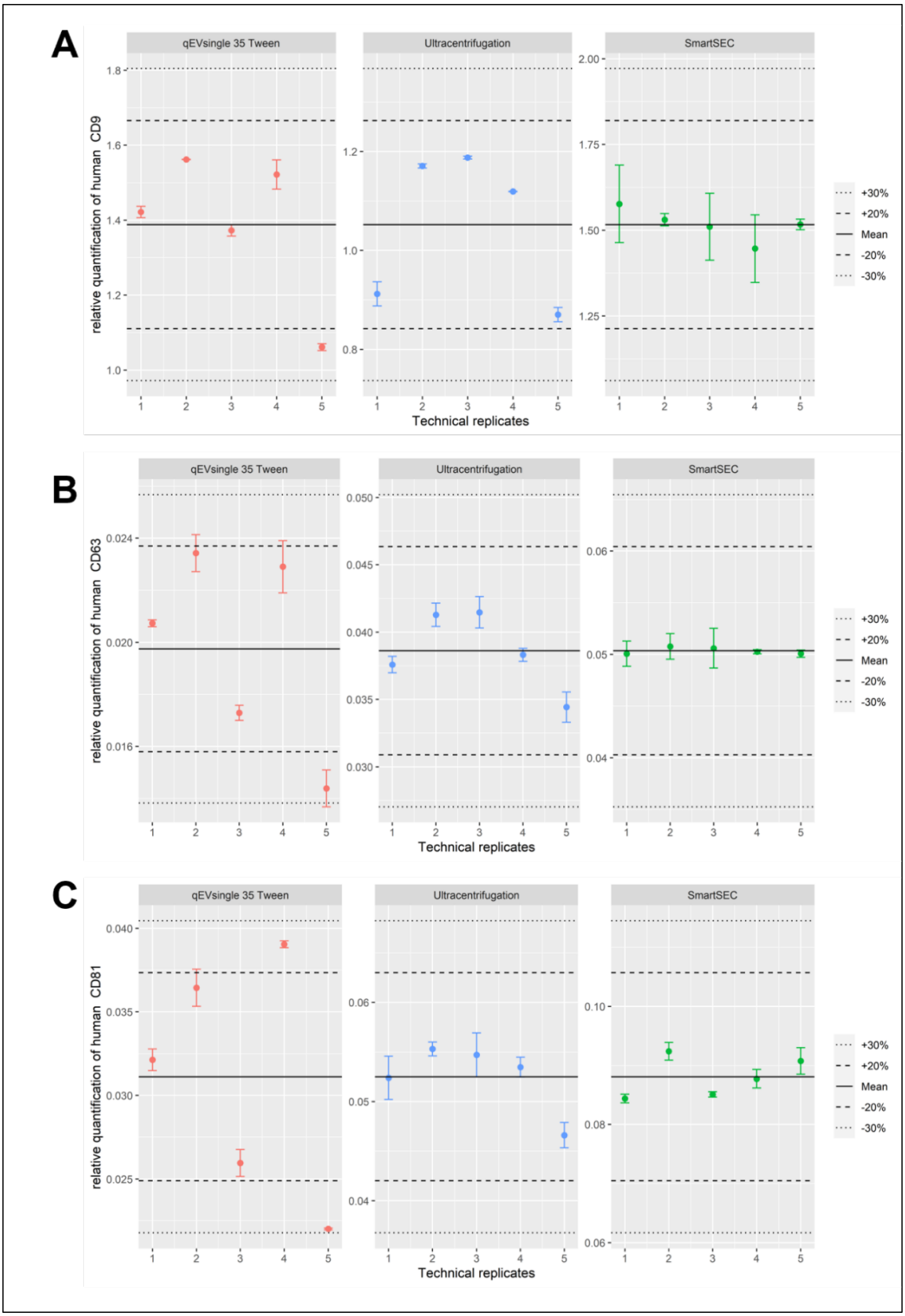

Figure 26 – MSD results for the relative quantification of EV-bound human TSPNs (CD9/CD63/CD81). The appearance of multiple identical TSPN on the surface of one vesicle is required for the analysis. Each dot represents the mean of two repeated measurements from the same sample and the error bars represent the standard deviation. The five dots show the relative quantity of five technical replicates of each isolation procedure. The quantification is relative to a standard of human cell culture derived EVs and the data is normalized to the plasma input volume.

3.2.1.2.NanoView

The characterization and quantification of EVs in the technical replicates of qEVsingle 35 Tween, Ultracentrifugation, and SmartSEC were performed using NanoView analysis.

The results (Figure 27) for the CD9-spot of the qEVsingle 35 Tween samples are above the upper limit of quantification and are not reported. For the other methods, the CD9 results were within a ±30 % error range. Again, the measured error between the different technical replicates is lower in SmartSEC, with a standard variation of 3.4 %. The standard deviation from the ultracentrifugation samples is 8.5 %. For CD63 and CD81, all three methods gave valid results.

The calculated standard deviation for CD63 is 23.6 % for qEVsingle 35 Tween, and the technical replicate five does not fit into the ±30 % error range. Other than that, all samples of the three isolation methods were measured within the range. The relative standard deviation was 12.7 % for Ultracentrifugation and 12.1 % for SmartSEC.

The measurement of CD81 demonstrated that the qEVsingle 35 Tween again shows the highest variation between the technical replicates with an 18.2 % relative standard deviation. Ultracentrifugation and SmartSEC show 7.4 % and 5.7 % much less variation between the replicates. All measured technical replicates fall within the ±30 % margin of error for CD81 across all isolation methods.

Conclusively, the NanoView measurement of the 5 replicates from 3 isolation methods did, like the MSD measurement, fit into our acceptance criteria. Only one replicate of the qEVsingle 35 Tween method was not measured within the acceptance range. The results demonstrate that also the semi-quantitative NanoView method does give coherent data suggesting that the SmartSEC is the most reproducible method, followed by Ultracentrifugation. The qEVsingle 35 Tween isolation is the most error-prone in our setting. Still, all methods revealed reproducibility within our expected criteria.

When analyzing the colocalization data of the TSPN (Figure 28), more CD9-positive EVs can be found in the qEV35 samples compared to the other methods. At the same time, the amount of, e.g., CD81 and CD63 positive EVs is lower compared to the other isolation methods. In contrast to qEVsingle 35 Tween, the other isolation methods show an almost identical colocalization pattern of the TSPNs.

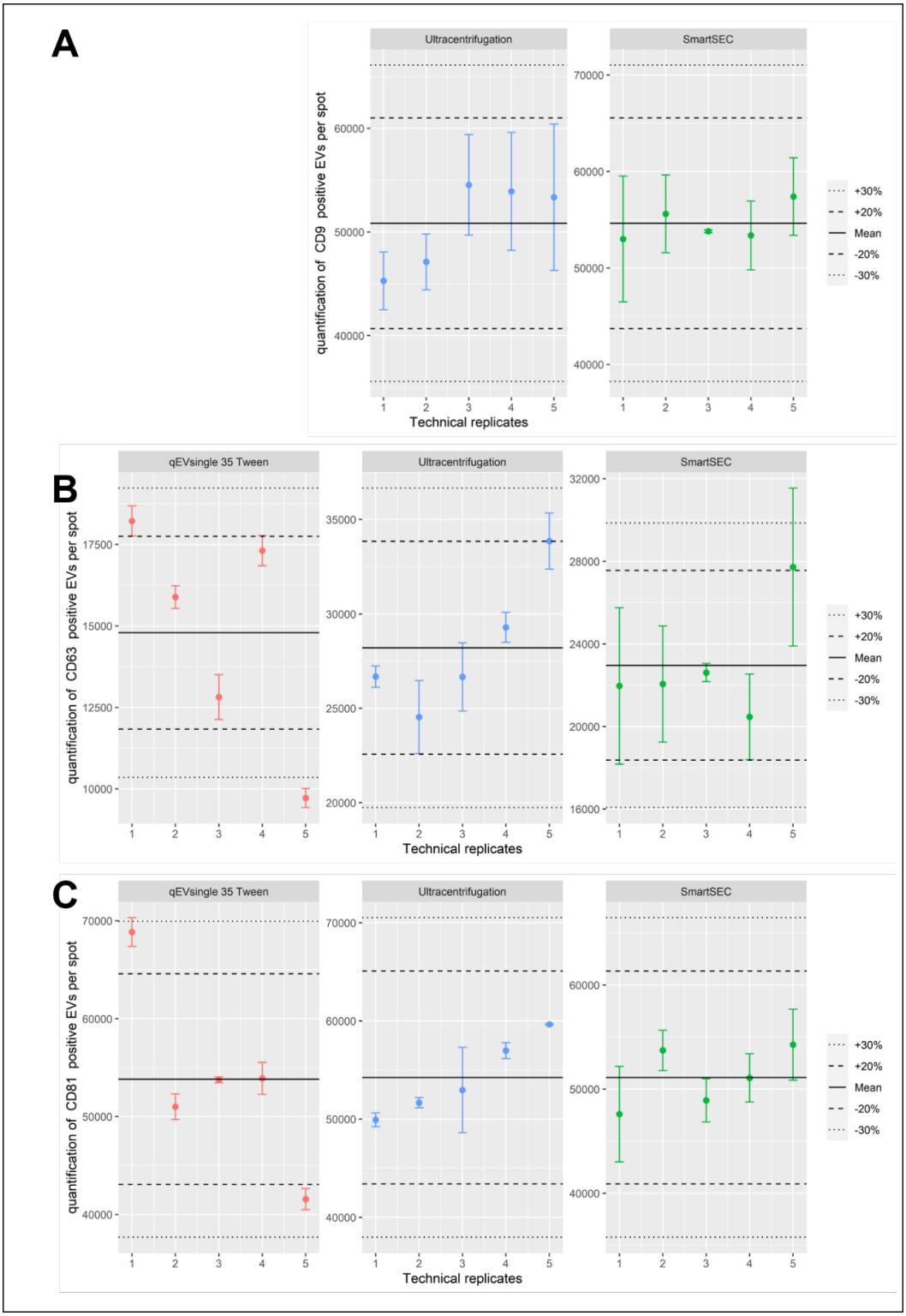

Figure 27 – NanoView-based quantification of extracellular vesicles (EVs) isolated from human plasma pool by three different methods: I) qEVsingle 35 Tween, II) Ultracentrifugation, and III) SmartSEC. The double-positive EVs for CD9, CD63, or CD81 will be captured and stained based on the same antigen. The number of double-positive markers is reported after analyzing five different technical replicates. The dots represent the mean of the three analyzed spots, and the error bar is the standard deviation. Before measurement, all values were normalized for the plasma input and the dilution factor. The solid line indicates the mean of the five measurements, whereas the dashed and the dotted lines indicate a deviation of ±20 % and ±30 % percent deviation from the mean.

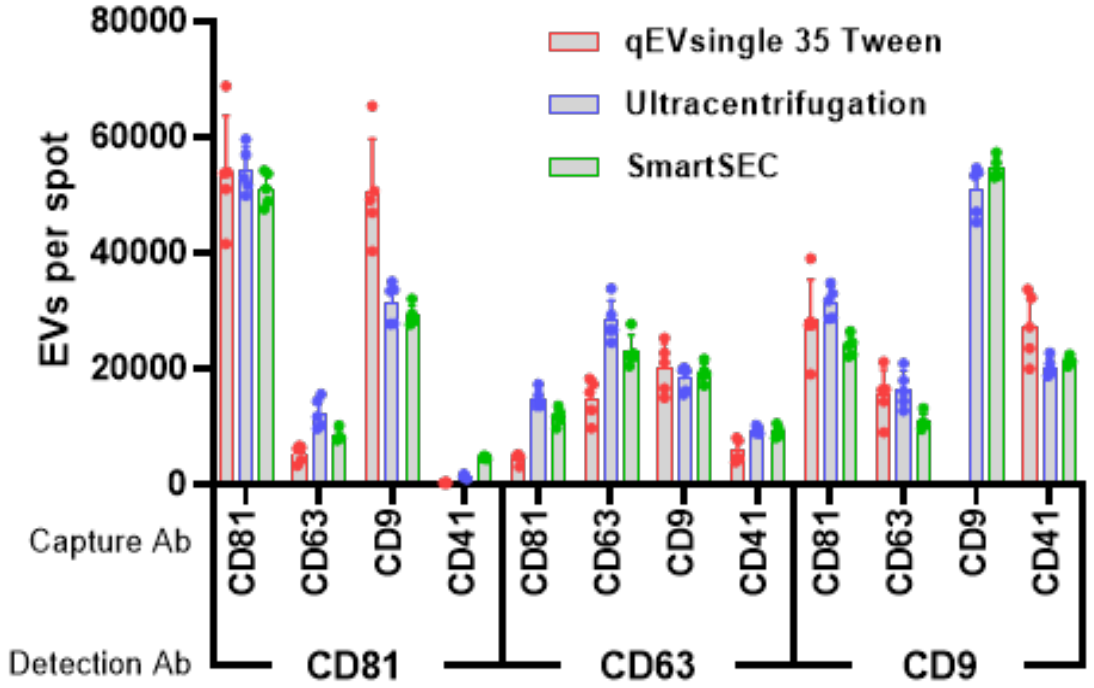

Figure 28 – NanoView-based quantification of colocalization of the different TSPNs and the platelet marker CD41 on the surface of plasma extracellular vesicles (EVs) isolated with qEVsingle 35 Tween column, Ultracentrifugation, and SmartSEC. The individual points represent the mean of three spots analyzed as replicates. Consequently, one technical replicate is illustrated by a point. The bar represents the mean of the five technical replicates, and the error bars represent the standard error. Since the analyzed spot surface is the same for each, the relative amount is comparable and allows relative quantification. The bar for the CD9 double positive EVs is missing because the results where above the limit of quantification. The number of EVs per spot is normalized to the plasma input volume.

3.2.1.3. Western Blot

The semi-quantitative analysis of CD9, CD81, and Flotillin-1 via WB verifies the presence of the markers and allows a comparison of the different technical replicates (Figure 29). Since this method has been thought to be qualitative instead of quantitative, we performed this method in single replicates. As anticipated, the relative quantification shows a much higher variability than other characterization methods. In total, three measurements did not meet the criteria, including the CD9 quantification in the Ultracentrifugation method (A), the CD81 quantification in the qEVsingle 35 Tween method (B), and the Flotillin 1 quantification for the Ultracentrifugation method (C).

Overall, only the SmartSEC method could fulfill the acceptance criteria in all the replicates. Nevertheless, even here, the CD81 quantification showed a much higher variation in

Western Blot analysis compared to other characterization methods. This indicates that with the WB, the variation in the method is significantly higher, which can not be attributed to the isolation error.

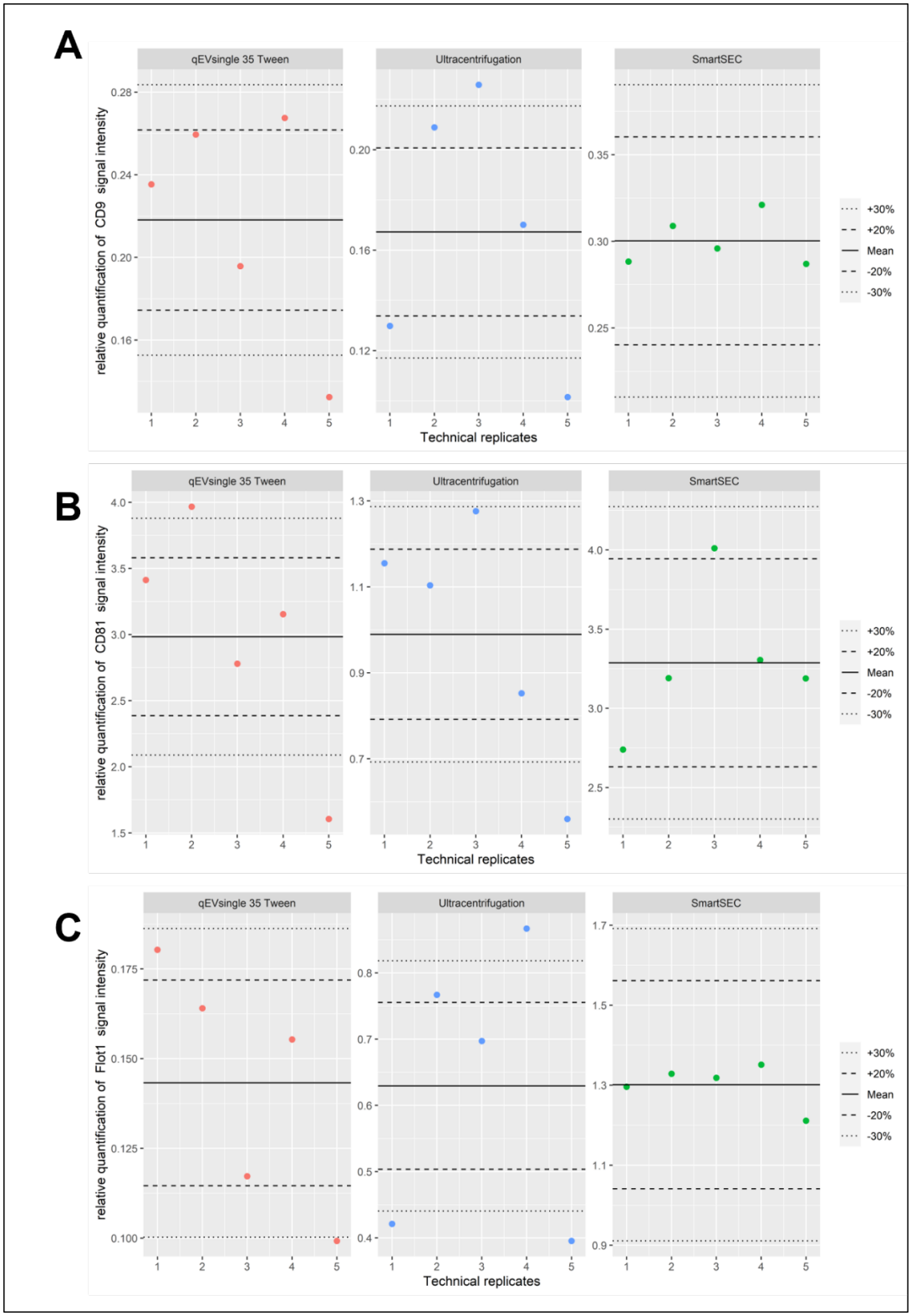

Figure 29 – Relative quantification of CD9, CD81, and Flotillin-1 (Flot1) by western blot analysis in three different isolation protocols (qEVsingle 35 Tween, Ultracentrifugation, SmartSEC).The isolations were performed in five technical replicates originating from the same healthy human plasma pool. The analysis was not repeated; consequently, no standard error can be reported. The solid line indicates the mean of the five measurements, whereas the dashed and the dotted lines indicate a deviation of ±20 % and ±30 % percent deviation from the mean. The data is normalized for the positive controls band intensity of the Exo Standard (Table 6) and the plasma input volume.

3.2.1.4. Impurities

Total protein

The variation of total protein concentration in the technical replicates of the EV isolation methods was estimated by BCA measurement. The BCA results show that the amount of protein is constant within the technical replicates and stays in a ±30 % deviation range from the mean concentration. The absolute mean concentration between the three isolation methods differed significantly and ranged from 265.2 µg/mL plasma (qEVsingle 35 Tween) to 4657.6 µg/mL plasma (SmartSEC). This explains the higher relative error report for the repeated measurement of the qEVsingle 35 Tween. The relative standard deviation between the technical replicates is 12.9 %, which is lower than the Ultracentrifugation methods, which is 21.2 %, but higher than the SmartSEC reproducibility with 6.0 %.

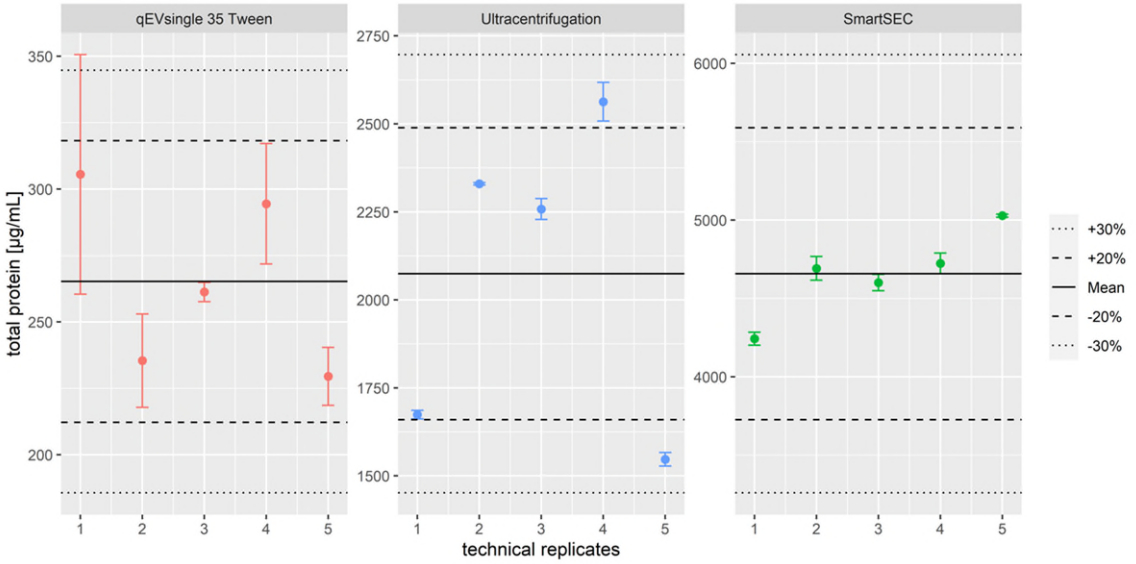

Figure 30 – Amount of total protein determined by BCA assay in isolates from healthy human plasma by qEVsingle 35 Tween, Ultracentrifugation, and SmartSEC methods normalized for plasma input volume. Thus, the values describe the carry-over of the protein from the originating plasma sample in µg/mL. Each dot represents the mean of a measurement repeated twice, and the error bars illustrate the standard deviation between these measurements. The solid line describes the mean on the five technical replicates for each method, and the dashed and dotted lines are a ±20 and ±30 % deviation from the mean.

High-density lipoprotein

The ELISA-based measurement of ApoA1 in the technical replicates of the isolation procedures quantifies the residual high-density lipoprotein. The contamination between

the three isolation methods varies greatly (Figure 31), ranging from 51.9 ng/mL plasma (qEVsingle 35 Tween) to 9072.7 ng/mL plasma (SmartSEC). The mean ApoA1 concentration in the qEVsingle 35 Tween method is 51.9 ng/mL plasma. Technical replicate four has a much higher ApoA1 concentration. Here, the normalized ApoA1 is 79.8 ng/mL plasma. Besides this technical replicate, all further ones are within a ±30 % error range. The relative standard deviation is 34.8 %. Even though the relative standard deviation is smaller in the Ultracentrifugation replicates (27.3 %), two technical replicates are not within the ±30 % error range.

Nevertheless, the criteria we defined are only applicable for the EV markers. Still, the impurity variation might lead to unpredictable effects during sample measurement. The SmartSEC method shows less variation but the highest degree of impurity. The technical replicate with the highest deviation from the mean shows a deviation of only 14.7 %. In summary, the residual high-density lipoprotein contamination differs a lot between the three enrichment methods. The qEVsingle 35 Tween method is most effective in depleting HDL, and the residual concentration in the sample is very low compared to the other isolation methods. Ultracentrifugation and SmartSEC do lead to similar HDL contamination. The contamination is higher in the SmartSEC method and can be quantified more reproducible. Ultracentrifugation combines a high HDL contamination with a high level of variation.

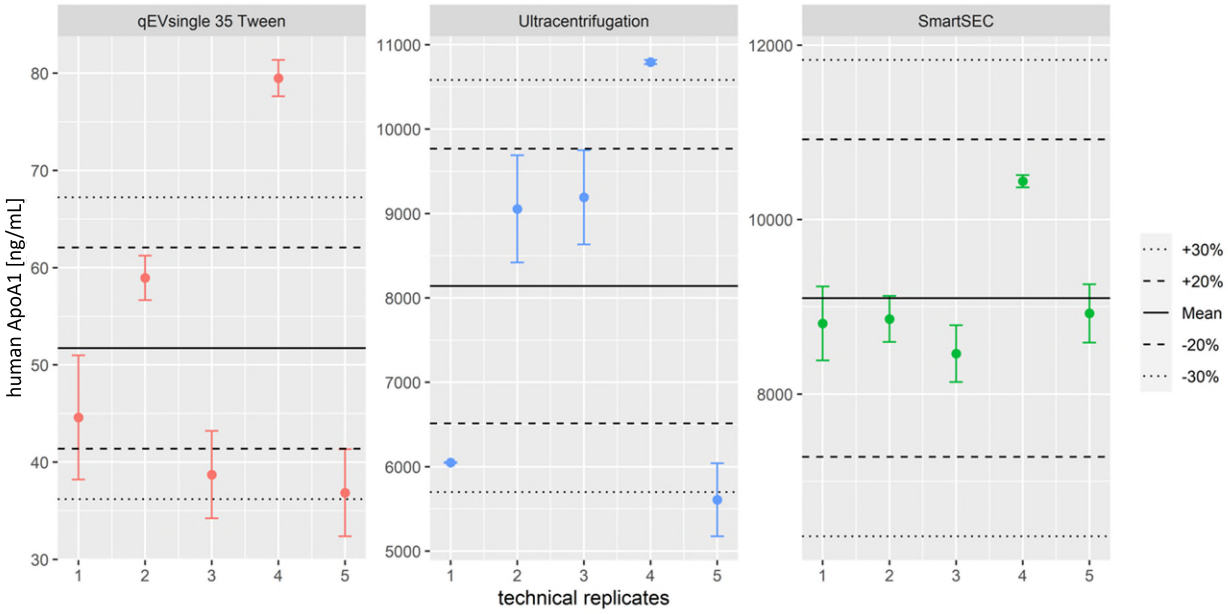

Figure 31 – The normalized amount of apolipoprotein A1 (ApoA1) in isolates from healthy human plasma by qEVsingle 35 Tween, Ultracentrifugation, and SmartSEC methods. The measured concentrations are normalized for the dilution factor during isolation and in preparation for quantification. Consequently, the shown values describe the carry-over of the quantified protein from the originating plasma sample in ng/mL. The solid line describes the mean on the five technical replicates for each method, and the dashed and dotted lines a ±20 and ±30 % deviation from the mean. Each dot represents the mean on a measurement repeated twice, and the error bars illustrate the standard deviation between these measurements.

Low-density lipoprotein

The quantification of low-density lipoprotein (LDL) based on the protein apolipoprotein B100 (ApoB100) is visualized in Figure 32. The depletion factor between the methods is highly diverse, ranging from 168.0 ng/mL plasma (Ultracentrifugation) to 522.2 µg/mL plasma (SmartSEC). The deviation from the mean is highest for the qEVsingle 35 Tween method, which shows a relative standard deviation of 27.1 %. Concerning that, the variety between the replicates is lower in the Ultracentrifugation with a 19.9 % standard deviation. The SmartSEC shows the lowest variation with a relative standard deviation of only 4.8 %. Only one technical replicate of the qEVsingle 35 Tween method is not within the ±30 % error range – it shows a deviation from the mean of 39.1 %.

Succinctly, the Ultracentrifugation samples show the lowest contamination with LDL. Overall, the SEC-based methods SmartSEC and qEVsingle 35 Tween show higher LDL contaminations.

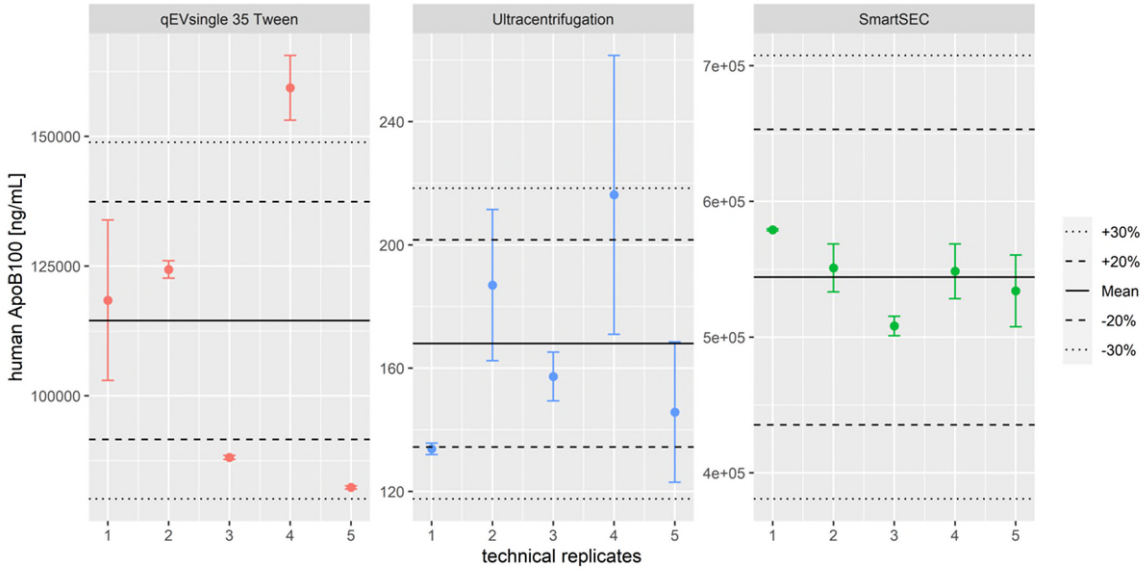

Figure 32 – Measured low-density lipoprotein (LDL) contamination by determination of the apolipoprotein B100 (ApoB100) levels. In the EV isolates from a healthy human plasma pool by qEVsingle 35 Tween, Ultracentrifugation, and SmartSEC, the concentration of ApoB100 is determined by ELISA and reported after normalizing for the dilution factor during the isolation procedure. Thus, the given contamination reflects the amount of residual protein from the originating plasma. For each method, five replicates were measured, and the reported data for each replicate describes the repeated (2X) measurement with the mean (dot) and standard error (error bars). The solid line describes the mean of all five replicates, and the dashed and dotted lines the 20 and 30 % deviation range.

3.2.1.5.MACSPlex

The MACSPlex is a flow cytometry-based method where the median intensity per bead population is used as a semi-quantitative readout. The MACSPlex analysis reveals the reproducibility of the methods investigated based on EV markers and further surface markers (see Table 8). Here the data reported included only the surface markers that gave valid results for all the technical replicates of the three isolation methods (Figure 27). The qEVsingle 35 Tween replicates show the highest variation with a relative standard deviation of 26.4 % for CD9, 32.7 % for CD63, and 33.8 % for CD81. If the acceptance criteria were applicated to the MACSPlex method, only the CD9 quantification would fit. CD63 and CD81 quantification show two technical replicates each that do not fit into the ±30 % error range. The other methods (Ultracentrifugation and SmartSEC) do not show replicates with a high (>30 %) deviation from the mean for none of the TSPN. Here, the mean variation for each analyte lies below 10 %. The TSPN-positive EVs are again high in

the qEVsingle 35 Tween method for CD9 compared to the other methods. Especially CD81 positive EV signals are about twice as high in the Ultracentrifugation and SmartSEC samples compared to the qEVsingle 35 Tween method. On average, the qEVsingle 35 Tween method still shows the highest results for TSPN-positive EVs.

However, since neither the kit comes with a standard curve nor was a dilution test performed with the matrices investigated, the reported results should not be treated as quantitative data. Another limitation of the validity of the results is the absence of repeated measurements due to the high sample consumption and limited sample volume.

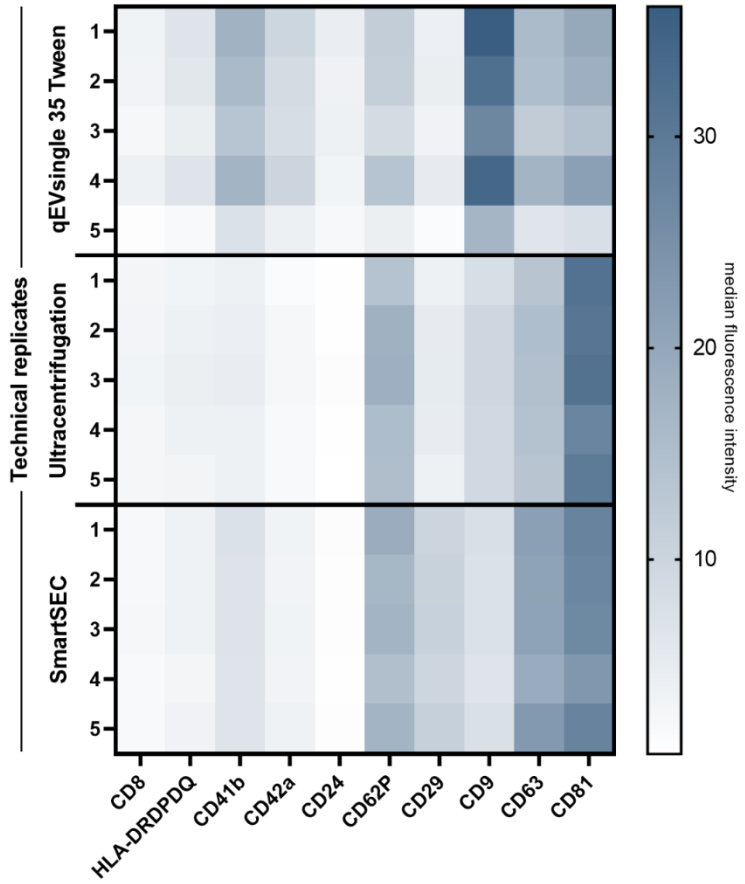

Figure 33 – Heatmap of the semi-quantitative MACSPlex analysis of extracellular vesicles positive for the surface markers CD8, HLA-DRDPDQ, CD41b, CD42a, CD24, CD62P, CD29, CD9, CD63, and CD81. The analysis includes five replicates of each method (qEVsingle 35 Tween, Ultracentrifugation, SmartSEC) originating from the same healthy human plasma pool. The intensity of the blue coloration reflects the median fluorescence intensity for each bead population (analyte). The data were normalized for dilution during the isolation and plasma sample input. The measured data does not include repeated measurements of each technical replicate.

3.2.1.6.Summary

The data in *3.2 Part 2 – Reproducibility of superior EV isolation methods* shows the reproducibility of the sEV isolation methods Ultracentrifugation, SmartSEC, and qEVsingle 35 Tween. All EV marker detection methods reached the acceptance criteria except western blot, meaning the variation of two-thirds of the determined values did not exceed a ±30 % deviation from the mean. Thus, for further experiments the qEVsingle 35 Tween method was picked due to the good compromise between yield, impurities, throughput, and reproducibility.

3.2.2 Discussion

The reproducibility data should allow the identification of methods that fulfill the acceptance criteria. Moreover, it should help to identify pitfalls of the analyzed isolation methods and point out if further method development could improve the reproducibility. Further, the test for variability can improve the understanding of the source of variation and thus, help to identify the critical steps. [134] Once the isolation methods have shown their reproducibility, one method should be further evaluated to ascertain if the method without further optimization can represent interindividual differences. For that the qEVsingle 35 Tween was further characterized since the method provides a good yield, high purity and fits the acceptance criteria.

3.2.2.1. SmartSEC – *Highly reproducible but low purity*

The reproducibility test data suggests a preferential use of the SmartSEC method, as the variation is exceptionally low for the different EV markers. Since this result is unexpected due to the reasons mentioned in *3.1 Part 1 – Isolation method feasibility*, the technological applicability of the method for clinical use seems to be high. Still, the high contamination with plasma proteins restricts the informative value of the resulting isolates. Even after the isolation, there is a tremendous amount of total protein, HDL, and LDL. The technological progress toward single vesicle characterization and EV-specific assay formats allows the question of whether isolation with low specificity is necessary, e.g., for EV surface marker quantification. Here, the measurement of plasma alone already has a good informative value and thus certifies this consideration. For instance,

the CellStream can quantify TSPN-positive EVs in precleared plasma and compared to the qEVsingle 35 Tween isolated EVs from the same sample revealed a good correlation (0.72 < R <0.87) (data not included). Since the SmartSEC sample still comes with a significant loss of sEVs and a potentially unfavorable preselection of EV subpopulations, the raw sample might be the better matrix to work with. Conclusively, the SmartSEC method will not be chosen as the method of choice to proceed. However, it has the potential to be used when high purity is not required for the biomarker analysis. Hirschberg et al. (2022) concluded from their evaluation of the SmartSEC EV isolation that the purity of the isolation is sufficient for further biomarker studies. [143] Since the study was performed with CSF pools and the amount of proteins and lipoproteins is much lower than plasma, SmartSEC might be a suitable method. There is no study published comparing different isolation methods, including the SmartSEC methods, and evaluating the reproducibility.

3.2.2.2. Ultracentrifugation – *Not a gold standard for purifying circulating EVs*

The Ultracentrifugation method results in sEV samples with a higher variation compared to the SmartSEC samples. Nevertheless, it reached the acceptance criteria and revealed good reproducibility in our experiment. Anyhow, equipment and operator seem to impact the outcome significantly, hindering method transfer and data comparability. [144] In our experiments, the degree of impurity is lower than the SmartSEC samples but still exceeds the qEVsingle 35 Tween method. The only exception is the ApoB100, representing the LDL, VLDL, and chylomicrons detected in higher concentrations after qEV isolation. This, together with the apprehensions already stated in *3.1 Part 1 – Isolation method feasibility*, the advantage in reproducibility compared to the qEVsingle 35 Tween method is not sufficient to be used in a clinical sample EV preparation. Baranyai et al. (2015) come to a comparable result using much shorter ultracentrifugation protocols for the isolation of plasma EVs. [138]

The reproducibility results still provide essential information to evaluate data from the literature since Ultracentrifugation is the field's most commonly used EV isolation method. [145] Furthermore, the Ultracentrifugation method has been shown to have many advantages in settings where the samples are less contaminated, e.g., cell

supernatant, and the throughput and sample requirements are neglectable. As such, it can be an essential method during early biomarker discovery.

3.2.2.3. qEVsingle 35 Tween – *Reproducible but improvable*

The qEVsingle 35 Tween method shows a reproducibility that fits our criteria and seems to give purer and better definable sEV-isolations compared to SmartSEC and Ultracentrifugation. Nevertheless, the fact that SEC-based isolation is superior for the isolation of intact plasma sEVs has been stated several times, and often, a combination of methods was suggested to enhance the depletion of the remaining LDL, e.g., by additional ultracentrifugation. [146, 147] Indeed, this sample processing would lead to higher purity, but the applicability is limited. The yield of the combined approach would be reduced, reproducibility lower, and the time requirements would be significantly higher. A method combination approach might be valuable when a biomarker in plasma EVs needs to be verified. There, a manageable number of samples could be purified, followed by targeted or untargeted detection. Another reason the combination might not be feasible is the addition of error that every method would contribute. Since the single-step isolation already shows high variation in the reproducibility analysis for both qEVsingle 35 Tween and Ultracentrifugation, a combination would likely not reach the criteria.

Ter-Ovenesyan et al. (2021) tested the reproducibility of different SEC columns with three types of Sepharose: Sepharose CL--6B, Sepharose CL--4B, and Sepharose CL--2B. Their result indicates a comparable relative standard deviation for CD63 ($CV\%^{(CD63)}$ = 14.9-31.7). In contrast, the deviation of CD9 is higher ($CV\%^{(CD9)}$ = 32.2-57.6) while the deviation of CD81 is lower ($CV\%^{(CD81)}$ = 8-17.8). Even though another assay was used to measure the TSPN concentrations, the results fall into a comparable range. [128]

To enhance reproducibility and detect process errors, an internal standard as a spike-in might be helpful to determine the EV loss during the isolation and thus normalize the result. For example, an EV preparation from another species would be interesting quality control for size exclusion. If this standard would be applicable in a specific experimental setup has to be verified. Here, the EV population used as the internal standard should not

interfere with any downstream characterization methods, particularly the biomarker measurement. Another source of positive control and internal standard might be viruses, virus capsids, nanoparticles, or liposomes. They have a more defined phenotype, and the quantification could be more straightforward. Simultaneously, the size is more uniform compared to sEVs, and there might be a size-dependent error source that the viruses will not display. It is essential to pick a virus within the sEV size range and evaluate the feasibility of the normalization as an internal standard. Geeurickx et al. (2021) were able to show that the normalization based on recombinant EVs reduced the relative standard deviation by 40 % for conditioned medium sEV isolation by differential centrifugation. [148]

Another possibility to improve the reproducibility of the size-exclusion-based isolation might be the weight determination of the void volume and the EV fraction. Since this results in lower throughput and the advantages have not been shown yet, the current method uses the applied volume as a predictor of flow volume. However, available options for weight-based SEC fractionation (IZON, AFC) reduce the sample throughput to roughly two samples per hour and device and lack reliability. A comparison of the reproducibility of both methods has not yet been published.

The qEVsingle 35 Tween method reproducibly isolates sEVs from a human plasma pool and depletes the large majority of proteins and HDL. While the variance observed by MSD and NanoView stayed well within the criteria, the Western Blot analysis showed a higher variation. This seemed to occur due to the technical variation of the Western Blot. However, EV marker detection was possible in all the technical replicates.

3.2.2.4. Impurities – *Acceptance criteria needed?*

Classification of impurity reproducibility data is difficult because none of the isolates exhibited tremendous variability. Nevertheless, the variation in lipoprotein markers is higher in qEVsingle 35 Tween than the variation in EV markers. This indicates a fraction collection close to the peak shoulder of the lipoproteins. Thus, slight changes in the collection volume led to high variations between the technical replicates. Overall, higher deviations of the impurities could indicate an error during the isolation protocol. Setting

acceptance criteria might be beneficial in the future to have internal controls to exclude samples for the analysis.

Interestingly all impurities, including total protein, show the same pattern in the five technical replicates in the Ultracentrifugation samples. These deviations could occur, e.g., during the removal of the supernatant. Since the same pattern can also be observed in the MSD results, an error source might affect all proteins, but the observed impact is lower for the TSPNs.

For the analysis of the interindividual variation of the superior EV isolation method, we chose to continue with the qEVsingle 35 Tween method because it has shown to be the most versatile method with a good compromise of yield and purity, reproducibility, and good throughput.

3.3. Part 3 – Interindividual variation of qEVsingle 35 Tween EV isolation

3.3.1. Results

In *3.1 Part 1 – Isolation method feasibility* and *3.2 Part 2 – Reproducibility of superior EV isolation methods* of this thesis, the feasibility, yield, purity, and reproducibility of different EV isolation methods were evaluated, which identified the qEV35 Tween isolation as the most superior method for EV isolation. The interindividual variation of the qEV35 Tween method is further evaluated based on the EV isolation and characterization of ten healthy human individuals (visualized in Figure 34). The isolation was performed again after the pre-clearing of each plasma sample, followed by the EV isolation by qEVsingle 35 Tween size exclusion procedure. A single isolation was performed since the volume is sufficient for the characterization procedure established and demonstrated in *3.2 Part 2 – Reproducibility of superior EV isolation methods*. Since the variation has been described already, the single isolation best represents a clinical workflow with limited sample volume and required throughput. The characterization was performed according to the *3.2 Part 2 – Reproducibility of superior EV isolation methods*, but no western blot analysis was performed due to the poor reproducibility of the technic compared to the other methods. In addition to the characterization workflow in *3.2 Part 2 – Reproducibility of superior EV isolation methods*, an in-house established flow cytometry-based single vesicle

quantification method (CellStream) was performed on the isolated plasma EV samples. Overall, the variability between individuals should be shown by different methods; additionally, characterization methods should be compared to prove their resolution capabilities, disclose the interchangeability, and verify their reciprocal readouts.

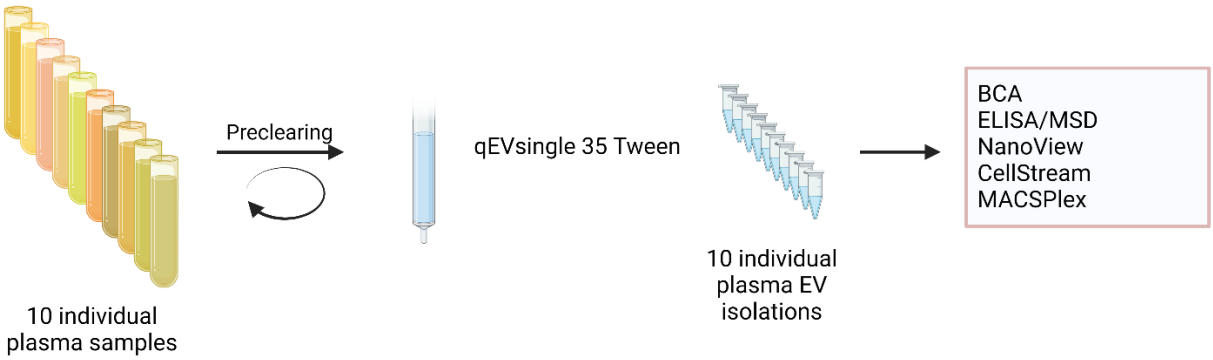

Figure 34 – Experimental workflow to test the interindividual variability in circulating EV composition in a population of ten healthy human individuals. All plasma samples get precleared by a two-step centrifugation protocol, and the EVs are purified by qEVsingle 35 Tween. The Individual EV isolations are analyzed by a set of methods capable of clinical study analysis, including total protein quantification by bicinchoninic acid assay (BCA), quantification of HDL and LDL by enzyme-linked immunosorbent assay (ELISA), quantification of vesicular CD9, CD63, and CD81 by electrochemiluminescence (ECL), the single vesicle characterization methods NanoView and CellStream and the vesicular surface marker panel MACSPlex.

3.3.1.1. TSPN

CD81

CD63

CD9

3.3.1.2. Impurities

3.3.1.3. Summary

3.3.1.4. Analytical variation vs. biological variation

3.3.1.1. TSPN

CD81

The variety of CD81-positive circulating EVs in a homogenous healthy group of individuals can be evaluated by looking at the data from the TSPN CD81 positive EV quantification methods (NanoView, MSD, CellStream, and MACSPlex, Figure 35).

Cross-platform, Individuum (IND) 6 reveals the highest number of CD81 positive EVs in plasma, whereas IND 9 consistently shows weak signals in all assays. The commonalities between the different characterization platforms are valid and can be proven by correlation analysis (Figure 36).

The data from the **MSD** analysis reveals a higher variation between the individuals (relative standard deviation = 42.3 %) compared to the technical replicated (22.8 %) (further evaluated in Figure 43), indicating that the variation is not due to the isolation or analytical variety but results from differences in the individual's EV composition.

The results from the **MACSPlex** analysis show values of 6.2 (IND 9) to 36.8 (IND 6) median fluorescence intensity/mL plasma. The relative standard deviation from the average is 40.1 %.

The **NanoView** shows a relative standard deviation of 49.1 %. IND 6 has the highest values from the ten individuals' mean, which shows 78.6 % more CD81 positive EVs per mL plasma than the mean. The lowest sample measured by the NanoView is IND 10, with only 21.7 % of the average.

The data originating from the **CellStream** can prove its significance by showing a strong correlation (Pearson $R \geq 0.88$) with all other methods. The error bars indicate that none of the methods used are too inaccurate to resolve the sample differences in CD81-positive sEV expressions (not determined for MACSPlex – no replicated measurement). However, the CellStream has the highest variability between the repeated measurements.

In summary, the slight variations between the observed methods indicate either the measurement differences or the appearance of minor experimental variations (e.g., pipetting errors).

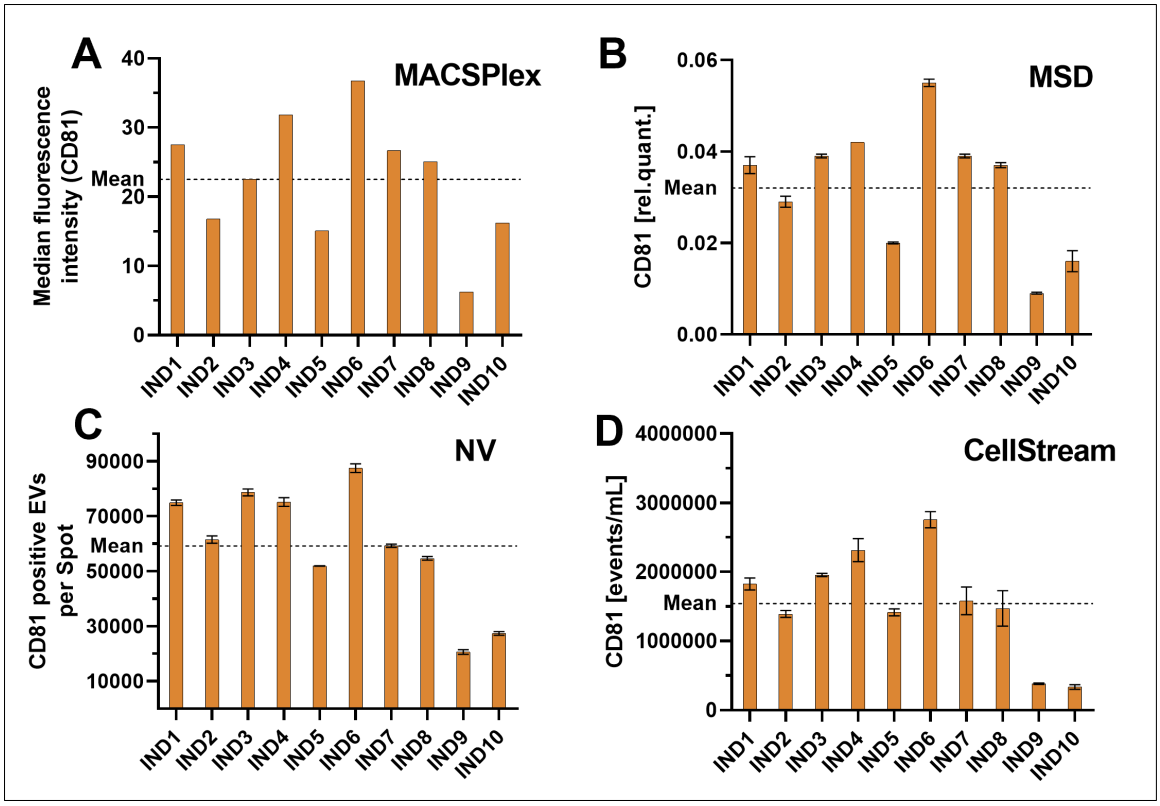

Figure 35 – Quantifying CD81 positive EVs by MACSPlex, MSD, NanoView (NV), and CellStream in ten individuals (IND1-10). In each graph, the average signal intensity of the ten individuals is demonstrated with a dashed line. A) MACSPlex results give a semi-quantitative analysis of CD81 captured EVs stained with a TSPN mix. The measurement was not repeated; thus, the bars indicated the back-calculated median fluorescence intensity of the CD81-coated bead population. B) MSD results reveal the intensity of CD81 on the surface of CD81 captured EVs. Given is the signal intensity relative to a standard of human cell culture-derived EVs. The results were back-calculated for plasma input. The error bars indicate the standard error between the two repeated measurements. C) NanoView results of CD81 positive EVs on the surface of CD81 spot, back-calculated for plasma input. The error bars demonstrate the standard error between the three measured spots. D)The CellStream single EV characterization allows quantifying EVs based on the expression of multiple surface markers (CD81). Multiple staining leads to a recognition of the particle and thus to a counting of the vesicle. The experiment was repeated once on the ten individuals; the standard error is indicated by the error bars. All results are normalized to the plasma input volume.

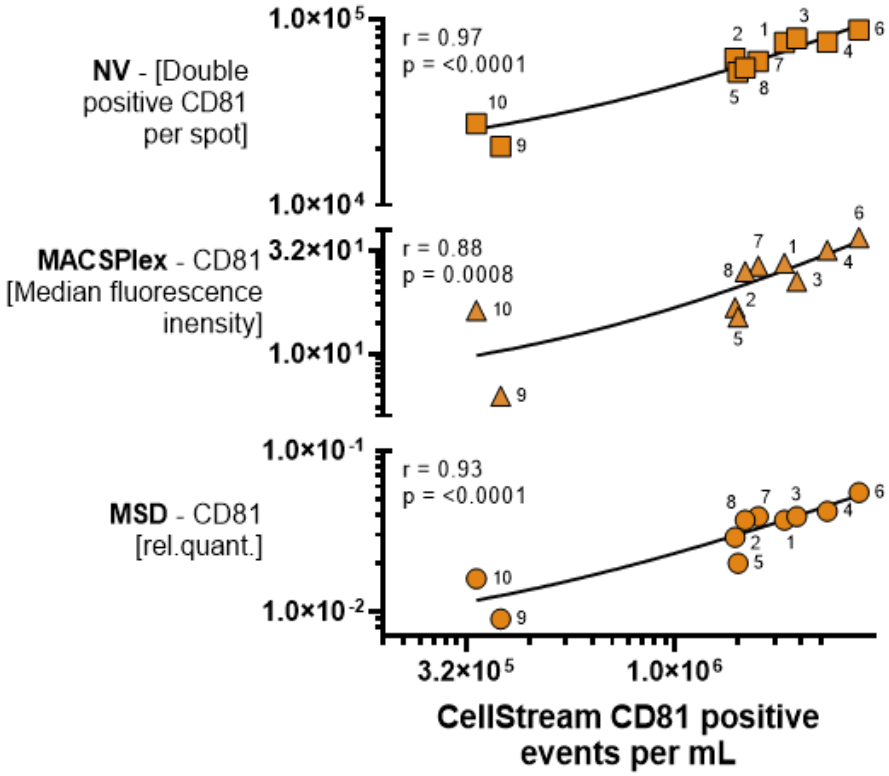

Figure 36 – Correlation analysis of different quantification methods (NanoView (NV), MACSPlex, MSD) of CD81 positive extracellular vesicles (EVs) with the CellStream method. The X-axis shows the amount of CD81 positive events per mL of plasma, whereas the Y-axis gives: top) amount of double positive CD81 EVs per spot measured on the NanoView, middle) the median fluorescence intensity in the anti-CD81 antibody-coated bead population of the MACSPlex kit, bottom) the relative signal intensity of CD81 captured and detected vesicles. The identification number is noted for every individual plasma donor. Pearson R is given from each correlation analysis with p-value and linear regression. The data is reported normalized for the plasma input volume.

CD63

The CD63 analysis of the EV isolates of ten plasma samples reveals a high variation between the individuals (Figure 37). In all methods, IND 2 shows the highest signals for CD63-positive EVs. The variation in the EV composition can be demonstrated by this individual, as it shows low or average CD81 positive EV quantities. IND 5 and 9 constantly have low signals in contrast to the mean, which is congruent with the CD81 results.

For the **MSD**, the mean of all individuals lies at a relative intensity of 0.02, and the relative standard deviation is at 85.7 %. The relative signal intensity of 0.07 can be found in IND 1, which has the highest value for CD63 positive EVs. IND 9 reveals a relative CD63 signal intensity of only 0.005 and thus is the individual with the lowest occurrence. As the

relative standard error between the repeated measurements is low (3.07 % on average), the validity of the quantitative output of the method is high.

The **NanoView** method, which gives the amount of CD63 labeled EVs on the CD63 spot, reports having a mean value between the ten individuals of 13352 CD63-positive EVs/spot. Here, IND 2 is more than three times as high as the mean (3.33-fold higher), whereas IND 9 is 4.66 times lower. Overall, this results in a relative standard deviation of 88.4 %.

The **MACSPlex** data shows a 59.2 % of relative variation from the mean. The IND 2 sample has a 2.66-fold higher value compared to the mean of all individuals that lies at 17 median fluorescence intensity/mL plasma. IND9 has a value of 6.1; thus, it is close to 3-fold lower than the average.

The **CellStream** data shows the highest variability among the individuals, with a relative standard deviation of 89.3 %. With an average of 963679.5 CD63 positive EVs per mL plasma, the values vary within a ±3.3-fold range (IND 2: +3.35x; IND 9: -3.27x).

The correlation analysis (Figure 38) of the CellStream data with the other methods demonstrates a good correlation ($r \geq 0.93$) with all the other methods with an elevated level of significance ($p \leq 0.0001$). Especially for the correlation analysis between CellStream and MSD, Pearson's R of 0.98 reveals a high linear relationship.

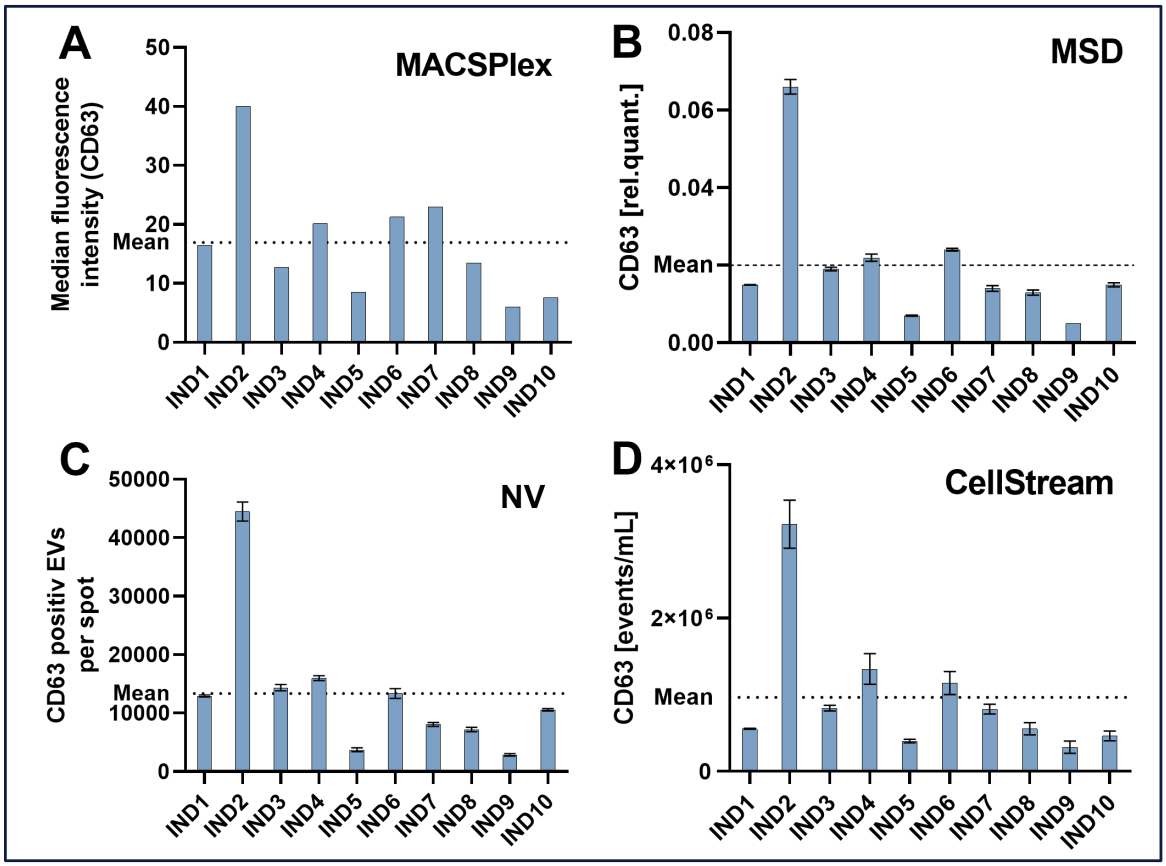

Figure 37 – Quantification of CD63 positive EVs by MACSPlex, MSD, NanoView (NV), and CellStream in ten individuals (IND1-10). In each graph, the average signal intensity of the ten individuals is demonstrated with a dashed line. A) MACSPlex results give a semi-quantitative analysis of CD63 captured EVs stained with a TSPN mix. The measurement was not repeated; thus, the bars indicated the back-calculated median fluorescence intensity of the CD63-coated bead population. B) MSD results reveal the intensity of CD63 on the surface of CD63-captured EVs. Given is the signal intensity relative to a standard of human cell culture-derived EVs. The results were back calculated for plasma input. The standard error between the two repeated measurements is indicated by the error bars. C) NanoView results of CD63-positive EVs on the surface of the CD63 spot are back-calculated for plasma input. The error bars demonstrate the standard error between the three measured spots. D) The CellStream single EV characterization allows quantifying EVs just based on the expression of multiple surface markers (CD9). Multiple staining leads to a recognition of the particle and thus to a counting of the vesicle. The experiment was repeated once on the ten individuals; the standard error is indicated by the error bars. The data is reported normalized to the plasma input volume.

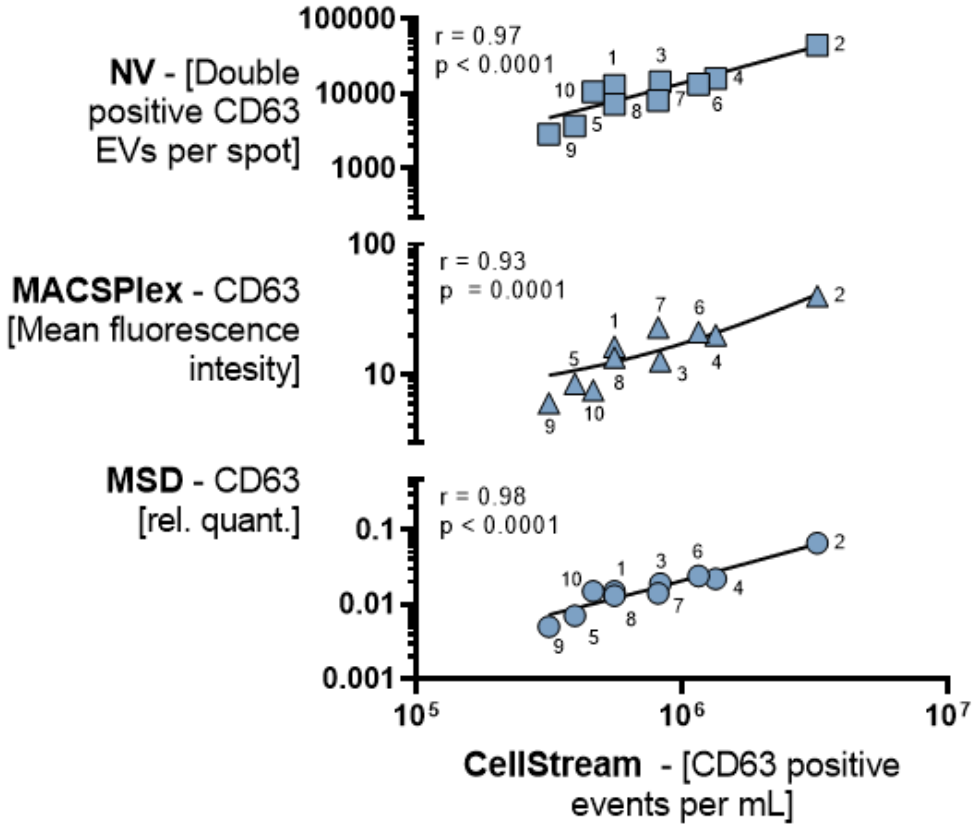

Figure 38 – Correlation analysis of different quantification methods (NanoView (NV), MACSPlex, MSD) of CD63 positive extracellular vesicles (EVs) with the CellStream method. The X-axis shows the amount of CD63 positive events per mL of plasma, whereas the Y-axis gives: top) amount of double positive CD63 EVs per spot measured on the NanoView, middle) the median fluorescence intensity in the anti-CD63 antibody-coated bead population of the MACSPlex kit, bottom) the relative signal intensity of CD63 captured and detected vesicles. The identification number is noted for every individual plasma donor. Pearson R is given from each correlation analysis with p-value and linear regression. All data is reported normalized for the plasma input volume.

CD9

MACSPlex, MSD, CellStream, and NanoView measured the amount of CD9-positive plasma EVs from ten individuals (). The NanoView values of CD9-positive vesicles on the anti-CD9 spot were above the semi-quantitative range. Therefore, the **NanoView** data are not reported. The other methods confirm each other so that IND 2, 6, and 7 show high values for all the methods. Again IND 5 and 9 are comparably low in all the analyses. Interestingly in the CellStream method, IND 10 has the lowest amount of CD9-positive EVs/mL plasma, but the other methods can not confirm that.

MACSPlex data shows a low variation compared to the other TSPN, with only a 33.1 % standard deviation. The average lies at 36.51 MFI/mL plasma and is notably higher than the other TSPNs.

The **MSD** methods demonstrate a variation of 33.8 %, which is close to the result obtained by MACSPlex. The average relative signal intensity of 1.38 is calculated, and the maximal deviations can be measured in IND6 with 2.0 relative signal intensity and IND 9 with 0.8 relative signal intensity.

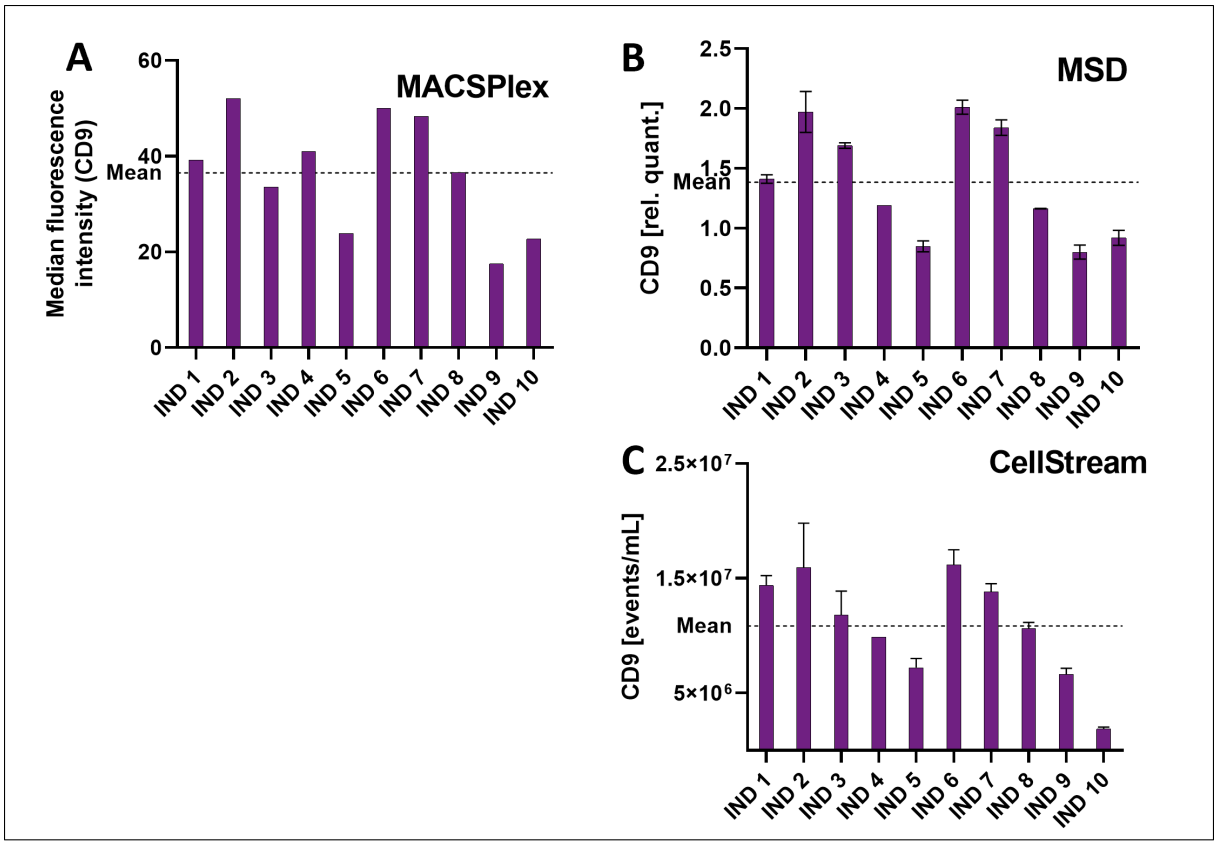

Figure 39 –Quantification of CD9 positive EVs by MACSPlex, MSD, NanoView (NV), and CellStream in ten individuals (IND1-10). In each graph, the average signal intensity of the ten individuals is demonstrated with a dashed line. A) MACSPlex results give a semi-quantitative analysis of CD9-captured EVs stained with a TSPN mix. The measurement was not repeated; thus, the bars indicated the back-calculated median fluorescence intensity of the CD9-coated bead population. B) MSD results reveal the intensity of CD9 on the surface of CD9-captured EVs. Given is the signal intensity relative to a standard of human cell culture derived EVs. The results were back-calculated for plasma input. The standard error between the two repeated measurements is indicated by the error bars. C) NanoView results of CD9-positive EVs on the surface of the CD9 spot are back-calculated for plasma input. The error bars demonstrate the standard error between the three measured spots. D) The CellStream single EV characterization allows quantifying EVs just based on the expression of multiple surface markers (CD9). Multiple staining leads to a recognition of the particle and thus to a counting of the vesicle. The experiment was repeated once on the ten individuals; the standard error is indicated by the error bars. The results is normalized for the dilution factor during EV isolation.

The **CellStream** results show similar CD9 quantities in the ten individuals like the other methods that is also indicated in Figure 42. In contrast to the other individuals IND 10 showed a reduced presence of CD9 positive EVs. Overall, there is still a good correlation between the CellStream and the other TSPN quantification methods.

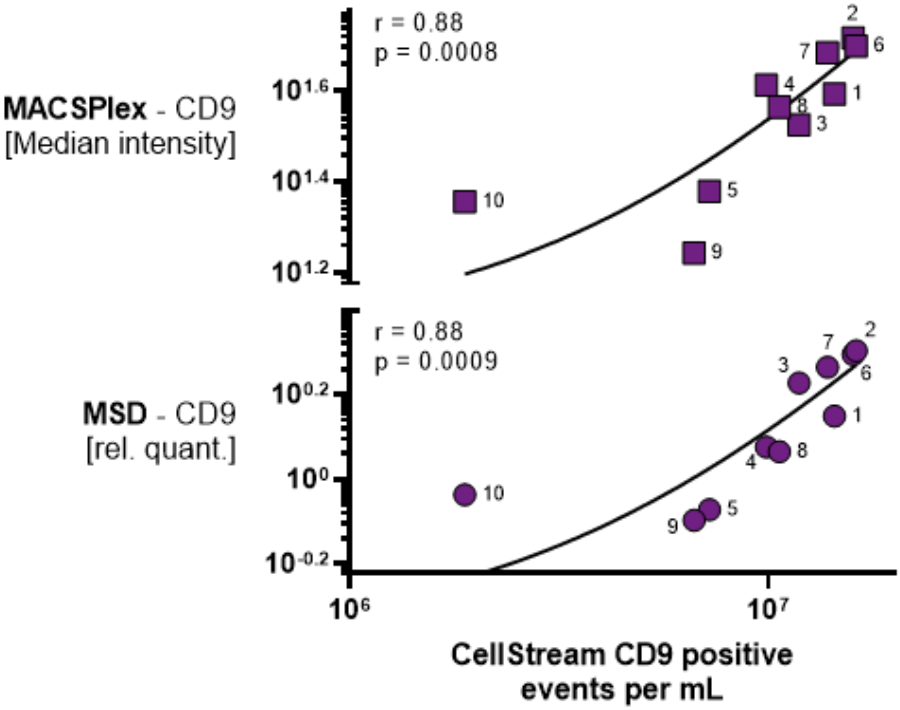

Figure 40 – Correlation analysis of different quantification methods (NanoView (NV), MACSPlex, MSD) of CD9 positive extracellular vesicles (EVs) with the CellStream method. The X-axis shows the amount of CD9 positive events per mL of plasma, whereas the Y-axis gives: top) amount of double positive CD9 EVs per spot measured on the NanoView, middle) the median fluorescence intensity in the anti-CD9 antibody-coated bead population of the MACSPlex kit, bottom) the relative signal intensity of CD9 captured and detected vesicles. The identification number is noted for every individual plasma donor. Pearson R is given from each correlation analysis with p-value and linear regression. The data is normalized for the plasma input volume.

3.3.1.2. Impurities

The amount of impurities is riven by the results of the BCA assay as well as the ELISAs for ApoA1 and ApoB100. The impurities are total protein, HDL, and LDL that are quantified in the ten plasma EV preparations of ten different donors (IND 1-10) (Figure 41).

The analysis of total protein by BCA reveals that the average of all ten EV preparations lies at 267.8 µg protein/mL plasma (A). The relative variability is comparably low at 23.6 %. The maximal deviation from the mean can be found in IND 1 with 40 % higher total

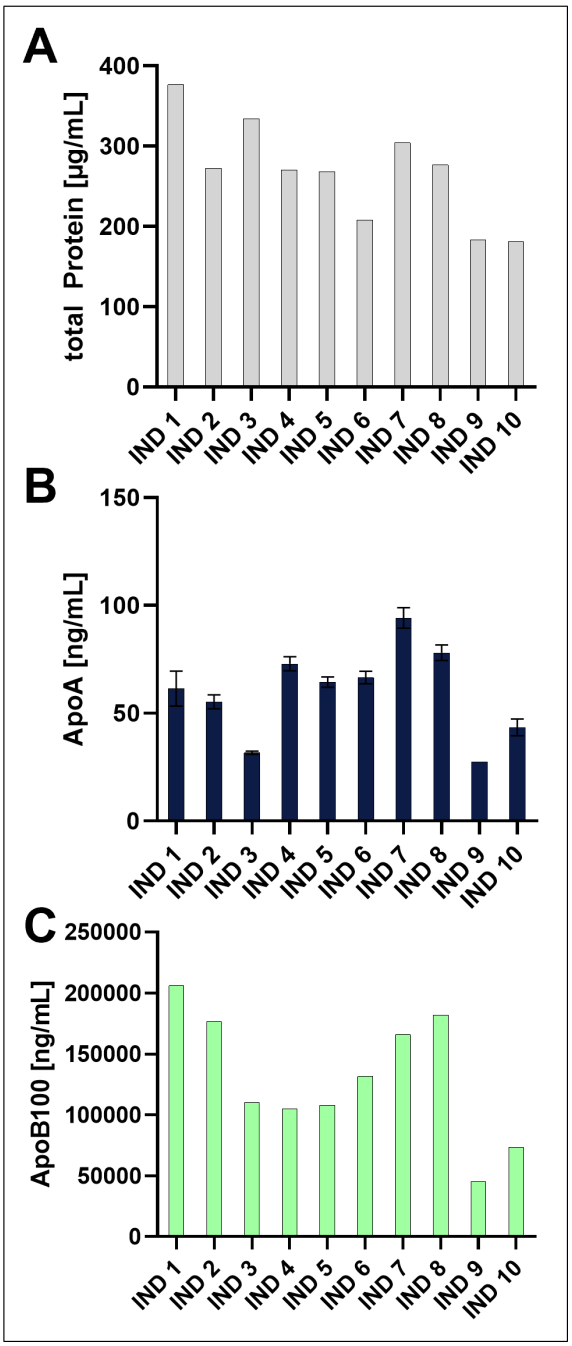

protein concentration. The samples IND 9 and IND 10 show only a low residual plasma concentration with 183.5 and 181.5 µg protein/mL of plasma. The standard error for the repeated measurement lies at 0.02 %, making the determination very accurate.

The HDL contamination of the plasma EV preparation is determined by the ELISA-based quantification of ApoA1 (B). The relative interindividual variation lies at 34.8 % from the mean, which is defined to be 59.6 ng ApoA1/mL plasma. Due to the low concentrations within the qEVsingle 35 Tween preparations, the relative standard error is relatively high (mean = 5.35 %) and reaches up to 13.2 % (IND 1).

The quantification of ApoB100 allows conclusions about the levels of LDL contaminations in the EV preparation originating from plasma (C). The data is not given in replicates due to a pipetting error; thus, there is no error bar. The data suggests that the average ApoB100 concentration lies at 130 µg/mL plasma. The variation between the individuals lies at 39.3 %, where IND 1 again shows the highest values, 57 % more than the mean. The IND 9 exhibits the lowest ApoB100 contamination, 65.1 % less than the average.

Figure 41 – Quantification of protein (a), ApoA1 (B), and ApoB100 (C) in the plasma EVs from ten individuals (IND 1-10). The individuals are indicated on the x-axis whereas the concentrations normalized for plasma input are given on the Y-axis. The error bars in plot A and B show the standard variation. The ApoB100 quantification was only analyzed once due to a pipetting error.

3.3.1.3. Summary

The correlation matrix (Figure 42) summarizes the results of the interindividual variation analysis. The data for the TSPNs shows that there is a correlation ($r \geq 0.8$) for the different methods analyzing the same target. Other than the comparison of the same TSPN, the cross-TSPN analysis reveals a lower correlation of nearly all the combinations. Only the correlation of MACSPlex data of CD9 and CD63 shows a higher degree of correlation ($r = 0.88$), as well as of the CD9 MACSPlex analysis with the CD81 MSD data ($r = 0.80$). There is a low correlation coefficient for the TSPNs CD81 and CD63 ($r < 0.5$), whereas CD9 correlates more with the other TSPNs ($r > 0.5$). Mainly the MACSPlex data must be analyzed with caution because the signal intensity of every analyte bead population is based on the colocalization of the TSPN CD9, CD63, and CD81 since the APC-staining of the EVs is performed with this antibody mix. At the same time, the excellent correlation of the CD63 analysis methods might be due to IND 2 being an outlier in all the methods that sample enhances the correlation coefficient. Interestingly, the CD9 measurement by CellStream and MACSPlex shows a higher correlation to ApoA1 than any other TSPN measurement ($r = 0.73$ and $r= 0.72$).

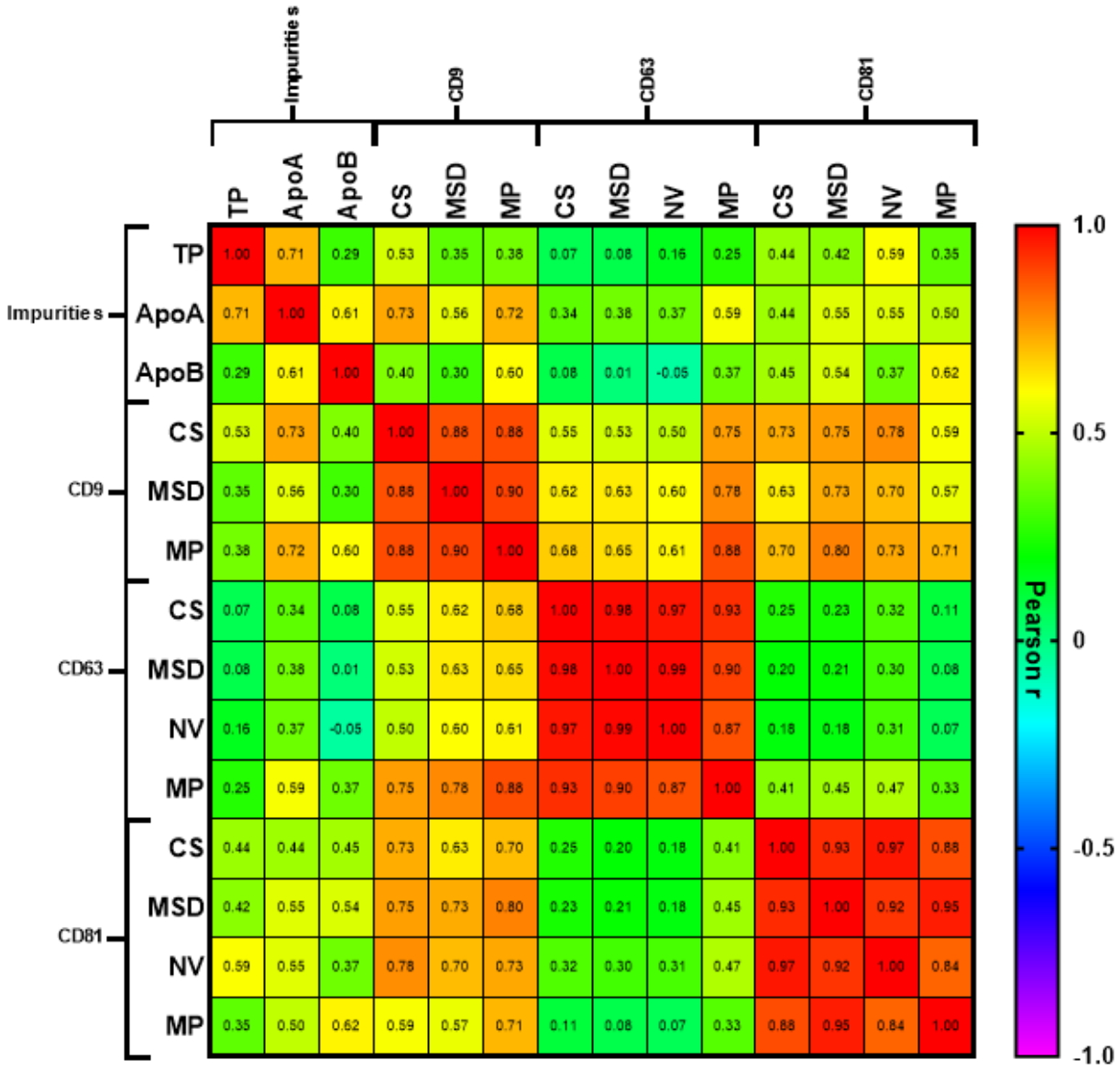

Figure 42 – Correlation matrix of the different characterization methods for the qEVsingle 35 Tween purified sEVs from ten healthy human individuals. The analysis includes impurities like total protein (TP), ApoA1 (ApoA), and ApoB100 (ApoB), as well as the TSPNs CD9, CD63, and CD81, all analyzed with different methods, including CellStream (CS), MSD, MACSPlex (MP), and NanoView (NV). The correlation is analyzed, and Pearson's R is given and indicated by the color.

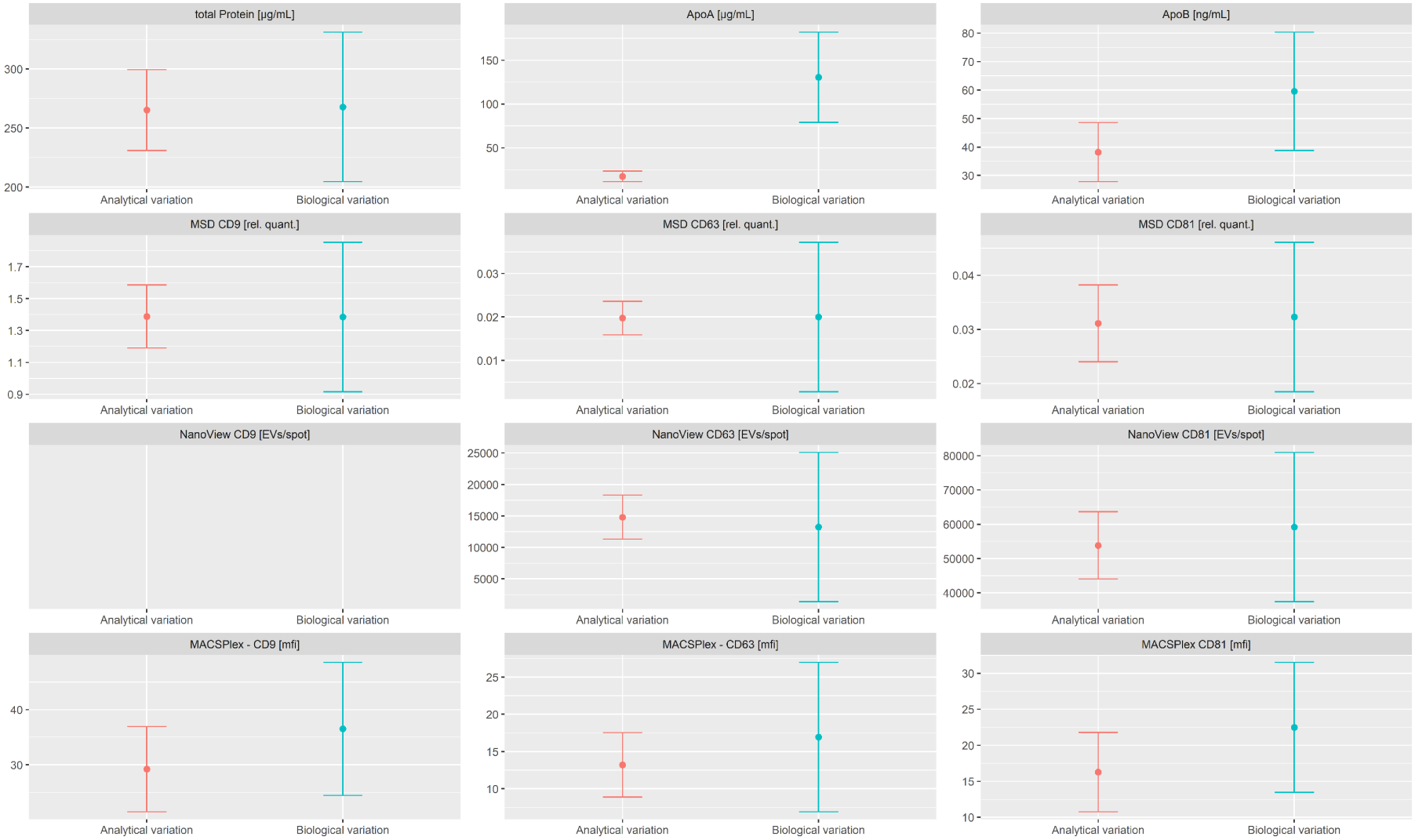

Figure 43 – The graphs display the data of the reproducibility analysis of the qEVsingle 35 Tween method performed with the merged plasma from ten healthy humans in red (n=5) and the data of the same ten individuals isolated by the same method in blue (n=10). The dots indicate the mean values normalized by plasma input. The error bars in analytical variation represents the standard error that is brought in by the sample preparation and the variation of the characterization method; the error bar of the biological variation additionally includes the interindividual variation. That comparison is shown for the quantification of total protein by BCA; ApoA and ApoB by ELISA; TSPN (CD9, CD63, CD81) by MSD,

3.3.1.4. Analytical variation vs. biological variation

To compare the analytical and the biological variation observed in this study, Figure 43 shows the mean and the variation of the repeated isolation of the pooled plasma sample in red and the ten plasma sample isolated individually in blue. In all cases, the variation of the individuals is higher compared to the variation analyzed in *3.2 Part 2 – Reproducibility of superior EV isolation methods*, indicating that the description of the individual variations is possible. Even though the mean values are not identical in all the cases, most methods show high comparability. Especially, the mean values measured by MSD are almost identical for the repeated experiments indicating good stability of the quantification method and a constant and reproducible error brought in by the isolation procedure. The relative standard deviation is up to 4.4 times higher (MSD CD63), representing the biological variation. In the mean, the MSD measurements of the individuals show a 2.9 times higher variation compared to the pooled sample. Comparing the TSPN measurements by MACSPlex shows a constant shift in the mean value, which indicates a systematic error in one of the experiments. Nevertheless, the relative standard error is constantly higher in the group of the individual measurements depending on the TSPN between 1.2- to 1.9-fold. (CD81 and CD63). NanoView also reveals a good reproducibility of the mean values in both experiments and a constant increase in the standard error when analyzing the biological variation. Again, the relative standard deviation of the CD63 analysis shows the highest increase by a factor of 3.8. The quantification of total protein also shows approximately the same mean in both experiments and an increase of the relative standard error of 1.8-fold.

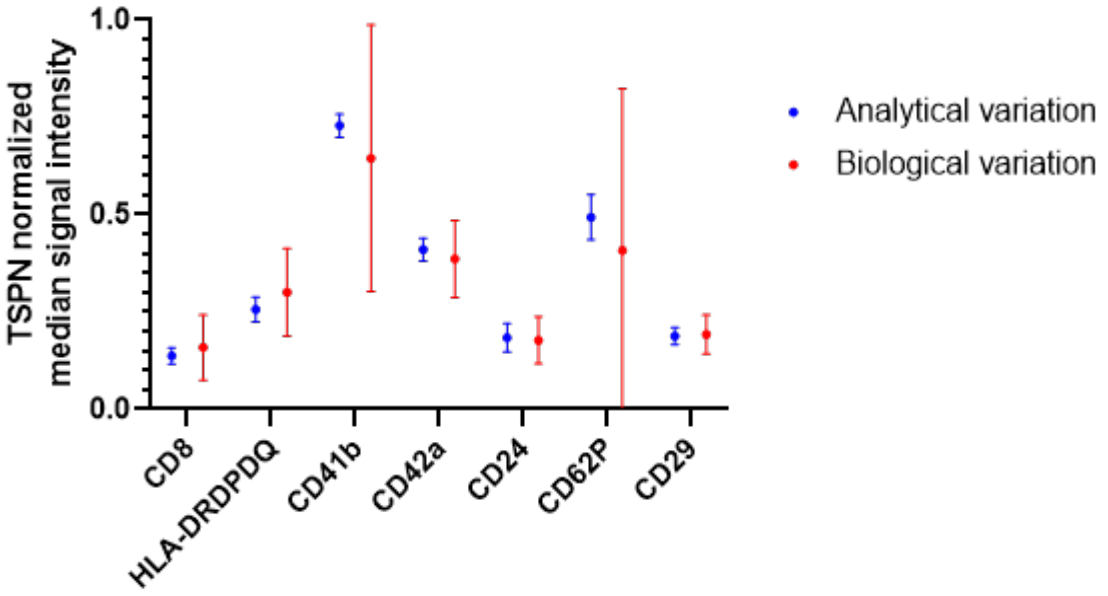

Figure 44 – qEVsingle 35 Tween isolated EVs from the reproducibility analysis (Analytical variation) and the analysis of the interindividual variation (Biological variation) analyzed by MACSPlex. The mean normalized median fluorescence intensity is indicated by a dot, whereas the error bars show the standard error. The normalization was performed by the mean of the TSPNs CD9, CD63, and CD81. Shown are the markers CD8, HLA-DRDPDQ, CD41b, CD42a, CD24, CD62P, and CD29.

The results of the MACSPlex analysis show the normalized median fluorescence intensity for several surface markers (Figure 44). For all markers, an increased error is demonstrated in the measurement of individuals compared to the repeated isolation of the pooled sample. In particular, CD41b and CD62P have a much higher variation when analyzing individual plasma samples. For CD42b, the relative standard deviation is more than 10-fold higher (Analytical variation – 4.0 %, Biological variation – 53.1 %). In comparison, other markers like CD24 show a milder increase in variation when analyzing individuals (Analytical variation – 20.0 %, Biological variation – 34.1 %). The average relative variation is 11.7 % in the analytical variation and 47.3 % in the biological variation.

Since the whole analytical variation, including the purification and the characterization, has already been evaluated in *3.2 Part 2 – Reproducibility of superior EV isolation methods*, the same error can be presumed in the individual sEV preparation. As an example, in Figure 45, the relative variation has been adapted to the results of the individuals measured in *3.3 Part 3 – Interindividual variation of qEVsingle 35 Tween EV isolation* measured by MSD. The error bars in green indicate the standard deviation of the

duplicates, whereas the red error bar demonstrates the theoretical variation (19.47 %) of both the isolation and measurement determined in *3.2 Part 2 – Reproducibility of superior EV isolation methods*.

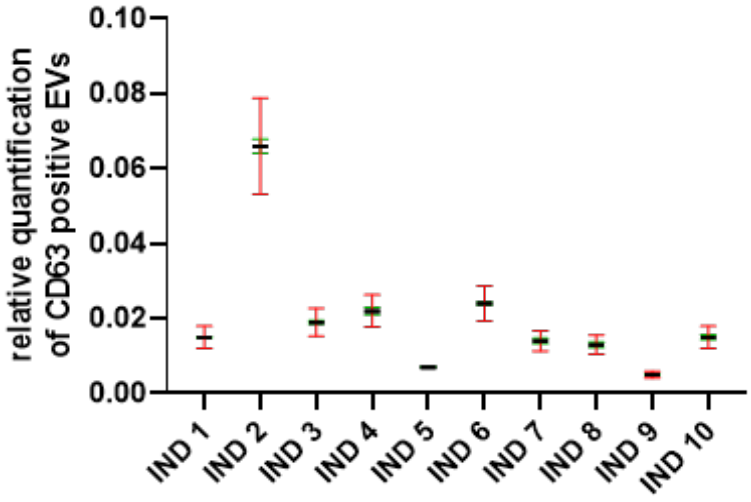

Figure 45 – Relative quantification of CD63 positive EVs by MSD for ten healthy human individuals (IND 1-10) reported with two different error bars. The error bars in green show the standard deviation of the two measurements of the identical aliquots of isolated sEVs. Indicated in red is the relative standard deviation calculated in the reproducibility analysis, including the theoretical error by isolation. The signal intensity is normalized to the calibrator and the plasma input.

3.3.2. Discussion

The purification of circulating sEVs from ten individuals with qEVsingle 35 Tween, followed by the characterization by MSD, NanoView, MACSPlex, and CellStream, gives insights into the differences in the TSPN distribution between individuals. Also, it allows for comparing which characterization methods are suitable to detect inter-individual differences.

3.3.2.1. TSPN distribution – *High variety in inter-individual EV composition emphasizes the need for correct normalization*

The analysis of the TSPN levels in ten individuals revealed a high variation in the expression. There is a tendency in some individuals (e.g., IND 9) to have low levels in all three TSPNs, indicating a low EV abundance. On the other hand, the data also shows individuals with a strong expression of specific TSPNs (e.g., IND 2 with high CD63). This indicates that there is indeed a high variation in specific individuals' EV number and their composition. This illustrates a significant issue for biomarker analysis; There is a strong need to understand the connection between the EV-based biomarker and the EV marker used for normalization. Depending on which TSPN would have been picked for normalization, the results would vary significantly for specific individuals. Still, selecting specific EV markers like CD9 or TSG101 is commonly used for normalization. [149, 150] Since no ubiquitous EV has been detected so far, and the TSPN expression differs in subclasses of EVs, a normalization based on multiple EV makers might be most valid. [151] The variations in the surface marker composition shown by MACSPlex and MSD (Figure 44, Figure 45) between the technical replicates and the individuals highlight the capability of the methods to reveal the interindividual variation for many potential biomarkers. The variability in TSPNs is constantly higher when analyzing the sEVs from different individuals compared to the pooled sample, highlighting that the variations we see are not just artifacts of the isolation procedure.

3.3.2.2.Comparison of characterization methods

Overall, the data indicates good comparability of the different characterization methods MACSPlex, NanoView, MSD, and CellStream. The R-values given for correlation analysis allow high confidence in the data even though the principles of the measurements differ. The characterization methods used can be divided into bulk analysis and single vesicle characterization methods. The single vesicle characterization methods are NTA, NanoView, and CellStream; they simultaneously allow visual detection of single vesicles to associate attributes like size and surface marker expression. These techniques can dispaly the EV heterogeneity and allow the setting of further criteria by defining subpopulations for the analysis in a single experiment. Since the EV source and function have been shown to vary between subpopulations, single vesicle characterization methods are essential tools in biomarker analysis. [152]

MACSPlex, for example, gives a result indicating a colocalization of TSPN and CD41b, but MACSPlex, as a bulk analysis, does not facilitate the determination of the intersection set and single positives at the same time. The NanoView instead can identify these characteristics for each vesicle, allowing to answer questions like: how many of the CD63 positive EVs are also biomarker positive.

As such, single vesicle characterization methods can, e.g., predefine the EV origin by surface markers and determine the percentage of biomarker-positive vesicles. [153] Similar approaches would be conceivable by bulk methods, but several experiments would be required. The CellStream, as a single vesicle characterization method, stands out due to its capability to determine the number of positive vesicles per volume and the possibility of determining the expression of a particular marker per vesicle. This allows answering questions like: Is an increased amount of biomarker measured due to a higher number of EVs carrying this or a higher amount per vesicle?

Since many of the single vesicle characterization methods are discussed to give valid results even in raw biofluids, the variation by the isolation methods might be bypassed in some situations in the future.

3.3.2.3.MSD – R*eproduceable and reliable method for the bulk analysis of intact EV*

The MSD methods showed great reproducibility and a versatile application for the detection of TSPN-positive EVs. The fact that the method has been proven to be able to give colocalization data and thus, reveal their biochemical signature, makes the method very important for EV-biomarker analysis. [154] The standard curve allows relative quantification of EV surface markers. The reproducibility and throughput of the method exceed the other characterization methods. Nevertheless, there is no established protocol for the quantification of intraluminal markers, even though the conventional ECL-based protein quantification could be applied with purified and then lysed samples. The EVs are analyzed in bulk; thus, the technic has a disadvantage in the early stages of the biomarker analysis, where a deeper understanding of different colocalizing markers and the EV heterogeneity is beneficial. [154, 155] Still, the simplicity of the acquired data also has advantages since the analysis is less error-prone, and the evaluation is less susceptible to the user's cognitive bias. [156]

It should be noted that, if the assay is used to research biomarkers that are rarely expressed on the surface of EVs, there might be no good calibrator or positive control and, thus, no relative quantification possible. This is also the case if cell-type specific markers need to be evaluated; the provided standard might not be the adequate positive control. Still, the assay is easily adaptable to the specific needs by exchanging the antibodies. Till now, there are no publications available using the MSD based analysis of intact EVs in the field of biomarker research and colocalization analysis.

3.3.2.4. NanoView – *Comprehensive EV characterization for early biomarker development*

The NanoView method also gives highly reproducible data and allows the quantification of different TSPNs as well as the colocalization analysis in a single experiment application. The analysis includes a non-binding control antibody and a visual read-out. This increases confidence in the acquired data and allows the identification of false positive results and handling-based errors. The data comprises the EV number in interferometric and fluorescent mode and a size distribution profile for every immobilized antibody. The NanoView method identifies co-localization of surface proteins and thus, a comparison of

distribution patterns and relative quantification. [157] Often the data acquired on one chip fail to fall into the acceptance range for every read-out; thus, multiple sample dilutions would be required. Since decisive factors like fluorescence detection threshold can also be configured manually after each experiment, the analysis and evaluation are error-prone and requires user expertise. The NanoView is limited in throughput due to the ExoView-instrument design. Also, the data read-out and restructuring are elaborate, error-prone, and time-consuming.

Nevertheless, the assay is versatile and allows extensive phenotyping of the vesicles. The method shows its advantages in an experimental setup, e.g., by analyzing single vesicles. The adaption of the assay for biomarker analysis is simple and allows the evaluation of colocalization with TSPN and unspecific antibody binding. In early biomarker research several surface marker based EV characterizations via the NanoView are already published and the method is established. [158–160] In later stage of biomarker discovery the analysis of bigger cohorts on the NanoView is possible, but the correlation data with the MSD and CellStream suggests these methods to use instead of NanoView, since NanoView is more laborious.

Interestingly, the company also offers a kit that allows the detection of intraluminal markers of EVs like syntenin on the NanoView device. The kit has been tested initially in our lab and the number of syntenin positive EVs has proven to have good dilution linearity (data not shown). All the data, from EV quantification over colocalization to intraluminal protein determination can be gathered by the NanoView disclosing a high potential for biomarker discovery.

3.3.2.5. MACSPlex – *Multiple surface marker detection in single experiment setup*

The MACSPlex method gives a good overview of the EVs in the preparation and the tissue origin. The method's advantage is based on the variety of analytes that can be measured on the EV surface. The fact that changes in EV composition and number can be visualized by the method has been confirmed. [161] This plays a role in the early biomarker discovery and colocalization analysis, but for later phases, especially clinical sample analysis, this method requires too much sample volume. Once a potential surface biomarker is identified, and MACSPlex has evaluated the colocalization, other

characterization methods, including MSD and CellStream, can substitute the assay. Still, the adaption of the assay by substitution of the detection antibodies allows interesting experiments based on a high number of membrane-bound analytes. If each capture antibody gives valid results in a certain setting would have to be evaluated. Here a positive control sample would highly increase the confidence. The assay can be performed in a 96-well plate format, but a suitable flow cytometer is required for the read-out. The data extraction and visualization are work intensive, but the values acquired are clear, and only a limited amount of user expertise is required once the system has been established. The recommended normalization based on the TSPNs is under debate due to the high variations observed in different individuals. [162] Since the detection is based on the colocalization of the TSPNs it might be a valid way to interpret the data. Promising data showing how MACSPlex can improve the field of biomarker research has already been published. [163–165]

3.3.2.6.CellStream – *Strong single EV characterization and quantification tool that need to prove its full potential*

The single vesicle characterization based on the CellStream instrument gives a good correlation to MSD, MACSPlex, and NanoView. The assay is highly adaptable to the markers of choice, but intraluminal staining has not yet been established in-house. Even though the measurement principle is simple, and the protocol is easy to perform, the initial establishment of a new assay takes time and requires suitable antibodies. The importance of negative controls is still under debate [166] .If all the negative controls need to be performed for each sample, the required sample volume is much higher, and the throughput of samples per plate is severely disadvantaged. At least during the validation phase of a new antibody many controls, including isotype control and serial dilution control, need to be performed. [167] Nevertheless, the advantages of the methods are visible in the later phase of biomarker analysis. While the appearance and the colocalization of the biomarker with the TSPN can be evaluated on the, e.g., NanoView first, the same assay can be transferred to the CellStream platform. Here the single vesicle characterization can not only give relative signal intensity like the MSD platform. The

simultaneous measurement of two or more markers can also give the relative colocalization as well as the absolute concentration of positive events per mL. [154, 168] The repeated measurement of the samples indicates a higher variation compared to the MSD and NanoView methods, but the CellStream is a valuable compromise between throughput and information.

3.3.2.7.Summary

We have established several characterization methods that, in combination with the qEVsingle 35 Tween method, show the variability between individuals. The methods analyzed have different advantages and disadvantages, can be used under different circumstances, and depend on the sample and biomarker to analyze. The toolbox of methods will help to tackle different challenges on the way to EV-based biomarkers and the measurement under early scientific and clinical conditions. All methods investigated showed good correlation by comparing ten individuals. There is nearly no correlation in the CD81-positive and CD63-positive EV composition ($r < 0.5$), indicating the need for a suitable marker to normalize with. CD9 correlates better with the other TSPN ($0.5 < R < 0.88$), but mainly the MACSPlex correlation data must be handled with caution since the detection of the EVs is still based on the mixed anti-TSPN antibodies.

4. Conclusion

This work aimed to identify methods to isolate sEV from plasma that is feasible for clinical studies. It should help to evaluate the usefulness and reliability of the data gathered by different characterization methods from the according isolation methods; several different isolation methods were tested to purify circulating sEVs. All the isolation methods assessed were able to isolate sEV from the plasma. However, the quality of the isolation methods varied tremendously in terms of sEV yield and impurities. For example, the qEVsingle70 and the Miltenyi Pan Bead isolation methods have been shown to isolate very pure sEVs, but their yield was inadequate for further characterization of EV populations. These techniques have advantages and can be used in other experimental settings, e.g., in early biomarker discovery. Since the biomarker quantification and read-out validity rely on the number of sEVs analyzed and the required sample volume is restricted, these methods are unsuitable to be used for EV biomarker evaluation in a clinical setting. Same is true for the ExoQuick method, which has been shown to be much lower in yield and higher in impurities compared to size exclusion-based EV isolation. Ultracentrifugation and SmartSEC, instead, have proven a high yield of sEVs when purifying plasma, but the purity of the preparation is low. These methods are highly dependent on the biomarker and its appearance in an EV-bound and soluble form. Also, the high number of proteins can falsify the detection methods. The qEVsingle 35 Tween method represents an sEV isolation method with a good balance of yield and impurities.

The critical element of the first part of the experimental setup was the good standardization of the source plasma and the high number of commonly used isolation methods compared. This, with a comprehensive characterization workflow, allows conclusions to select the suitable isolation methods and characterization workflow for their individual needs.

The second part of the experiments describes a validation-like test of the reproducibility of isolation methods. Especially in the biomarker field, the systematic reproducibility of EV isolations has not yet been shown. The variation is crucial to know if the data gathered represents the interindividual variation. Even though the qEVsingle 35 Tween reproducibility reached the acceptance criteria, a higher isolation method robustness would be advantageous for biomarker measurement.

Ultracentrifugation and especially SmartSEC provided good reproducibility with minor variations from the mean.

In the third part of the experiment, ten healthy human plasma samples were isolated via the qEVsingle 35 Tween method. The experiments demonstrated that the variation is higher when evaluating the variation between individuals (part3) compared to the variation observed during reproducibility investigation (part 2). This verifies the applicability of the isolation method and the usefulness of the characterization workflow. However, it also confirms that normalization for one or multiple TSPNs holds pitfalls since there is a wide variety in EV marker expression. Still, the more markers are used to normalize the results, the more accurate the read-out may be.

Even though the correlation data indicated the same trend observed with different techniques, the results indicated a distinct difference between the characterization methods. The MSD-based TSPN quantification showed the most lucid difference between the error based on the isolation method and the interindividual variation. This method is easily integrable into a clinical study and can quickly provide results in a standardized and robust manner.

Nevertheless, the other TSPN quantification methods investigated also have their place in earlier biomarker discovery. We were able to show that the platforms and read-outs are interchangeable. The different platforms' differences, strengths, and disadvantages have been disclosed and discussed. The data comparing the characterization methods in the third part help to drive the decision-making forward once a potential biomarker has been investigated and encouraged to adapt their biomarker assay to a platform that is easier and faster in assay execution and data analysis.

We were able to show that reliable isolation of circulating vesicles can be performed by the qEVsingle 35 Tween method with only 150 µL of plasma resulting in a high sEV yield and a reduction in lipoprotein and protein contaminations. The method is reproducible, up-scalable for bigger cohorts, and allows the revelation of the sEV composition in individual samples. The established characterization workflow requires minimal sample input and is adaptable to different scientific questions and challenges. The semi-quantitative readouts show a good correlation between the platforms, verifying their results. This also indicates that early EV biomarker assays on the NanoView or MACSPlex

are easily transferable to platforms like CellStream or MSD on the way from biomarker discovery to clinical application.

5. Literature

[1] FDA-NIH. BEST (Biomarkers, EndpointS, and other Tools) Resource; 2021

[2] Aronson JK, Ferner RE. Biomarkers-A General Review. Curr Protoc Pharmacol 2017; 76: 9.23.1-9.23.17. doi:10.1002/cpph.19

[3] Varesi A, Carrara A, Pires VG, et al. Blood-Based Biomarkers for Alzheimer's Disease Diagnosis and Progression: An Overview. Cells 2022; 11. doi:10.3390/cells11081367

[4] Jain KK. The Handbook of Biomarkers. 2nd ed. New York, NY: Springer New York; 2017

[5] Mayeux R. Biomarkers: potential uses and limitations. NeuroRx 2004; 1: 182–188. doi:10.1602/neurorx.1.2.182

[6] Chung L, Shibli S, Moore K, et al. Tissue biomarkers of breast cancer and their association with conventional pathologic features. Br J Cancer 2013; 108: 351–360. doi:10.1038/bjc.2012.552

[7] Olsson B, Lautner R, Andreasson U, et al. CSF and blood biomarkers for the diagnosis of Alzheimer's disease: a systematic review and meta-analysis. The Lancet Neurology 2016; 15: 673–684. doi:10.1016/S1474-4422(16)00070-3

[8] Wei R, Zhao L, Kong G, et al. Combination of Size-Exclusion Chromatography and Ultracentrifugation Improves the Proteomic Profiling of Plasma-Derived Small Extracellular Vesicles. Biol Proced Online 2020; 22: 12. doi:10.1186/s12575-020-00125-5

[9] Yu W, Hurley J, Roberts D, et al. Exosome-based liquid biopsies in cancer: opportunities and challenges. Ann Oncol 2021; 32: 466–477. doi:10.1016/j.annonc.2021.01.074

[10] Colburn WA. Biomarkers in drug discovery and development: from target identification through drug marketing. J Clin Pharmacol 2003; 43: 329–341. doi:10.1177/0091270003252480

[11] Frank R, Hargreaves R. Clinical biomarkers in drug discovery and development. Nat Rev Drug Discov 2003; 2: 566–580. doi:10.1038/nrd1130

[12] Davis KD, Aghaeepour N, Ahn AH, et al. Discovery and validation of biomarkers to aid the development of safe and effective pain therapeutics: challenges and opportunities. Nat Rev Neurol 2020; 16: 381–400. doi:10.1038/s41582-020-0362-2

[13] Taube SE, Clark GM, Dancey JE, et al. A perspective on challenges and issues in biomarker development and drug and biomarker codevelopment. J Natl Cancer Inst 2009; 101: 1453–1463. doi:10.1093/jnci/djp334

[14] Dancey JE, Dobbin KK, Groshen S, et al. Guidelines for the development and incorporation of biomarker studies in early clinical trials of novel agents. Clin Cancer Res 2010; 16: 1745–1755. doi:10.1158/1078-0432.CCR-09-2167

[15] FDA/CDER/"Clampet J. Enrichment Strategies for Clinical Trials to Support Determination of Effectiveness of Human Drugs and Biological Products - Guidance for Industry. In: Gough J, Nettleton D, Hrsg. Managing the Documentation Maze. Hoboken, NJ, USA: John Wiley & Sons, Inc; 2010: 431–450. doi:10.1002/9780470597507.app2

[16] Cheng L, Sharples RA, Scicluna BJ, et al. Exosomes provide a protective and enriched source of miRNA for biomarker profiling compared to intracellular and cell-free blood. Journal of extracellular vesicles 2014; 3. doi:10.3402/jev.v3.23743

[17] Jin X, Chen Y, Chen H, et al. Evaluation of Tumor-Derived Exosomal miRNA as Potential Diagnostic Biomarkers for Early-Stage Non-Small Cell Lung Cancer Using Next-Generation Sequencing. Clin Cancer Res 2017; 23: 5311–5319. doi:10.1158/1078-0432.CCR-17-0577
[18] Pang B, Zhu Y, Ni J, et al. Extracellular vesicles: the next generation of biomarkers for liquid biopsy-based prostate cancer diagnosis. Theranostics 2020; 10: 2309–2326. doi:10.7150/thno.39486
[19] Cui C, Yu B, Jiang Q, et al. The roles of PD-1/PD-L1 and its signalling pathway in gastrointestinal tract cancers. Clin Exp Pharmacol Physiol 2019; 46: 3–10. doi:10.1111/1440-1681.13028
[20] Twomey JD, Zhang B. Cancer Immunotherapy Update: FDA-Approved Checkpoint Inhibitors and Companion Diagnostics. AAPS J 2021; 23: 39. doi:10.1208/s12248-021-00574-0
[21] Zheng X-H, Cui C, Zhou X-X, et al. Centrifugation: an important pre-analytic procedure that influences plasma microRNA quantification during blood processing. Chin J Cancer 2013; 32: 667–672. doi:10.5732/cjc.012.10271
[22] Ballman KV. Biomarker: Predictive or Prognostic? J Clin Oncol 2015; 33: 3968–3971. doi:10.1200/JCO.2015.63.3651
[23] Raimondo S, Pucci M, Alessandro R, et al. Extracellular Vesicles and Tumor-Immune Escape: Biological Functions and Clinical Perspectives. Int J Mol Sci 2020; 21. doi:10.3390/ijms21072286
[24] Chen G, Huang AC, Zhang W, et al. Exosomal PD-L1 contributes to immunosuppression and is associated with anti-PD-1 response. Nature 2018; 560: 382–386. doi:10.1038/s41586-018-0392-8
[25] Ballman KV. Biomarker: Predictive or Prognostic? J Clin Oncol 2015; 33: 3968–3971. doi:10.1200/JCO.2015.63.3651
[26] Tripepi G, Jager KJ, Dekker FW, et al. Statistical methods for the assessment of prognostic biomarkers (Part I): discrimination. Nephrol Dial Transplant 2010; 25: 1399–1401. doi:10.1093/ndt/gfq018
[27] Guan M, Chen X, Ma Y, et al. MDA-9 and GRP78 as potential diagnostic biomarkers for early detection of melanoma metastasis. Tumour Biol 2015; 36: 2973–2982. doi:10.1007/s13277-014-2930-9
[28] Mukohara T. PI3K mutations in breast cancer: prognostic and therapeutic implications. Breast Cancer (Dove Med Press) 2015; 7: 111–123. doi:10.2147/BCTT.S60696
[29] Califf RM. Biomarker definitions and their applications. Exp Biol Med (Maywood) 2018; 243: 213–221. doi:10.1177/1535370217750088
[30] Sarker D, Workman P. Pharmacodynamic Biomarkers for Molecular Cancer Therapeutics. Bd. 96. doi:10.1016/S0065-230X(06)96008-4
[31] FitzGerald GA. Measure for Measure: Biomarker standards and transparency. Sci Transl Med 2016; 8: 343fs10. doi:10.1126/scitranslmed.aaf8590
[32] Ileana Dumbrava E, Meric-Bernstam F, Yap TA. Challenges with biomarkers in cancer drug discovery and development. Expert Opin Drug Discov 2018; 13: 685–690. doi:10.1080/17460441.2018.1479740

[33] Sistare FD, Dieterle F, Troth S, et al. Towards consensus practices to qualify safety biomarkers for use in early drug development. Nat Biotechnol 2010; 28: 446–454. doi:10.1038/nbt.1634
[34] Dieterle F, Marrer E. New technologies around biomarkers and their interplay with drug development. Anal Bioanal Chem 2008; 390: 141–154. doi:10.1007/s00216-007-1688-y
[35] Context of Use. FDA, <time datetime="2021-07-07T16:13:18Z">Wed, 07.07.2021 - 16:13</time>. Im Internet: https://www.fda.gov/drugs/biomarker-qualification-program/context-use; Stand: 16.11.2022
[36] Hunter DJ, Losina E, Guermazi A, et al. A pathway and approach to biomarker validation and qualification for osteoarthritis clinical trials. Curr Drug Targets 2010; 11: 536–545. doi:10.2174/138945010791011947
[37] Alix-Panabières C, Pantel K. Liquid Biopsy: From Discovery to Clinical Application. Cancer Discov 2021; 11: 858–873. doi:10.1158/2159-8290.CD-20-1311
[38] Kwapisz D. The first liquid biopsy test approved. Is it a new era of mutation testing for non-small cell lung cancer? Ann Transl Med 2017; 5: 46. doi:10.21037/atm.2017.01.32
[39] Zhou E, Li Y, Wu F, et al. Circulating extracellular vesicles are effective biomarkers for predicting response to cancer therapy. EBioMedicine 2021; 67: 103365. doi:10.1016/j.ebiom.2021.103365
[40] Poulet G, Massias J, Taly V. Liquid Biopsy: General Concepts. Acta Cytol 2019; 63: 449–455. doi:10.1159/000499337
[41] Yu D, Li Y, Wang M, et al. Exosomes as a new frontier of cancer liquid biopsy. Mol Cancer 2022; 21: 56. doi:10.1186/s12943-022-01509-9
[42] Riethdorf S, O'Flaherty L, Hille C, et al. Clinical applications of the CellSearch platform in cancer patients. Adv Drug Deliv Rev 2018; 125: 102–121. doi:10.1016/j.addr.2018.01.011
[43] Ignatiadis M, Sledge GW, Jeffrey SS. Liquid biopsy enters the clinic - implementation issues and future challenges. Nat Rev Clin Oncol 2021; 18: 297–312. doi:10.1038/s41571-020-00457-x
[44] FDA. Guardant360 CDx – P200010 (09.10.2022). Im Internet: https://www.fda.gov/medical-devices/recently-approved-devices/guardant360-cdx-p200010
[45] Becerra MF, Atluri VS, Bhattu AS, et al. Serum and urine biomarkers for detecting clinically significant prostate cancer. Urol Oncol 2021; 39: 686–690. doi:10.1016/j.urolonc.2020.02.018
[46] Margolis E, Brown G, Partin A, et al. Predicting high-grade prostate cancer at initial biopsy: clinical performance of the ExoDx (EPI) Prostate Intelliscore test in three independent prospective studies. Prostate Cancer Prostatic Dis 2022; 25: 296–301. doi:10.1038/s41391-021-00456-8
[47] Akiyama H. Inflammation and Alzheimer's disease. Neurobiology of Aging 2000; 21: 383–421. doi:10.1016/s0197-4580(00)00124-x
[48] Hansson O. Biomarkers for neurodegenerative diseases. Nat Med 2021; 27: 954–963. doi:10.1038/s41591-021-01382-x

[49] Shaw LM, Korecka M, Clark CM, et al. Biomarkers of neurodegeneration for diagnosis and monitoring therapeutics. Nat Rev Drug Discov 2007; 6: 295–303. doi:10.1038/nrd2176
[50] Parnetti L, Gaetani L, Eusebi P, et al. CSF and blood biomarkers for Parkinson's disease. The Lancet Neurology 2019; 18: 573–586. doi:10.1016/S1474-4422(19)30024-9
[51] Blennow K, Mattsson N, Schöll M, et al. Amyloid biomarkers in Alzheimer's disease. Trends Pharmacol Sci 2015; 36: 297–309. doi:10.1016/j.tips.2015.03.002
[52] Hanahan D, Weinberg RA. The Hallmarks of Cancer. Cell 2000; 100: 57–70. doi:10.1016/S0092-8674(00)81683-9
[53] Hanahan D. Hallmarks of Cancer: New Dimensions. Cancer Discov 2022; 12: 31–46. doi:10.1158/2159-8290.CD-21-1059
[54] Dagogo-Jack I, Shaw AT. Tumour heterogeneity and resistance to cancer therapies. Nat Rev Clin Oncol 2018; 15: 81–94. doi:10.1038/nrclinonc.2017.166
[55] Sankin A, Hakimi AA, Mikkilineni N, et al. The impact of genetic heterogeneity on biomarker development in kidney cancer assessed by multiregional sampling. Cancer Med 2014; 3: 1485–1492. doi:10.1002/cam4.293
[56] Cyll K, Ersvær E, Vlatkovic L, et al. Tumour heterogeneity poses a significant challenge to cancer biomarker research. Br J Cancer 2017; 117: 367–375. doi:10.1038/bjc.2017.171
[57] Marrugo-Ramírez J, Mir M, Samitier J. Blood-Based Cancer Biomarkers in Liquid Biopsy: A Promising Non-Invasive Alternative to Tissue Biopsy. Int J Mol Sci 2018; 19. doi:10.3390/ijms19102877
[58] Gainor JF, Longo DL, Chabner BA. Pharmacodynamic biomarkers: falling short of the mark? Clin Cancer Res 2014; 20: 2587–2594. doi:10.1158/1078-0432.CCR-13-3132
[59] Sandfeld-Paulsen B, Aggerholm-Pedersen N, Bæk R, et al. Exosomal proteins as prognostic biomarkers in non-small cell lung cancer. Mol Oncol 2016; 10: 1595–1602. doi:10.1016/j.molonc.2016.10.003
[60] van der Pol E, Böing AN, Harrison P, et al. Classification, functions, and clinical relevance of extracellular vesicles. Pharmacol Rev 2012; 64: 676–705. doi:10.1124/pr.112.005983
[61] Younas N, Fernandez Flores LC, Hopfner F, et al. A new paradigm for diagnosis of neurodegenerative diseases: peripheral exosomes of brain origin. Transl Neurodegener 2022; 11: 28. doi:10.1186/s40035-022-00301-5
[62] Krämer-Albers E-M. Extracellular Vesicles at CNS barriers: Mode of action. Curr Opin Neurobiol 2022; 75: 102569. doi:10.1016/j.conb.2022.102569
[63] Shi M, Sheng L, Stewart T, et al. New windows into the brain: Central nervous system-derived extracellular vesicles in blood. Prog Neurobiol 2019; 175: 96–106. doi:10.1016/j.pneurobio.2019.01.005
[64] Morales-Prieto DM, Stojiljkovic M, Diezel C, Streicher P-E, Röstel F, Lindner J, Weis S, Schmeer C, Marz M. Peripheral blood exosomes pass blood-brain-barrier and induce glial cell activation. Bd. 13; 2018. doi:10.1101/471409
[65] Guedes VA, Devoto C, Leete J, et al. Extracellular Vesicle Proteins and MicroRNAs as Biomarkers for Traumatic Brain Injury. Front Neurol 2020; 11: 663. doi:10.3389/fneur.2020.00663

[66] Zhang Y, Liu Y, Liu H, et al. Exosomes: biogenesis, biologic function and clinical potential. Cell Biosci 2019; 9: 19. doi:10.1186/s13578-019-0282-2
[67] Thompson AG, Gray E, Heman-Ackah SM, et al. Extracellular vesicles in neurodegenerative disease - pathogenesis to biomarkers. Nat Rev Neurol 2016; 12: 346–357. doi:10.1038/nrneurol.2016.68
[68] Vlassov AV, Magdaleno S, Setterquist R, et al. Exosomes: current knowledge of their composition, biological functions, and diagnostic and therapeutic potentials. Biochimica et Biophysica Acta 2012; 1820: 940–948. doi:10.1016/j.bbagen.2012.03.017
[69] Vader P. Extracellular Vesicle Heterogeneity: Subpopulations, Isolation Techniques, and Diverse Functions in Cancer Progression
[70] Doyle LM, Wang MZ. Overview of Extracellular Vesicles, Their Origin, Composition, Purpose, and Methods for Exosome Isolation and Analysis. Cells 2019; 8. doi:10.3390/cells8070727
[71] Huang C, Quinn D, Sadovsky Y, et al. Formation and size distribution of self-assembled vesicles. Proc Natl Acad Sci U S A 2017; 114: 2910–2915. doi:10.1073/pnas.1702065114
[72] Borges FT, Reis LA, Schor N. Extracellular vesicles: structure, function, and potential clinical uses in renal diseases. Braz J Med Biol Res 2013; 46: 824–830. doi:10.1590/1414-431X20132964
[73] Abels ER, Breakefield XO. Introduction to Extracellular Vesicles: Biogenesis, RNA Cargo Selection, Content, Release, and Uptake. Cell Mol Neurobiol 2016; 36: 301–312. doi:10.1007/s10571-016-0366-z
[74] Brennan K, Martin K, FitzGerald SP, et al. A comparison of methods for the isolation and separation of extracellular vesicles from protein and lipid particles in human serum. Sci Rep 2020; 10: 1039. doi:10.1038/s41598-020-57497-7
[75] Battistelli M, Falcieri E. Apoptotic Bodies: Particular Extracellular Vesicles Involved in Intercellular Communication. Biology (Basel) 2020; 9. doi:10.3390/biology9010021
[76] Gebara N, Rossi A, Skovronova R, et al. Extracellular Vesicles, Apoptotic Bodies and Mitochondria: Stem Cell Bioproducts for Organ Regeneration. Curr Transpl Rep 2020; 7: 105–113. doi:10.1007/s40472-020-00282-2
[77] Ratajczak MZ, Ratajczak J. Extracellular microvesicles/exosomes: discovery, disbelief, acceptance, and the future? Leukemia 2020; 34: 3126–3135. doi:10.1038/s41375-020-01041-z
[78] Witwer KW, Théry C. Extracellular vesicles or exosomes? On primacy, precision, and popularity influencing a choice of nomenclature. Journal of extracellular vesicles 2019; 8: 1648167. doi:10.1080/20013078.2019.1648167
[79] Zhang Y, Chen X, Gueydan C, et al. Plasma membrane changes during programmed cell deaths. Cell Res 2018; 28: 9–21. doi:10.1038/cr.2017.133
[80] Mathivanan S. New Frontiers. v.97. Subcellular Biochemistry Ser. Cham: Springer International Publishing AG; 2021
[81] Wu D, Ingram A, Lahti JH, et al. Apoptotic release of histones from nucleosomes. J Biol Chem 2002; 277: 12001–12008. doi:10.1074/jbc.M109219200
[82] Prokhorova EA, Kopeina GS, Lavrik IN, et al. Apoptosis regulation by subcellular relocation of caspases. Sci Rep 2018; 8: 12199. doi:10.1038/s41598-018-30652-x

[83] Mulcahy LA, Pink RC, Carter DRF. Routes and mechanisms of extracellular vesicle uptake. Journal of extracellular vesicles 2014; 3. doi:10.3402/jev.v3.24641
[84] Brock CK, Wallin ST, Ruiz OE, et al. Stem cell proliferation is induced by apoptotic bodies from dying cells during epithelial tissue maintenance. Nat Commun 2019; 10: 1044. doi:10.1038/s41467-019-09010-6
[85] van Niel G, D'Angelo G, Raposo G. Shedding light on the cell biology of extracellular vesicles. Nat Rev Mol Cell Biol 2018; 19: 213–228. doi:10.1038/nrm.2017.125
[86] Lai CP-K, Breakefield XO. Role of exosomes/microvesicles in the nervous system and use in emerging therapies. Front Physiol 2012; 3: 228. doi:10.3389/fphys.2012.00228
[87] Cocucci E, Racchetti G, Meldolesi J. Shedding microvesicles: artefacts no more. Trends Cell Biol 2009; 19: 43–51. doi:10.1016/j.tcb.2008.11.003
[88] Tricarico C, Clancy J, D'Souza-Schorey C. Biology and biogenesis of shed microvesicles. Small GTPases 2017; 8: 220–232. doi:10.1080/21541248.2016.1215283
[89] Sidhom K, Obi PO, Saleem A. A Review of Exosomal Isolation Methods: Is Size Exclusion Chromatography the Best Option? Int J Mol Sci 2020; 21. doi:10.3390/ijms21186466
[90] Chuo ST-Y, Chien JC-Y, Lai CP-K. Imaging extracellular vesicles: current and emerging methods. J Biomed Sci 2018; 25: 91. doi:10.1186/s12929-018-0494-5
[91] Konoshenko MY, Lekchnov EA, Vlassov AV, et al. Isolation of Extracellular Vesicles: General Methodologies and Latest Trends. Biomed Res Int 2018; 2018: 8545347. doi:10.1155/2018/8545347
[92] Cordonnier M, Nardin C, Chanteloup G, et al. Tracking the evolution of circulating exosomal-PD-L1 to monitor melanoma patients. Journal of extracellular vesicles 2020; 9: 1710899. doi:10.1080/20013078.2019.1710899
[93] Xuan H, Hu X, Huang J. Role of motility-related protein-1 in promoting the development of several types of cancer (Review). Oncol Lett 2014; 7: 611–615. doi:10.3892/ol.2014.1786
[94] Mathivanan S, Simpson RJ. ExoCarta: A compendium of exosomal proteins and RNA. Proteomics 2009; 9: 4997–5000. doi:10.1002/pmic.200900351
[95] Fernanda G. Kugeratski, Kelly Hodge, Sergio Lilla, et al. Quantitative proteomics identifies the core proteome of exosomes with syntenin-1 as the highest abundant protein and a putative universal biomarker
[96] Schnatz A, Müller C, Brahmer A, et al. Extracellular Vesicles in neural cell interaction and CNS homeostasis. FASEB Bioadv 2021; 3: 577–592. doi:10.1096/fba.2021-00035
[97] Mathieu M, Névo N, Jouve M, et al. Specificities of exosome versus small ectosome secretion revealed by live intracellular tracking of CD63 and CD9. Nat Commun 2021; 12: 4389. doi:10.1038/s41467-021-24384-2
[98] Men Y, Yelick J, Jin S, et al. Exosome reporter mice reveal the involvement of exosomes in mediating neuron to astroglia communication in the CNS. Nat Commun 2019; 10: 4136. doi:10.1038/s41467-019-11534-w
[99] Duffield A, Kamsteeg E-J, Brown AN, et al. The tetraspanin CD63 enhances the internalization of the H,K-ATPase beta-subunit. Proc Natl Acad Sci U S A 2003; 100: 15560–15565. doi:10.1073/pnas.2536699100

[100] Berditchevski F, Odintsova E. Tetraspanins as regulators of protein trafficking. Traffic 2007; 8: 89–96. doi:10.1111/j.1600-0854.2006.00515.x
[101] Pompa A, Marchis F de. Unconventional Protein Secretion 2016; 1459. doi:10.1007/978-1-4939-3804-9
[102] Martins VR, Dias MS, Hainaut P. Tumor-cell-derived microvesicles as carriers of molecular information in cancer. Curr Opin Oncol 2013; 25: 66–75. doi:10.1097/CCO.0b013e32835b7c81
[103] Nickel W, Rabouille C. Mechanisms of regulated unconventional protein secretion. Nat Rev Mol Cell Biol 2009; 10: 148–155. doi:10.1038/nrm2617
[104] Rabouille C. Pathways of Unconventional Protein Secretion. Trends Cell Biol 2017; 27: 230–240. doi:10.1016/j.tcb.2016.11.007
[105] Lombardi M, Gabrielli M, Adinolfi E, et al. Role of ATP in Extracellular Vesicle Biogenesis and Dynamics. Front Pharmacol 2021; 12: 654023. doi:10.3389/fphar.2021.654023
[106] Buschow SI, Nolte-'t Hoen ENM, van Niel G, et al. MHC II in dendritic cells is targeted to lysosomes or T cell-induced exosomes via distinct multivesicular body pathways. Traffic 2009; 10: 1528–1542. doi:10.1111/j.1600-0854.2009.00963.x
[107] Yang C, Robbins PD. The roles of tumor-derived exosomes in cancer pathogenesis. Clin Dev Immunol 2011; 2011: 842849. doi:10.1155/2011/842849
[108] Juan T, Fürthauer M. Biogenesis and function of ESCRT-dependent extracellular vesicles. Semin Cell Dev Biol 2018; 74: 66–77. doi:10.1016/j.semcdb.2017.08.022
[109] Yáñez-Mó M, Siljander PR-M, Andreu Z, et al. Biological properties of extracellular vesicles and their physiological functions. Journal of extracellular vesicles 2015; 4: 27066. doi:10.3402/jev.v4.27066
[110] Logozzi M, Milito A de, Lugini L, et al. High levels of exosomes expressing CD63 and caveolin-1 in plasma of melanoma patients. PloS one 2009; 4: e5219. doi:10.1371/journal.pone.0005219
[111] Frühbeis C, Fröhlich D, Kuo WP, et al. Extracellular vesicles as mediators of neuron-glia communication. Front Cell Neurosci 2013; 7: 182. doi:10.3389/fncel.2013.00182
[112] Kriebel PW, Barr VA, Rericha EC, et al. Collective cell migration requires vesicular trafficking for chemoattractant delivery at the trailing edge. J Cell Biol 2008; 183: 949–961. doi:10.1083/jcb.200808105
[113] Raposo G, Nijman HW, Stoorvogel W, et al. B lymphocytes secrete antigen-presenting vesicles. J Exp Med 1996; 183: 1161–1172. doi:10.1084/jem.183.3.1161
[114] Conzelmann C, Groß R, Zou M, et al. Salivary extracellular vesicles inhibit Zika virus but not SARS-CoV-2 infection. Journal of extracellular vesicles 2020; 9: 1808281. doi:10.1080/20013078.2020.1808281
[115] Valadi H, Ekström K, Bossios A, et al. Exosome-mediated transfer of mRNAs and microRNAs is a novel mechanism of genetic exchange between cells. Nat Cell Biol 2007; 9: 654–659. doi:10.1038/ncb1596
[116] Thietart S, Rautou P-E. Extracellular vesicles as biomarkers in liver diseases: A clinician's point of view. J Hepatol 2020; 73: 1507–1525. doi:10.1016/j.jhep.2020.07.014

[117] Enderle D, Noerholm M. Are extracellular vesicles ready for the clinical laboratory? Journal of Laboratory Medicine 2022; 46: 273–282. doi:10.1515/labmed-2022-0064
[118] Simonsen JB. What Are We Looking At? Extracellular Vesicles, Lipoproteins, or Both? Circ Res 2017; 121: 920–922. doi:10.1161/CIRCRESAHA.117.311767
[119] Helwa I, Cai J, Drewry MD, et al. A Comparative Study of Serum Exosome Isolation Using Differential Ultracentrifugation and Three Commercial Reagents. PloS one 2017; 12: e0170628. doi:10.1371/journal.pone.0170628
[120] Varga Z, Fehér B, Kitka D, et al. Size Measurement of Extracellular Vesicles and Synthetic Liposomes: The Impact of the Hydration Shell and the Protein Corona. Colloids Surf B Biointerfaces 2020; 192: 111053. doi:10.1016/j.colsurfb.2020.111053
[121] Théry C, Witwer KW, Aikawa E, et al. Minimal information for studies of extracellular vesicles 2018 (MISEV2018): a position statement of the International Society for Extracellular Vesicles and update of the MISEV2014 guidelines. Journal of extracellular vesicles 2018; 7: 1535750. doi:10.1080/20013078.2018.1535750
[122] Wojczynski MK, Glasser SP, Oberman A, et al. High-fat meal effect on LDL, HDL, and VLDL particle size and number in the Genetics of Lipid-Lowering Drugs and Diet Network (GOLDN): an interventional study. Lipids Health Dis 2011; 10: 181. doi:10.1186/1476-511X-10-181
[123] Böing AN, van der Pol E, Grootemaat AE, et al. Single-step isolation of extracellular vesicles by size-exclusion chromatography. Journal of extracellular vesicles 2014; 3. doi:10.3402/jev.v3.23430
[124] Mørk M, Handberg A, Pedersen S, et al. Prospects and limitations of antibody-mediated clearing of lipoproteins from blood plasma prior to nanoparticle tracking analysis of extracellular vesicles. Journal of extracellular vesicles 2017; 6: 1308779. doi:10.1080/20013078.2017.1308779
[125] Buzas EI. Opportunities and challenges in studying the extracellular vesicle corona. Nat Cell Biol 2022; 24: 1322–1325. doi:10.1038/s41556-022-00983-z
[126] Jung HH, Kim J-Y, Lim JE, et al. Cytokine profiling in serum-derived exosomes isolated by different methods. Sci Rep 2020; 10: 14069. doi:10.1038/s41598-020-70584-z
[127] Bachurski D, Schuldner M, Nguyen P-H, et al. Extracellular vesicle measurements with nanoparticle tracking analysis - An accuracy and repeatability comparison between NanoSight NS300 and ZetaView. Journal of extracellular vesicles 2019; 8: 1596016. doi:10.1080/20013078.2019.1596016
[128] Ter-Ovanesyan D, Norman M, Lazarovits R, et al. Framework for rapid comparison of extracellular vesicle isolation methods. Elife 2021; 10. doi:10.7554/eLife.70725
[129] Witwer KW, Buzás EI, Bemis LT, et al. Standardization of sample collection, isolation and analysis methods in extracellular vesicle research. Journal of extracellular vesicles 2013; 2. doi:10.3402/jev.v2i0.20360
[130] Tóth EÁ, Turiák L, Visnovitz T, et al. Formation of a protein corona on the surface of extracellular vesicles in blood plasma. Journal of extracellular vesicles 2021; 10: e12140. doi:10.1002/jev2.12140
[131] IZON. Summary of qEV recommendation and sample preparation by sample type

[132] Rider MA, Hurwitz SN, Meckes DG. ExtraPEG: A Polyethylene Glycol-Based Method for Enrichment of Extracellular Vesicles. Sci Rep 2016; 6: 23978. doi:10.1038/srep23978
[133] Bruce TF, Slonecki TJ, Wang L, et al. Exosome isolation and purification via hydrophobic interaction chromatography using a polyester, capillary-channeled polymer fiber phase. Electrophoresis 2019; 40: 571–581. doi:10.1002/elps.201800417
[134] Vergauwen G, Dhondt B, van Deun J, et al. Confounding factors of ultrafiltration and protein analysis in extracellular vesicle research. Sci Rep 2017; 7: 2704. doi:10.1038/s41598-017-02599-y
[135] Zhou B, Xu K, Zheng X, et al. Application of exosomes as liquid biopsy in clinical diagnosis. Signal Transduct Target Ther 2020; 5: 144. doi:10.1038/s41392-020-00258-9
[136] Stranska R, Gysbrechts L, Wouters J, et al. Comparison of membrane affinity-based method with size-exclusion chromatography for isolation of exosome-like vesicles from human plasma. J Transl Med 2018; 16: 1. doi:10.1186/s12967-017-1374-6
[137] Holcar M, Ferdin J, Sitar S, et al. Enrichment of plasma extracellular vesicles for reliable quantification of their size and concentration for biomarker discovery. Sci Rep 2020; 10: 21346. doi:10.1038/s41598-020-78422-y
[138] Tamás Baranyai, Kata Herczeg, Zsófia Onódi, István Voszka, Károly Módos, Nikolett Marton, György Nagy, Imre Mäger, Matthew J. Wood, Samir El Andaloussi, Zoltán Pálinkás, Vikas Kumar, Péter Nagy, Ágnes Kittel, Edit Irén Buzás, Péter Ferdinandy, Zoltán Giricz. Isolation of Exosomes from Blood Plasma: Qualitative and Quantitative Comparison of Ultracentrifugation and Size Exclusion Chromatography Methods
[139] Shimomura R, Nezu T, Hosomi N, et al. Alpha-2-macroglobulin as a Promising Biological Marker of Endothelial Function. J Atheroscler Thromb 2018; 25: 350–358. doi:10.5551/jat.41335
[140] Nordin JZ, Lee Y, Vader P, et al. Ultrafiltration with size-exclusion liquid chromatography for high yield isolation of extracellular vesicles preserving intact biophysical and functional properties. Nanomedicine 2015; 11: 879–883. doi:10.1016/j.nano.2015.01.003
[141] Serrano-Pertierra E, Oliveira-Rodríguez M, Rivas M, et al. Characterization of Plasma-Derived Extracellular Vesicles Isolated by Different Methods: A Comparison Study. Bioengineering (Basel) 2019; 6. doi:10.3390/bioengineering6010008
[142] Malenica M, Vukomanović M, Kurtjak M, et al. Perspectives of Microscopy Methods for Morphology Characterisation of Extracellular Vesicles from Human Biofluids. Biomedicines 2021; 9. doi:10.3390/biomedicines9060603
[143] Hirschberg Y, Boonen K, Schildermans K, et al. Characterising extracellular vesicles from individual low volume cerebrospinal fluid samples, isolated by SmartSEC. J of Extracellular Bio 2022; 1. doi:10.1002/jex2.55
[144] Torres Crigna A, Fricke F, Nitschke K, et al. Inter-Laboratory Comparison of Extracellular Vesicle Isolation Based on Ultracentrifugation. Transfus Med Hemother 2021; 48: 48–59. doi:10.1159/000508712
[145] Royo F, Théry C, Falcón-Pérez JM, et al. Methods for Separation and Characterization of Extracellular Vesicles: Results of a Worldwide Survey Performed by the ISEV Rigor and Standardization Subcommittee. Cells 2020; 9. doi:10.3390/cells9091955

[146] Mol EA, Goumans M-J, Doevendans PA, et al. Higher functionality of extracellular vesicles isolated using size-exclusion chromatography compared to ultracentrifugation. Nanomedicine 2017; 13: 2061–2065. doi:10.1016/j.nano.2017.03.011
[147] Böing AN, van der Pol E, Grootemaat AE, et al. Single-step isolation of extracellular vesicles by size-exclusion chromatography. Journal of extracellular vesicles 2014; 3. doi:10.3402/jev.v3.23430
[148] Geeurickx E, Lippens L, Rappu P, et al. Recombinant extracellular vesicles as biological reference material for method development, data normalization and assessment of (pre-)analytical variables. Nat Protoc 2021; 16: 603–633. doi:10.1038/s41596-020-00446-5
[149] Koritzinsky EH, Street JM, Chari RR, et al. Circadian variation in the release of small extracellular vesicles can be normalized by vesicle number or TSG101. Am J Physiol Renal Physiol 2019; 317: F1098-F1110. doi:10.1152/ajprenal.00568.2017
[150] Miguel-Perez D de, Russo A, Arrieta O, et al. Extracellular vesicle PD-L1 dynamics predict durable response to immune-checkpoint inhibitors and survival in patients with non-small cell lung cancer. J Exp Clin Cancer Res 2022; 41: 186. doi:10.1186/s13046-022-02379-1
[151] Mizenko RR, Brostoff T, Rojalin T, et al. Tetraspanins are unevenly distributed across single extracellular vesicles and bias sensitivity to multiplexed cancer biomarkers. J Nanobiotechnology 2021; 19: 250. doi:10.1186/s12951-021-00987-1
[152] Bordanaba-Florit G, Royo F, Kruglik SG, et al. Using single-vesicle technologies to unravel the heterogeneity of extracellular vesicles. Nat Protoc 2021; 16: 3163–3185. doi:10.1038/s41596-021-00551-z
[153] Crescitelli R, Lässer C, Lötvall J. Isolation and characterization of extracellular vesicle subpopulations from tissues. Nat Protoc 2021; 16: 1548–1580. doi:10.1038/s41596-020-00466-1
[154] Woud WW, van der Pol E, Mul E, et al. An imaging flow cytometry-based methodology for the analysis of single extracellular vesicles in unprocessed human plasma. Commun Biol 2022; 5: 633. doi:10.1038/s42003-022-03569-5
[155] Bağcı C, Sever-Bahcekapili M, Belder N, et al. Overview of extracellular vesicle characterization techniques and introduction to combined reflectance and fluorescence confocal microscopy to distinguish extracellular vesicle subpopulations. Neurophotonics 2022; 9: 21903. doi:10.1117/1.NPh.9.2.021903
[156] *[Anonym]*. doi:10.1016/j.trac.2006.10.007
[157] Chiodi E, Daaboul GG, Marn AM, et al. Multiplexed Affinity Measurements of Extracellular Vesicles Binding Kinetics. Sensors (Basel) 2021; 21. doi:10.3390/s21082634
[158] Eren E, Leoutsakos J-M, Troncoso J, et al. Neuronal-Derived EV Biomarkers Track Cognitive Decline in Alzheimer's Disease. Cells 2022; 11. doi:10.3390/cells11030436
[159] Park S, Moon HY. Urinary extracellular vesicle as a potential biomarker of exercise-induced fatigue in young adult males. Eur J Appl Physiol 2022; 122: 2175–2188. doi:10.1007/s00421-022-04995-3
[160] Mahida RY, Price J, Lugg ST, Li H, Parekh D, Scott A, Harrison P, Matthay MA, Thickett DR. CD14 Positive Extracellular Vesicles in Broncho-Alveolar Lavage Fluid as a New

Biomarker of Acute Respiratory Distress Syndrome; 2021. doi:10.1101/2021.09.25.21264053
[161] Brahmer A, Neuberger E, Esch-Heisser L, et al. Platelets, endothelial cells and leukocytes contribute to the exercise-triggered release of extracellular vesicles into the circulation. Journal of extracellular vesicles 2019; 8: 1615820. doi:10.1080/20013078.2019.1615820
[162] Archibald SJ, Hisada Y, Bae-Jump VL, et al. Evaluation of a new bead-based assay to measure levels of human tissue factor antigen in extracellular vesicles in plasma. Res Pract Thromb Haemost 2022; 6: e12677. doi:10.1002/rth2.12677
[163] Ekström K, Crescitelli R, Pétursson HI, et al. Characterization of surface markers on extracellular vesicles isolated from lymphatic exudate from patients with breast cancer. BMC Cancer 2022; 22: 50. doi:10.1186/s12885-021-08870-w
[164] Bandini E, Rossi T, Scarpi E, et al. Early Detection and Investigation of Extracellular Vesicles Biomarkers in Breast Cancer. Front Mol Biosci 2021; 8: 732900. doi:732900
[165] Signorelli D, Ghidotti P, Proto C, et al. Circulating CD81-expressing extracellular vesicles as biomarkers of response for immune-checkpoint inhibitors in advanced NSCLC. Front Immunol 2022; 13: 987639. doi:10.3389/fimmu.2022.987639
[166] Welsh JA, van der Pol E, Arkesteijn GJA, et al. MIFlowCyt-EV: a framework for standardized reporting of extracellular vesicle flow cytometry experiments. Journal of extracellular vesicles 2020; 9: 1713526. doi:10.1080/20013078.2020.1713526
[167] Welsh JA, Arkesteijn GJA, Bremer M, et al. A compendium of single extracellular vesicle flow cytometry. Journal of extracellular vesicles 2023; 12: e12299. doi:10.1002/jev2.12299
[168] Volpert O, Gershun E, Elgart K, Erden E, Kapogiannis D, Verma A, Levin A, Kalia V, Wu H, Baccarelli A, Eitan E. Novel modification of Luminex assay for characterization of extracellular vesicle populations in biofluids; 2022. doi:10.21203/rs.3.rs-1723261/v1